The Toxicity of a Novel Antifungal Compound Is Modulated by Endoplasmic Reticulum-Associated Protein Degradation (ERAD) Components

Shriya S Raj, Karthik Krishnan, David S Askew, Olivier S Helynck, Peggy Suzanne, Aurélien Lesnard, Sylvain Rault, Ute S Zeidler, Christophe d'Enfert, Jean-Paul S Latgé, et al.

Toxicity of a novel antifungal compound is modulated by ERAD components

Shriya Raj[1], Karthik Krishnan[2], David S. Askew[2], Olivier Helynck[3,4], Peggy Suzanne[5], Aureslien Lesnard[5], Sylvain Rault[5], Ute Zeidler[6,7,@], Christophe d'Enfert[6,7], Jean-Paul Latgé[1,#], Hélène Munier-Lehmann[3,4,#], Cosmin Saveanu[8,9,#]

[1] Institut Pasteur, Unité des Aspergillus, Département Mycologie, 25-28 rue du docteur Roux 75015, Paris, France

[2] Department of Pathology & Laboratory Medicine, University of Cincinnati, Cincinnati, OH 45267-0529, USA

[3] Institut Pasteur, Unité de Chimie et Biocatalyse, 25-28 rue du docteur Roux 75015, Paris, France

[4] CNRS UMR3523, F-75015, Paris, France

[5] Centre d'Etudes et de Recherche sur le Médicament de Normandie, EA4258, UFR des Sciences Pharmaceutiques, University of Caen Basse-Normandie, Caen, France

[6] Institut Pasteur, Unité Biologie et Pathogénicité Fongiques, Département Mycologie, 25-28 rue du docteur Roux 75015, Paris, France

[7] INRA USC2019, F-75015 Paris, France

[8] Institut Pasteur, Unité de Génétique des Interactions Macromoléculaires, Département Génomes et Génétique, 25-28 rue du docteur Roux 75015, Paris, France

[9] CNRS UMR3525, F-75015 Paris, France

[@] Current address: Sandoz, Unterach, Austria

[#] Corresponding authors: jean-paul.latge@pasteur.fr (JPL), helene.munier-lehmann@pasteur.fr (HML), cosmin.saveanu@pasteur.fr (CS)

Running title: Endoplasmic reticulum-related antifungal toxicity

Abstract

In a search for new antifungal compounds, we screened a library of 4454 chemicals for toxicity against the human fungal pathogen *Aspergillus fumigatus*. We identified sr7575, a molecule that inhibits growth of the evolutionary distant fungi *A. fumigatus, Cryptococcus neoformans, Candida albicans,* and *Saccharomyces cerevisiae* but lacks acute toxicity for mammalian cells. To gain insight into the mode of inhibition, sr7575 was screened against 4885 *S. cerevisiae* mutants from the systematic collection of haploid deletion strains and 977 barcoded haploid DAmP strains in which the function of essential genes was perturbed by the introduction of a drug resistance cassette downstream of the coding sequence region. Comparisons with previously published chemogenomic screens revealed that the set of mutants conferring sensitivity to sr7575 was strikingly narrow, affecting components of the endoplasmic-associated protein degradation (ERAD) stress response and the ER membrane protein complex (EMC). ERAD-deficient mutants were hypersensitive to sr7575 in both *S. cerevisiae* and *A. fumigatus*, indicating a conserved mechanism of growth inhibition between yeast and filamentous fungi. Although the unfolded protein response (UPR) is linked to ERAD regulation, sr7575 did not trigger the UPR in *A. fumigatus* and UPR mutants showed no enhanced sensitivity to the compound. The data from this chemogenomic analysis demonstrate that sr7575 exerts its antifungal activity by disrupting ER protein quality control in a manner that requires ERAD intervention but bypasses the need for the canonical UPR. ER protein quality control is thus a specific vulnerability of fungal organisms that might be exploited for antifungal drug development.

Introduction

The burden of fungal infections in the human population is very high, with an estimated 1.5 million annual deaths worldwide, despite antifungal prophylaxis (1–3). The evolutionary proximity between mammalian and fungal cells creates a challenge for the identification of selective drug targets. Consequently, there are only a few mechanistically distinct classes of antifungal agents. The major antifungal drugs in clinical use disrupt membrane homeostasis by targeting ergosterol (4), impair cell wall integrity by inhibiting β-(1,3)-glucan synthase (5), or perturb nucleic acid synthesis via a fluorinated nucleotide analogue (6). The limited number of therapeutic options impedes effective management of invasive fungal infections, particularly when resistance to a drug is either emerging or an intrinsic characteristic of the fungal pathogen.

The identification of novel drugs and their targets can follow several strategies, ranging from the inhibition of a known protein target with a panel of inhibitors to the analysis of mutant strain sensitivity to toxic compounds (7). Chemical genomic screens analyze large collections of genetically defined mutant strains for their sensitivity to chemical libraries in a systematic manner. Data from these screens can provide insight into candidate targets for a given drug, as well as the cellular pathways required to buffer drug toxicity (8–11). The interpretation of chemogenomic screens depends on the type of mutant collection utilized for the analysis. For example, the absence of a general dosage compensation mechanism in yeast (12) allows heterozygous deletion strains to be used as tools to determine how a reduction in the level of a gene product impacts drug sensitivity. However, since heterozygous deletion strains retain some level of gene function, compensatory mechanisms could mask changes in

drug sensitivity. Haploid deletion strains can circumvent this problem and increase the sensitivity of the screen. The resulting chemogenomic profile, or pattern of mutants that are affected by a given compound, is predictive of the mechanism of action and has been successfully applied to drug lead identification and target classification in yeast (13). Further insight into pathways that are modulated by a compound can be obtained by developing *in silico* comparison tools that link the results of a chemogenomic analysis to the data of other published large-scale chemogenomic or genetic interaction screens (14, 15, for examples).

Most of the large chemogenomic data sets currently available have investigated non-essential gene deletions in haploid strains (10, 16). Essential genes, representing about one sixth of all *S. cerevisiae* genes, are more difficult to study in haploid or heterozygous deletion strains, so an alternative approach is the use of Decreased Abundance by mRNA Perturbation (DAmP) strains. DAmP strains contain a drug resistance marker inserted into the 3' untranslated region (UTR) of a gene, resulting in defects in mRNA stability that can create hypomorphic alleles for phenotypic analysis of essential gene function (17). These strains have provided important insights into gene function, as well as the response of cells to stress (18, for example).

In this study, we report the identification of sr7575, a small molecule with fungistatic activity against *S. cerevisiae* and three genera of human fungal pathogens: *A. fumigatus*, *C. neoformans*, and *C. albicans*. We employed a genome-wide approach to characterize the mode of action of sr7575, using a systematic determination of *S. cerevisiae* deletion and DAmP mutant sensitivity to the drug, combined with extensive *in silico* comparisons with large-scale datasets from published chemogenomic and genetic interaction screens. The strategy led to the conclusion that *S. cerevisiae* and *A. fumigatus* mutants that are deficient in ER-associated

degradation (ERAD), a degradative pathway that disposes of misfolded proteins that arise in the ER membrane or lumen (19) are hypersensitive to sr7575. Collectively, these data implicate ER protein quality control as the target of sr7575 toxicity in evolutionarily distant fungi, and suggest that further analysis of compounds that disrupt ER homeostasis may provide novel avenues for antifungal drug development.

Materials and Methods

Screening procedure of the CERMN chemical library.

All robotic steps were performed on a Tecan Freedom EVO platform. Compounds were transferred from mother plates into clear, flat bottom, barcoded tissue culture 96-well plates (Greiner Bio One): 1 µL of a DMSO solution containing 3.3 mg/mL of each compound was spiked into dry wells of daughter plates (80 compounds per plate). For each plate, columns 1 and 12 served as controls: 8 positive controls spiked with DMSO alone provided the reference as 100% growth and 8 negative controls contained the antifungal drug amphotericin B at 15 µg/mL to kill all cells. 130 µL of a mixture containing 10 volumes of conidial suspension 10^5 conidia/mL (in RPMI with 0.1% Tween 20) and 3 volumes of resazurin 0.01% was added to each well. After 48 hours of incubation at 37°C, the absorbance at 570 nm (measurement wavelength) and 604 nm (reference wavelength) were measured on a Safire2 (Tecan) microplate reader. The data were normalized using the following formula: % viability = 100 x (sample value - average value of negative controls) / (average of positive controls - average of negative controls).

For analysis of toxicity to human cells, compounds were added to HeLa cells at a concentration of 10 µM (2.8 µg/mL for sr7575) and the release of cytoplasmic lactate

dehydrogenase was measured using the ELISA-based Cytotoxicity Detection Kit (Roche), according to the manufacturer's recommendations. Mutagenic activity was tested in the bacterial reverse mutation test, either in the presence or absence of a rat metabolizing system (performed by CiToxLAB Safety and Health Research Laboratories). To determine acute mouse toxicity, groups of four NMRI mice were given a single dose of sr7575 (100 mg/kg) by i.p. injection, and mortality was monitored for 3 days.

Yeast strains, growth, and media.

All strains used in this study are described in Table S4. The pooled haploid deletion library (MATa) contained deletions in 4885 non-essential genes along with DAmP modifications of 977 essential genes (20, 21). Wild type (WT) *S. cerevisiae* strain BY4741 was routinely maintained on YPD agar (1% yeast extract, 2% peptone, 2% dextrose, 2% bacto agar; YPDA).

For *S. cerevisiae* serial dilution spot assays, fresh colonies from plates were used to inoculate overnight cultures in YPD. The next morning, cultures were washed once, diluted to OD_{600} 1 in PBS and serial ten-fold dilutions were carried out in a 96-well plate. 10 µL of each dilution was spotted onto SC medium (containing 6.7 g/L yeast nitrogen base with ammonium sulfate, BD Difco, with all amino acids, 2% dextrose and 2% bacto agar) lacking or supplemented with 0.25 µg/mL sr7575. Plates were incubated at 30°C and growth was monitored every 24 h over three days. Spot assays on SC supplemented with the analog sr7576 were conducted in a similar fashion.

The same serial dilution spot assay used to assess sensitivity in *S. cerevisiae* was used for *C. albicans* and *C. neoformans*, with the exception that the plates were supplemented with

sr7575 between 1-8 μg/mL and were incubated at 37°C.

Verification of *S. cerevisiae* mutant strains.

The following mutants were extracted from the gene deletion library maintained in the 96-well format(8): *YBR283C* (*SSH1*), *YCL045C* (*EMC1*), *YDL020C* (*RPN4*), *YDL226C* (*GCS1*), *YER019C-A* (*SBH2*), *YER090W* (*TRP2*), *YKL126W* (*YPK1*), *YKL207W* (*EMC3*), *YML105C* (*SEC65*; DAmP strain), *YMR022W* (*UBC7*), *YMR264W* (*CUE1*), *YOL013C* (*HRD1*), *YOR008C* (*SLG1*), *YOR153W* (*PDR5*), *YPR060C* (*ARO7*), *YHR079C* (*IRE1*), *YFL031W* (*HAC1*), *YBR201W* (*DER1*), *YLR207W* (*HRD3*), *YIL030C* (*SSM4*/*DOA10*), *YDL190C* (*UFD2*), *YGL013C* (*PDR1*), *YNL181W* (DAmP strain), and *YML125C* (*PGA3*; DAmP strain). Genomic DNA was extracted using phenol-chloroform followed by ethanol precipitation. Mutants were verified by PCR amplification using a common forward primer annealing to the KanMX cassette (KaniF) and gene specific reverse primers (oligonucleotides listed in Table S5).

Complementation tests in *S. cerevisiae*.

Complementation tests were performed with plasmids from the Molecular Barcoded Yeast ORF collection (MoBY-ORF) (22). *URA3* plasmids carrying ORFs corresponding to genes *ARO7*, *CUE1*, *EMC1*, *EMC3*, *HRD1*, *RPN4*, *SSH1*, and *UBC7* (Table S4) were recovered from *E.coli* grown in LB medium (1% tryptone, 0.5% yeast extract, 1% NaCl, 1.5% bacto agar) supplemented with chloramphenicol (60 μg/ml) and kanamycin (50 μg/ml) (22). 500 ng of each plasmid was transformed into the appropriate yeast deletion parent following the lithium acetate protocol (23) and *URA3*-expressing transformants were selected on SC medium lacking uracil. The resulting transformants were purified by passaging onto fresh SC

(-URA) medium and four clones of each transformant-set were screened by colony PCR using a gene-specific primer pair (Table S5), generating product sizes ranging between 500-1000 bp. The deletion parent was always included as a negative control. Complemented strains were screened in parallel with the parental deletion strains in spot assays.

Overexpression tests in *S. cerevisiae*.

2 micron-based *LEU2* plasmids from the systematic overexpression library (24) corresponding to regions of the yeast genome that contain the ORFs *PDR1*, *PDR5*, *PDR12,* and a control lacking intact genes (Table S4) were recovered from *E. coli* DH10B cultures grown in LB medium supplemented with kanamycin (50 µg/mL), transformed into wild type BY4741, and transformants selected on SC (-LEU) plates. Transformants were purified by passaging onto fresh SC (-LEU) plates. Overexpressing strains were screened by serial dilution spot assays on SC medium supplemented with increasing concentrations of sr7575.

Chemogenomic profiling.

Concentrations of sr7575 that inhibit WT growth by 10-20% in liquid culture were determined using the haploid strain BY4741 (MATa; *his3*Δ1; *leu2*Δ0; *met15*Δ0; *ura3*Δ0). Single colonies from fresh YPDA plates were inoculated into 10 ml YPD and incubated at 30°C for 14 h. Cultures were diluted to OD_{600} of 0.01 and grown to an OD_{600} of 0.05 prior to the addition of increasing concentrations of sr7575 (0.0625 µg/mL to 0.5 µg/mL). DMSO was used as a vehicle control but there was no observable difference in growth rate between the no-vehicle and DMSO-treated cultures. Growth was monitored by measuring the OD_{600} every hour, starting from 0 h until 10 h (Fig. S2A).

Pooled 400 mL cultures of the haploid deletion library were grown for 12 generations in

the presence of sr7575 at 0.125 μg/mL or DMSO vehicle-control. Amplified TAG products from the pooled cultures were hybridized to Agilent barcode-specific microarrays (platform GPL18088, GEO) as previously described (14). Images obtained with a GenePix 4200AL scanner were annotated by using GenePix Pro 7 (Molecular Devices, CA, USA). Gpr files were normalized separately for the UP and DOWN barcodes and aggregated for each mutant. Raw and normalized data were deposited in the GEO database under identifier GSE60934. Only results for which data were obtained in two independent biological replicates were further considered for analysis. A total of 4909 mutants, including both deletion and DAmP-modified strains, showed consistent growth measurements (Table S6), with a Pearson correlation coefficient between the two series of log-transformed values of 0.78.

Gene set enrichment analysis and correlations.

Over-representation of GO terms in the chemogenomic screen results was analyzed using the web interface at http://go.princeton.edu/cgi-bin/GOTermFinder to the GO Term finder program (25). This program identifies enriched GO terms by calculating the frequency with which one expects to encounter a number of genes having the same annotation in a subset of genes (hypergeometric distribution). Correlations with published large-scale datasets were computed using the R project (https://cran.r-project.org/) function 'cor.test', using either "*pearson*" or "*spearman*" as comparison methods. Treatments or gene deletion perturbations were ranked in decreasing order of calculated correlation coefficients.

***A. fumigatus* strains, growth, and media.**

WT *A. fumigatus* strain kuA and deletion mutants *derA*Δ, *hacA*Δ, *hrdA*Δ, and *hrdA*Δ/*derA*Δ were maintained on malt slants (2% malt extract, 2% bacto agar) while strains

*ireA*Δ and *hacA*Δ/*derA*Δ were maintained on *Aspergillus* minimal medium (MM) with 5 mM ammonium tartrate as the nitrogen source and osmotically stabilized with 1.2 M sorbitol (26). G418 was obtained from Invitrogen and Sigma Aldrich was the source for ampicillin, kanamycin, and chloramphenicol.

Conidia from *ireA*Δ and *hacA*Δ/*hrdA*Δ strains were recovered from *Aspergillus* MM + 1.2 M sorbitol slants, while that of the parental kuA strain and the remaining deletion strains were recovered from 10-day old malt slants in 0.05% Tween. Conidia were diluted to 10^7 conidia/mL and serial 10-fold dilutions were carried out in a 96-well plate prior to spotting 10 µL of each dilution onto MOPS-buffered RPMI-1640 pH 7.0 plates in the presence or absence of 5 µg/mL sr7575. The analog sr7576 precipitated out of solution in RPMI-1640 media and was therefore not included in the analysis. Plates were incubated at 37°C and growth was monitored over four days.

MIC determination.

Determination of the minimal inhibitory concentration (MIC) for yeast strains was carried out by the CLSI M27-A3 broth microdilution method (27). Growth inhibition of *Aspergillus* strains was monitored using a colorimetric test described earlier (28). The MIC of *A. fumigatus* strain that constitutively expresses DsRed fluorescent protein (29) was determined following growth for 24 h at 37°C by measuring fluorescence using a Biotek Synergy fluorescent microplate reader with an excitation wavelength of 254 nm and emission filter set at 291 nm. The relative fluorescence units were plotted against the compound concentrations to determine MIC.

Measurement of fungistatic or fungicidal activity.

For yeast, freshly growingYPD cultures were diluted to OD_{600} 0.001. sr7575 was added at 0.625 µg/mL, amphotericin B at 0.5 µg/mL, and DMSO was used as a vehicle control. 100 µL aliquots were recovered for plating on YPDA. Cultures were grown for 16 h, cells were washed once in 1X PBS and 100 µL of serially diluted samples were plated. Colonies were counted following 48 h and normalized to the OD_{600}.

For *A. fumigatus*, 50 mL RPMI cultures with a starting cell number of $1x10^5$ conidia/ml were setup in the presence or absence of 5 µg/mL sr7575 (in duplicate). 100 µL aliquots were recovered for enumeration of colony forming units. Following 16 h of growth, mycelia from one pair of flasks were filtered and mycelial dry weight estimated. From the second pair, 100 µL from the drug-treated flask was serially diluted and plated to assess viability.

qRT-PCR.

A. fumigatus conidia were inoculated into YG medium (0.5% yeast extract, 2% glucose) and incubated overnight at 37°C, 200 rpm. The mycelium was treated with the indicated concentrations of sr7575 or dithiothreitol (DTT), along with appropriate vehicle controls, for 1 h. The mycelia were harvested by filtration and lysed by crushing in liquid nitrogen. RNA was isolated using the TRIzol reagent, treated with DNase to remove traces of DNA, and reverse-transcribed using M-MuLV reverse transcriptase (NEB) together with an oligo-d(T) primer. Quantitation of *bipA* and *tigA* mRNA expression was performed by qRT-PCR, as previously described (30).

Results

Identification of a new inhibitor of fungal growth

In a search for new antifungals, we tested the toxicity of 4454 chemicals from the CERMN compound library against *A. fumigatus* using the strategy outlined in Fig. 1A. The CERMN library is part of the French national collection of chemicals (31) and was built since 1998 to be used in the framework of partnerships with public research laboratories. The dynamic range and degree of separation between positive and negative controls in the screen was evaluated by computing the Z' score (32). The average Z' value was 0.92 ± 0.03, indicating a robust and reliable assay. Data analysis identified 76 hits showing greater than 90% fungal growth inhibition, which were clustered into 7 chemical families and 29 singletons (Table S1). Compounds with known effects on human physiology (33), or which showed cytotoxicity for HeLa cells in a lactate dehydrogenase release assay, were eliminated from further consideration. The compound sr1810 was active against *A. fumigatus* and was selected for further analysis. Since sr1810 consisted of a mixture of two isomers, 75% of sr7575 (1) (Fig. 1A) and 25% of sr7576 (2), we synthesized each isomer (Fig S1, A and B) and found that it was only sr7575 that was responsible for the antifungal activity. The sr7575 compound showed no mutagenic activity in the bacterial reverse mutation test, and no acute toxicity was observed in mice at a dose of 100 mg/kg.

To gain insight into the structural basis for sr7575 antifungal activity, we prepared thirty analogues using aniline derivatives with different substitutions in the first reaction (compounds 3-32, Tables S2 and S3, synthesis detailed in Text S1). Growth inhibition tests with these compounds showed that at least two features of sr7575 were required for its antifungal potency: the chlorine at position 4 of the phenyl group and the positioning of the

nitro group in relation to the pyrrole moiety (Table S2).

In addition to its effects on *A. fumigatus*, sr7575 was active against *A. flavus* (Fig. 1B), *C. neoformans, C. albicans* (Fig. 1C), and *S. cerevisiae* (Fig. 1D) on plates and in liquid medium at inhibitory concentrations ranging from 0.6 to 10 μg/mL (Fig. S2A, B, C, D). More than 90% of either *S. cerevisiae* or *A. fumigatus* cells were able to resume growth after a 16 h incubation in the presence of sr7575 (0.625 μg/mL and 5 μg/mL, respectively) indicating that the compound exerts a fungistatic effect.

ERAD-deficient mutants of *S. cerevisiae* are hypersensitive to sr7575

To gain insight into the mechanism by which sr7575 perturbs fungal physiology, the effect of sr7575 was tested on the growth rate of each of 4885 haploid yeast deletion strains in the systemic deletion collection (20). In addition, sr7575 activity was measured on 977 locus tagged barcoded DAmP (17) mutants of essential genes that were previously generated in our laboratory (21). This collection of gene knockout and DAmP strains contains molecular barcodes to facilitate detection and quantitation of DNA by custom Agilent microarrays (34, 35). Following the strategy outlined in Fig. 1A, the normalized ratio of the hybridization signal in the presence or absence of treatment was used as an estimate of relative growth rate in pools of mutants. Only a fraction of mutant strains showed hypersensitivity to sr7575, as indicated by the left tail of the distribution for sensitivity values (Fig. 2A). The strain that showed the most dramatic increase in sr7575 sensitivity harbors a deletion of the PDR1 gene, encoding the main regulator of multidrug resistance in yeast (36). Pdr1 is a transcriptional activator for xenobiotic efflux transporter genes, thereby governing resistance to numerous toxic compounds. It is likely that the effect of *PDR1* deletion on sensitivity to sr7575 is

mediated through the plasma membrane ATP-binding cassette (ABC) transporter Pdr5, since *PDR5* is a known target of Pdr1 (37) and the pdr5 mutant was ranked 6th among deletion strains that were most affected by sr7575.

To identify cellular pathways or protein complexes that allow cells to counteract sr7575 effects, we used a gene set enrichment analysis on 89 mutant strains that showed an average increase in generation time of at least 10% relative to WT in the presence of sr7575. The most over-represented pathway in the dataset was ER-associated protein degradation (ERAD), specifically the GO term "ER-associated ubiquitin-dependent protein catabolic process" (GO:0030433), with a p-value corrected for multiple hypotheses testing of 1.5 X 10^{-6}. This set included *CUE1*, *UBC7*, *HRD1*, *HRD3*, *UFD2*, *UBX4*, *SSM4* (*DOA10*), *DSK2*, and *UBX2*, encompassing one fifth of the total number of genes annotated to this term (Fig. 2B). The second most over-represented GO term was "aromatic amino acid family biosynthetic process" (GO:0009073). However, strains deficient in this pathway are known to exhibit a multidrug response signature (9), so the study of the corresponding strains was not pursued further.

Cellular component enrichment analysis was used to determine whether any of the 89 proteins selected in the screen were linked to the same protein complex or intracellular location. The ER membrane protein complex (EMC) was the most over-represented group by this analysis, with a p-value of 2 X 10^{-7}. In addition to gene deletions directly affecting *EMC1*, *EMC3*, *EMC4* and *EMC5*, deletions affecting dubious ORFs which overlap with *EMC2* (*YJR087W*) and *EMC1* (*YCL046W*) that are distinct mutants of these genes, were also present in this dataset. Members of the EMC complex are required for efficient protein folding in the ER (38), potentially through roles in phospholipid metabolism at the ER membrane (39).

Other components of the ER membrane showed enrichment, including 10 of 58 genes annotated as "intrinsic components of the ER membrane" (GO:0031227) and two DAmP-modified essential genes of uncharacterized function (*YNL181W* and *PGA3*). In addition, several genes encoding components of the signal recognition particle (SRP) involved in co-translational targeting of proteins into the ER showed enrichment: *sec65*-DAmP, *srp21*-DAmP, *shr3*-DAmP, *ssh1*Δ, and *sbh2*Δ. Taken together, these findings indicate that sensitivity to the inhibitory effects of sr7575 is exacerbated by defects in the ERAD stress response, as well as by alterations in ER membrane composition that affect optimal ER protein translocation and folding.

The sr7575 sensitivity profile suggests a UPR-independent stress response

The effects of sr7575 on haploid yeast deletion strains were compared to profiles obtained from 1,824 different chemicals in a recently published large-scale chemogenomic screen (16). The compound CMB4166 had the highest Spearman correlation coefficient in this comparison (Fig. 2C, r= 0.44) and showed a remarkably similar profile to that of sr7575 (Fig. 2D). Most of the strains showing sensitivity to sr7575 were also sensitive to CMB4166 (Fig. 2E), suggesting that the two compounds trigger similar cellular responses. However, CMB4166 is a macrolide (D. Hoepfner, personal communication) and shares no structural homology to sr7575.

To acquire insights into the specificity of the response to sr7575, we compared its sensitivity profile to published results on 3,356 other chemical compounds (10). The pattern of sr7575 sensitive mutants revealed little-to-no similarity to profiles obtained from the other compounds in this comparison. For example, the maximum computed Pearson correlation

coefficient was 0.27 for the compound k048-0007 (screen SGTC_352, Fig. S3A). However, this correlation was due to strains with deletions in *PDR1*, *RPN4*, or *GCS1*, which confer sensitivity to multiple stresses (Fig. S3C). To avoid the typically large effect of outliers on the Pearson correlation, we also tested correlation via the Spearman non-parametric test that uses ranks rather than values. The maximum correlation by this approach was also low (0.18), identifying the compound 4245-1575 used in screen SGTC_513 (Fig. S3B). Most of the correlation in this case could be attributed to the hypersensitivity of the *ubc7*Δ and *cue1*Δ ERAD mutants (Fig. S3D). Since this second compound was annotated as having an unfolded protein response (UPR) signature (10), we also tested the correlation between the profile of sr7575 and tunicamycin, a well-known and widely used inducer of the UPR (40, 41, for review). However, no similarity was found (Fig. S3E). Collectively, these comparisons suggest that while many sensitivity profiles are related and indicate the most frequent types of cellular responses to chemical toxicity (10), the profile obtained for sr7575 was specific, with similarity to only one compound out of over 5000 chemicals analyzed.

Large-scale chemical toxicity screens are complementary to synthetic genetic array analyses (SGA), in which double deletion mutant strains are used to determine functional interactions between genes. We compared the sensitivity profile of sr7575 with the results from 1711 SGA screens (42). The closest hit was the profile shown by a strain harboring a DAmP modification of the essential gene *PGA3* (17) (Fig. S4A). The correlation between the sr7575 and *PGA3* profiles was robust, since it also ranked 5th when estimated using Spearman correlation (Fig. S4B). Despite the low value of the correlation coefficient (0.23), several strains containing gene deletions were affected by both sr7575 treatment and replacement of *PGA3* with the *pga3*-DAmP allele, including the ERAD-associated genes *cue1*Δ, *ubc7*Δ,

353 *ufd2*Δ, *ssm4*Δ, and EMC complex components (Fig. S4C). A role in newly synthesized protein
354 trafficking has been proposed for Pga3 (43), raising the possibility that its presence in our
355 dataset is due to a function that impacts ER homeostasis.

356 The gene deletion that ranked second in terms of correlation with the sr7575 profile
357 involved *CHO2*, encoding a phosphatidyl N–methyltransferase required for phosphatidyl–
358 choline synthesis. The absence of *CHO2* renders yeast cells dependent on the UPR for survival
359 (42, 44), suggesting that *CHO2* contributes to ER homeostasis. Consistent with this, *CHO2*
360 deletion shows an aggravating interaction with the loss of EMC genes in terms of yeast growth
361 (39).

362 A summary of the correlations between sr7575 sensitivity profiles and those derived
363 from published chemogenomic screens is shown in Fig. 3. Since the numerical values reported
364 for genetic and chemogenomic screens are not readily comparable, the ranking of the different
365 mutants in each screen was used to generate a meaningful graphical display. The resulting
366 heatmap (Fig. 3A) highlights the unique ERAD signature of sr7575 relative to currently
367 published screens. A schematic illustrating the ER membrane proteins involved in the ERAD
368 pathway is shown for perspective (Fig. 3B). Since ERAD is known to work in concert with the
369 UPR to relieve ER stress, it is interesting to note that hypersensitivity to sr7575 was observed
370 for ERAD mutants, but not for the UPR-inactivated strains *ire1*Δ and *hac1*Δ. Taken together,
371 these data are consistent with a model in which sr7575 toxicity is counteracted by a functional
372 ERAD machinery, independent of signaling through the UPR pathway.

373 **Specific ERAD deficiencies enhance sr7575 toxicity in *S. cerevisiae***

374 Seventeen *S. cerevisiae* mutant strains were selected to validate the results of the

chemogenomic screen, encompassing strains with deletions in components of the ERAD and proteasome pathways, the EMC, the Ssh1 co-translocase, the PDR network, aromatic acid biosynthesis, and DAmP modifications of *YNL181W* and *PGA3*. Each strain was analyzed individually for sr7575 susceptibility, using a subinhibitory concentration for WT (Fig. 4A and Fig. S5). A strain deleted for aromatic amino acid biosynthesis (*aro7*Δ) showed increased sr7575 sensitivity (Fig. 4A), consistent with the pleiotropic effects of this mutation on stress response.

As predicted by the chemogenomic screen, mutants in the *PDR5* multidrug transporter and its transcriptional activator *PDR1* were hypersensitive to sr7575 (Fig. S5). Conversely, overexpression of *PDR1* and *PDR5*, but not *PDR12* rendered *S. cerevisiae* cells tolerant to high concentrations of sr7575 (Fig. S6A). This phenotype was conserved across fungal species, since clinical isolates and laboratory *C. albicans* strains that overexpress *CDR1*, the ortholog of *S. cerevisiae PDR5*, were also tolerant to sr7575 (Fig. S6B).

Deletions of genes coding for EMC members, *EMC1* and *EMC3*, and the co-translational translocase *SSH1* conferred increased sensitivity to sr7575, as suggested by the chemogenomic screen. However, a mutant in *SBH2*, which functions in the Ssh1 translocase complex (45), did not show increased sensitivity at least at this concentration (Fig. S5). Hypersensitivity to sr7575 was confirmed for components of the ERAD complex, including the Hrd1 E3 ubiquitin ligase, the E2 ubiquitin conjugating enzyme Ubc7, and the ER membrane-resident recruiter Cue1 (46–48) (Fig. 4A). Although the ERAD component Der1 (49) was not identified in our chemogenomic screen, a mild increase in sr7575 sensitivity was observed for this mutant (Fig. S5), consistent with ERAD involvement in sr7575 effects. sr7575 hypersensitivity was also validated for a strain lacking *RPN4*, encoding a

transcriptional activator of proteasome genes (Fig. 4A). Since proteasomal degradation is the final step in the disposal of misfolded proteins by ERAD, this finding is consistent with the notion that sr7575 affects protein quality control in the ER. In conclusion, these findings demonstrate that components of the ERAD pathway are necessary to protect yeast cells from the toxic effects of sr7575 in *S. cerevisiae*, suggesting a mechanism of action that involves perturbation of ER protein quality control.

ERAD protects against sr7575 toxicity in *A. fumigatus*, but is UPR-independent

The UPR is a stress response pathway that communicates information on ER homeostasis to the nucleus (40, 41). The pathway is triggered by misfolded proteins, which accumulate in the ER when the demand for secretion exceeds ER folding capacity, or when the cell encounters adverse environmental conditions. Unfolded proteins are sensed by the ER-transmembrane sensor Ire1, which triggers the synthesis of Hac1, a transcription factor. Hac1 translocates to the nucleus and upregulates the expression of chaperones, folding enzymes, and other proteins that support ER function (44, 50). Since ERAD mutants are hypersensitive to sr7575, and ERAD capacity can be regulated by the UPR, we were surprised to find that neither *HAC1* nor *IRE1* were identified in the sr7575 chemogenomic screen. The UPR independence of this response was confirmed by susceptibility testing: yeast *ire1*Δ and *hac1*Δ mutants were not affected by sr7575 at concentrations of up to 0.5 μg/mL (Fig. 4C). These findings suggest that ERAD protects against sr7575 toxicity through a mechanism that is independent of the UPR in *S. cerevisiae*.

Consistent with the results obtained in *S. cerevisiae*, UPR mutants of *A. fumigatus* that lack either the ER sensor IreA or the transcription factor HacA showed no hypersensitivity to

sr7575 (Fig. 5A). As in yeast, the *hrdA*Δ mutant, which lacks the ortholog of *S. cerevisiae* *HRD1*, showed increased sensitivity to sr7575. A *derA*Δ mutant that is deficient in the DerA component of the HrdA ERAD complex showed no increase in sr7575 sensitivity. However, a double deletion mutant lacking both DerA and HrdA showed greater sensitivity to sr7575 than a mutant lacking HrdA alone, underscoring the importance of the Hrd1 complex in the response to sr7575 toxicity. We conclude that sr7575 action involves the inhibition of an evolutionarily conserved target, necessitating the intervention of the ERAD complex Hrd1/HrdA in both *S. cerevisiae* and *A. fumigatus*.

The ERAD-enriched signature for sr7575 suggested that some aspect of ER protein quality control is adversely affected by this compound. However, since UPR deficient strains of *S. cerevisiae* or *A. fumigatus* showed no increase in sr7575 sensitivity, the results suggest that a UPR-independent mechanism of ERAD activity is involved in the sr7575 response. To confirm UPR independence, qRT-PCR was used to measure mRNA levels for two well-known UPR target genes: the ER chaperone *bipA* and the protein disulfide isomerase *tigA*. As expected, the expression of both genes was strongly induced by treatment with a sub-inhibitory concentration of dithiothreitol (DTT, 1 mM), a well-known inducer of the UPR (Fig. 5B). By contrast, no increase in expression was observed following treatment with a sub-inhibitory concentration of sr7575 (0.1 μg/mL). In addition, pretreatment with sr7575 for 1 h prior to DTT exposure failed to block UPR activation. These results indicate that while exposure to sr7575 does not trigger the UPR, it was also unable to prevent UPR activation by DTT. We conclude that sr7575 is unlikely to target UPR signaling for its toxic effects in *A. fumigatus* or *S. cerevisiae*, consistent with the UPR-independent response suggested by the chemogenomic screen.

Discussion

In this study, we describe the identification of a novel antifungal compound, sr7575 that was active against species from four fungal genera. Chemogenomic profiling in *S. cerevisiae* demonstrated that the set of genes required for protection against sr7575 was markedly narrow, involving components of the ERAD stress response and other components of the ER membrane. The function of the ERAD pathway is to maintain protein quality control in the ER by eliminating toxic unfolded proteins that may accumulate in the fungus during periods of high secretory activity, or when the organism encounters adverse environmental conditions. This disposal mechanism centers on a multi-protein complex in the ER membrane that selectively identifies misfolded proteins in the ER lumen or membrane and transports them back into the cytoplasm for degradation by the proteasome. The results from our chemogenomic screen demonstrate that mutants of this complex, either in *S. cerevisiae* or *A. fumigatus*, are hypersensitive to sr7575 inhibition, suggesting that the antifungal effects of this compound involves a disruption of ER protein quality control.

ER protein quality control is also affected by the UPR, a signaling pathway that counters the accumulation of unfolded proteins in the ER by increasing the expression of chaperones and other proteins involved in protein folding when the demand for secretion exceeds the folding capacity of the organelle. A tight coordination between the UPR and ERAD pathways was demonstrated in yeast where UPR mutants have decreased ERAD activity whereas ERAD mutants exhibit constitutive UPR upregulation (50). In addition, although ERAD is sufficient to eliminate misfolded proteins that continually arise during normal growth, it requires the UPR for optimal degradative capacity under conditions of severe ER stress (51). Basal ERAD activity is thus sufficient to handle low levels of unfolded proteins and is UPR-independent.

However, upregulation of ERAD activity by the UPR is needed when the level of unfolded proteins reaches a critical threshold of toxicity. The connection between these pathways is also evident in *A. fumigatus*, where mutants deficient in both the UPR and ERAD are less fit than those lacking the UPR or ERAD alone (52).

In view of the link between the UPR and ERAD pathways, we were surprised to find that neither *ire1*Δ nor *hac1*Δ were among the strains most affected by sr7575 in our chemogenomic screen, and that these strains showed no increase in sr7575 sensitivity when tested individually. In addition, our experiments revealed that sr7575 did not trigger the UPR, nor did it prevent the UPR from being activated by DTT, a strong inducer of unfolded proteins. These observations suggest that sr7575 does not cause the widespread protein unfolding that is typical of strong ER stress aggravators such as DTT and tunicamycin. Specific ER stress can be induced, for example, by expressing topologically abnormal ERAD-targeted integral membrane proteins without inducing the canonical UPR pathway in yeast (53).

The ability of sr7575 to inhibit the growth of fungi but not human cells raises the possibility that it targets a fungal-specific process. Our chemogenomic screen identified *ynl181w*-DAmP as one of the top 10 strains most affected by sr7575 toxicity. *YNL181W* encodes an essential ER-membrane protein, the function of which is currently unknown, but is speculated to involve an oxido-reductase activity (54, 55). The Ynl181w protein is conserved among fungi (Fig. 6A) and has no metazoan orthologue, as defined in the OrthoMCL database (56). Since the protein is essential, a heterozygous *YNL181W*/*ynl181w*Δ deletion strain was previously used to study its function in chemogenomic investigations (10, 16). We were especially interested in the effects of chemical CMB4166 in these studies because our data

revealed that the strain sensitivity profile for that compound (16) most closely resembled that of sr7575 (Fig. 2C, D, E). A striking finding from this comparison was that the heterozygous deletion strain of *YNL181W* was among the strains most affected by CMB4166 (Fig. 3A), indicating that the absence of Ynl181w sensitizes yeast to both sr7575 and CMB4166.

A DAmP modification of *YNL181W* has been previously combined with a large-scale genetic screen to identify mutations that synergize with loss of *YNL181W* function (42). A comparison of the sr7575 sensitivity profile with the results of this genetic screen identified several ERAD mutants that were affected by both DAmP modification of *YNL181W* and by treatment with sr7575, including *UBC7*, *CUE1*, and *RPN4* (Fig. 6B). The connection to *UBC7* was particularly remarkable because a similar synergistic growth defect associated with *ynl181w*-DAmP and *ubc7*Δ mutation was observed in two other large-scale studies (17, 57). The correlation between Ynl181w mutation and sr7575 sensitivity obtained by chemogenomics was confirmed on plates by showing that a *ynl181w*-DAmP mutant was hypersensitive to sr7575 (Fig. 6C). We speculate that Ynl181w could be involved in processes that are targeted by sr7575.

In conclusion, we report the identification of a novel compound that has activity against both *S. cerevisiae* and *A. fumigatus*. The data are consistent with a model for s7575 action in which the compound disrupts the structure of one or more proteins in the ER lumen or membrane, resulting in a situation that necessitates ERAD intervention to eliminate the abnormal protein(s) but does not require UPR activation. These findings underscore the importance of ER homeostasis to the growth fungi and suggest the presence of fungal-specific ER processes that could represent new opportunities for antifungal intervention.

Funding information

Funding was provided by AVIESAN *A. fumigatus* grant BAP109, Institut Carnot Pasteur Maladies Infectieuses grant FUNGI, Institut Pasteur, CNRS, and INSERM. The funders had no role in study design, data collection and interpretation, or the decision to submit the work for publication.

Acknowledgments

We thank Pr. Michel Boulouard (Groupe Mémoire et Plasticité Comportementale, GMPc, EA4259) for the *in vivo* toxicity tests on mice, Dominique Sanglard (CHUV Laussane, Switzerland) for the *C. albicans* strains, Françoise Dromer (CNRMA, Institut Pasteur) for the *A. fumigatus* clinical isolates, and Alain Jacquier (Unité de Génétique des Interactions Macromoléculaires, Institut Pasteur) for support and critical reading of the manuscript,.

References

1. **Brown GD**, **Denning DW**, **Levitz SM**. 2012. Tackling human fungal infections. Science **336**:647.
2. **Lai C-C**, **Tan C-K**, **Huang Y-T**, **Shao P-L**, **Hsueh P-R**. 2008. Current challenges in the management of invasive fungal infections. J Infect Chemother Off J Jpn Soc Chemother **14**:77–85.
3. **Park BJ**, **Wannemuehler KA**, **Marston BJ**, **Govender N**, **Pappas PG**, **Chiller TM**. 2009. Estimation of the current global burden of cryptococcal meningitis among persons living with HIV/AIDS. AIDS Lond Engl **23**:525–530.
4. **Odds FC**, **Brown AJP**, **Gow NAR**. 2003. Antifungal agents: mechanisms of action. Trends Microbiol **11**:272–279.
5. **Perlin DS**. 2011. Current perspectives on echinocandin class drugs. Future Microbiol **6**:441–457.
6. **Hope WW**, **Tabernero L**, **Denning DW**, **Anderson MJ**. 2004. Molecular mechanisms of primary resistance to flucytosine in Candida albicans. Antimicrob Agents Chemother **48**:4377–4386.
7. **Schenone M**, **Dančík V**, **Wagner BK**, **Clemons PA**. 2013. Target identification and mechanism of action in chemical biology and drug discovery. Nat Chem Biol **9**:232–240.
8. **Giaever G**, **Nislow C**. 2014. The Yeast Deletion Collection: A Decade of Functional

Genomics. Genetics **197**:451–465.
9. **Hillenmeyer ME**, **Fung E**, **Wildenhain J**, **Pierce SE**, **Hoon S**, **Lee W**, **Proctor M**, **St Onge RP**, **Tyers M**, **Koller D**, **Altman RB**, **Davis RW**, **Nislow C**, **Giaever G**. 2008. The chemical genomic portrait of yeast: uncovering a phenotype for all genes. Science **320**:362–365.
10. **Lee AY**, **St Onge RP**, **Proctor MJ**, **Wallace IM**, **Nile AH**, **Spagnuolo PA**, **Jitkova Y**, **Gronda M**, **Wu Y**, **Kim MK**, **Cheung-Ong K**, **Torres NP**, **Spear ED**, **Han MKL**, **Schlecht U**, **Suresh S**, **Duby G**, **Heisler LE**, **Surendra A**, **Fung E**, **Urbanus ML**, **Gebbia M**, **Lissina E**, **Miranda M**, **Chiang JH**, **Aparicio AM**, **Zeghouf M**, **Davis RW**, **Cherfils J**, **Boutry M**, **Kaiser CA**, **Cummins CL**, **Trimble WS**, **Brown GW**, **Schimmer AD**, **Bankaitis VA**, **Nislow C**, **Bader GD**, **Giaever G**. 2014. Mapping the cellular response to small molecules using chemogenomic fitness signatures. Science **344**:208–211.
11. **Parsons AB**, **Lopez A**, **Givoni IE**, **Williams DE**, **Gray CA**, **Porter J**, **Chua G**, **Sopko R**, **Brost RL**, **Ho C-H**, **Wang J**, **Ketela T**, **Brenner C**, **Brill JA**, **Fernandez GE**, **Lorenz TC**, **Payne GS**, **Ishihara S**, **Ohya Y**, **Andrews B**, **Hughes TR**, **Frey BJ**, **Graham TR**, **Andersen RJ**, **Boone C**. 2006. Exploring the mode-of-action of bioactive compounds by chemical-genetic profiling in yeast. Cell **126**:611–625.
12. **Springer M**, **Weissman JS**, **Kirschner MW**. 2010. A general lack of compensation for gene dosage in yeast. Mol Syst Biol **6**:368.
13. **Hillenmeyer ME**, **Ericson E**, **Davis RW**, **Nislow C**, **Koller D**, **Giaever G**. 2010. Systematic analysis of genome-wide fitness data in yeast reveals novel gene function and drug action. Genome Biol **11**:R30.
14. **Decourty L**, **Saveanu C**, **Zemam K**, **Hantraye F**, **Frachon E**, **Rousselle J-C**, **Fromont-Racine M**, **Jacquier A**. 2008. Linking functionally related genes by sensitive and quantitative characterization of genetic interaction profiles. Proc Natl Acad Sci U S A **105**:5821–5826.
15. **Tong AHY**, **Lesage G**, **Bader GD**, **Ding H**, **Xu H**, **Xin X**, **Young J**, **Berriz GF**, **Brost RL**, **Chang M**, **Chen Y**, **Cheng X**, **Chua G**, **Friesen H**, **Goldberg DS**, **Haynes J**, **Humphries C**, **He G**, **Hussein S**, **Ke L**, **Krogan N**, **Li Z**, **Levinson JN**, **Lu H**, **Ménard P**, **Munyana C**, **Parsons AB**, **Ryan O**, **Tonikian R**, **Roberts T**, **Sdicu A-M**, **Shapiro J**, **Sheikh B**, **Suter B**, **Wong SL**, **Zhang LV**, **Zhu H**, **Burd CG**, **Munro S**, **Sander C**, **Rine J**, **Greenblatt J**, **Peter M**, **Bretscher A**, **Bell G**, **Roth FP**, **Brown GW**, **Andrews B**, **Bussey H**, **Boone C**. 2004. Global mapping of the yeast genetic interaction network. Science **303**:808–813.
16. **Hoepfner D**, **Helliwell SB**, **Sadlish H**, **Schuierer S**, **Filipuzzi I**, **Brachat S**, **Bhullar B**, **Plikat U**, **Abraham Y**, **Altorfer M**, **Aust T**, **Baeriswyl L**, **Cerino R**, **Chang L**, **Estoppey D**, **Eichenberger J**, **Frederiksen M**, **Hartmann N**, **Hohendahl A**, **Knapp B**, **Krastel P**, **Melin N**, **Nigsch F**, **Oakeley EJ**, **Petitjean V**, **Petersen F**, **Riedl R**, **Schmitt EK**, **Staedtler F**, **Studer C**, **Tallarico JA**, **Wetzel S**, **Fishman MC**, **Porter JA**, **Movva NR**. 2014. High-resolution chemical dissection of a model eukaryote reveals targets, pathways and gene functions. Microbiol Res **169**:107–120.
17. **Schuldiner M**, **Collins SR**, **Thompson NJ**, **Denic V**, **Bhamidipati A**, **Punna T**, **Ihmels J**, **Andrews B**, **Boone C**, **Greenblatt JF**, **Weissman JS**, **Krogan NJ**. 2005. Exploration of the function and organization of the yeast early secretory pathway through an epistatic miniarray profile. Cell **123**:507–519.

18. **Berry DB**, **Guan Q**, **Hose J**, **Haroon S**, **Gebbia M**, **Heisler LE**, **Nislow C**, **Giaever G**, **Gasch AP**. 2011. Multiple means to the same end: the genetic basis of acquired stress resistance in yeast. PLoS Genet **7**:e1002353.
19. **Thibault G**, **Ng DTW**. 2012. The endoplasmic reticulum-associated degradation pathways of budding yeast. Cold Spring Harb Perspect Biol **4**.
20. **Giaever G**, **Chu AM**, **Ni L**, **Connelly C**, **Riles L**, **Véronneau S**, **Dow S**, **Lucau-Danila A**, **Anderson K**, **André B**, **Arkin AP**, **Astromoff A**, **El-Bakkoury M**, **Bangham R**, **Benito R**, **Brachat S**, **Campanaro S**, **Curtiss M**, **Davis K**, **Deutschbauer A**, **Entian K-D**, **Flaherty P**, **Foury F**, **Garfinkel DJ**, **Gerstein M**, **Gotte D**, **Güldener U**, **Hegemann JH**, **Hempel S**, **Herman Z**, **Jaramillo DF**, **Kelly DE**, **Kelly SL**, **Kötter P**, **LaBonte D**, **Lamb DC**, **Lan N**, **Liang H**, **Liao H**, **Liu L**, **Luo C**, **Lussier M**, **Mao R**, **Menard P**, **Ooi SL**, **Revuelta JL**, **Roberts CJ**, **Rose M**, **Ross-Macdonald P**, **Scherens B**, **Schimmack G**, **Shafer B**, **Shoemaker DD**, **Sookhai-Mahadeo S**, **Storms RK**, **Strathern JN**, **Valle G**, **Voet M**, **Volckaert G**, **Wang C**, **Ward TR**, **Wilhelmy J**, **Winzeler EA**, **Yang Y**, **Yen G**, **Youngman E**, **Yu K**, **Bussey H**, **Boeke JD**, **Snyder M**, **Philippsen P**, **Davis RW**, **Johnston M**. 2002. Functional profiling of the Saccharomyces cerevisiae genome. Nature **418**:387–391.
21. **Decourty L**, **Doyen A**, **Malabat C**, **Frachon E**, **Rispal D**, **Séraphin B**, **Feuerbach F**, **Jacquier A**, **Saveanu C**. 2014. Long open reading frame transcripts escape nonsense-mediated mRNA decay in yeast. Cell Rep **6**:593–598.
22. **Ho CH**, **Magtanong L**, **Barker SL**, **Gresham D**, **Nishimura S**, **Natarajan P**, **Koh JLY**, **Porter J**, **Gray CA**, **Andersen RJ**, **Giaever G**, **Nislow C**, **Andrews B**, **Botstein D**, **Graham TR**, **Yoshida M**, **Boone C**. 2009. A molecular barcoded yeast ORF library enables mode-of-action analysis of bioactive compounds. Nat Biotechnol **27**:369–377.
23. **Schiestl RH**, **Gietz RD**. 1989. High efficiency transformation of intact yeast cells using single stranded nucleic acids as a carrier. Curr Genet **16**:339–346.
24. **Jones GM**, **Stalker J**, **Humphray S**, **West A**, **Cox T**, **Rogers J**, **Dunham I**, **Prelich G**. 2008. A systematic library for comprehensive overexpression screens in Saccharomyces cerevisiae. Nat Methods **5**:239–241.
25. **Boyle EI**, **Weng S**, **Gollub J**, **Jin H**, **Botstein D**, **Cherry JM**, **Sherlock G**. 2004. GO::TermFinder--open source software for accessing Gene Ontology information and finding significantly enriched Gene Ontology terms associated with a list of genes. Bioinforma Oxf Engl **20**:3710–3715.
26. **Richie DL**, **Hartl L**, **Aimanianda V**, **Winters MS**, **Fuller KK**, **Miley MD**, **White S**, **McCarthy JW**, **Latgé J-P**, **Feldmesser M**, **Rhodes JC**, **Askew DS**. 2009. A role for the unfolded protein response (UPR) in virulence and antifungal susceptibility in Aspergillus fumigatus. PLoS Pathog **5**:e1000258.
27. 2008. Reference method for broth dilution antifungal susceptibility testing of yeasts; Approved Standard-Third Edition. CLSI document M27-A3. Clinical and Laboratory Standards Institute, Wayne, PA.
28. **Clavaud C**, **Beauvais A**, **Barbin L**, **Munier-Lehmann H**, **Latgé J-P**. 2012. The composition of the culture medium influences the β-1,3-glucan metabolism of Aspergillus fumigatus and the antifungal activity of inhibitors of β-1,3-glucan synthesis. Antimicrob Agents Chemother **56**:3428–3431.
29. **Jhingran A**, **Mar KB**, **Kumasaka DK**, **Knoblaugh SE**, **Ngo LY**, **Segal BH**, **Iwakura Y**, **Lowell CA**, **Hamerman JA**, **Lin X**, **Hohl TM**. 2012. Tracing conidial fate and measuring

host cell antifungal activity using a reporter of microbial viability in the lung. Cell Rep **2**:1762–1773.
30. **Feng X**, **Krishnan K**, **Richie DL**, **Aimanianda V**, **Hartl L**, **Grahl N**, **Powers-Fletcher MV**, **Zhang M**, **Fuller KK**, **Nierman WC**, **Lu LJ**, **Latgé J-P**, **Woollett L**, **Newman SL**, **Cramer RA**, **Rhodes JC**, **Askew DS**. 2011. HacA-Independent Functions of the ER Stress Sensor IreA Synergize with the Canonical UPR to Influence Virulence Traits in Aspergillus fumigatus. PLoS Pathog **7**.
31. **Hibert MF**. 2009. French/European academic compound library initiative. Drug Discov Today **14**:723–725.
32. **Zhang J-H**, **Chung TDY**, **Oldenburg KR**. 1999. A Simple Statistical Parameter for Use in Evaluation and Validation of High Throughput Screening Assays. J Biomol Screen **4**:67–73.
33. **Prunier H**, **Rault S**, **Lancelot JC**, **Robba M**, **Renard P**, **Delagrange P**, **Pfeiffer B**, **Caignard DH**, **Misslin R**, **Guardiola-Lemaitre B**, **Hamon M**. 1997. Novel and selective partial agonists of 5-HT3 receptors. 2. Synthesis and biological evaluation of piperazinopyridopyrrolopyrazines, piperazinopyrroloquinoxalines, and piperazinopyridopyrroloquinoxalines. J Med Chem **40**:1808–1819.
34. **Smith AM**, **Heisler LE**, **Mellor J**, **Kaper F**, **Thompson MJ**, **Chee M**, **Roth FP**, **Giaever G**, **Nislow C**. 2009. Quantitative phenotyping via deep barcode sequencing. Genome Res **19**:1836–1842.
35. **Eason RG**, **Pourmand N**, **Tongprasit W**, **Herman ZS**, **Anthony K**, **Jejelowo O**, **Davis RW**, **Stolc V**. 2004. Characterization of synthetic DNA bar codes in Saccharomyces cerevisiae gene-deletion strains. Proc Natl Acad Sci U S A **101**:11046–11051.
36. **Cannon RD**, **Lamping E**, **Holmes AR**, **Niimi K**, **Baret PV**, **Keniya MV**, **Tanabe K**, **Niimi M**, **Goffeau A**, **Monk BC**. 2009. Efflux-mediated antifungal drug resistance. Clin Microbiol Rev **22**:291–321, Table of Contents.
37. **Meyers S**, **Schauer W**, **Balzi E**, **Wagner M**, **Goffeau A**, **Golin J**. 1992. Interaction of the yeast pleiotropic drug resistance genes PDR1 and PDR5. Curr Genet **21**:431–436.
38. **Jonikas MC**, **Collins SR**, **Denic V**, **Oh E**, **Quan EM**, **Schmid V**, **Weibezahn J**, **Schwappach B**, **Walter P**, **Weissman JS**, **Schuldiner M**. 2009. Comprehensive characterization of genes required for protein folding in the endoplasmic reticulum. Science **323**:1693–1697.
39. **Lahiri S**, **Chao JT**, **Tavassoli S**, **Wong AKO**, **Choudhary V**, **Young BP**, **Loewen CJR**, **Prinz WA**. 2014. A conserved endoplasmic reticulum membrane protein complex (EMC) facilitates phospholipid transfer from the ER to mitochondria. PLoS Biol **12**:e1001969.
40. **Hampton RY**. 2000. ER stress response: getting the UPR hand on misfolded proteins. Curr Biol CB **10**:R518–521.
41. **Schröder M**. 2008. Endoplasmic reticulum stress responses. Cell Mol Life Sci CMLS **65**:862–894.
42. **Costanzo M**, **Baryshnikova A**, **Bellay J**, **Kim Y**, **Spear ED**, **Sevier CS**, **Ding H**, **Koh JLY**, **Toufighi K**, **Mostafavi S**, **Prinz J**, **St Onge RP**, **VanderSluis B**, **Makhnevych T**, **Vizeacoumar FJ**, **Alizadeh S**, **Bahr S**, **Brost RL**, **Chen Y**, **Cokol M**, **Deshpande R**, **Li Z**, **Lin Z-Y**, **Liang W**, **Marback M**, **Paw J**, **San Luis B-J**, **Shuteriqi E**, **Tong AHY**, **van Dyk N**, **Wallace IM**, **Whitney JA**, **Weirauch MT**, **Zhong G**, **Zhu H**, **Houry WA**, **Brudno M**, **Ragibizadeh S**, **Papp B**, **Pál C**, **Roth FP**, **Giaever G**, **Nislow C**, **Troyanskaya OG**, **Bussey**

H, **Bader GD**, **Gingras A-C**, **Morris QD**, **Kim PM**, **Kaiser CA**, **Myers CL**, **Andrews BJ**, **Boone C**. 2010. The genetic landscape of a cell. Science **327**:425–431.
43. **Yu L**, **Peña Castillo L**, **Mnaimneh S**, **Hughes TR**, **Brown GW**. 2006. A survey of essential gene function in the yeast cell division cycle. Mol Biol Cell **17**:4736–4747.
44. **Thibault G**, **Shui G**, **Kim W**, **McAlister GC**, **Ismail N**, **Gygi SP**, **Wenk MR**, **Ng DTW**. 2012. The membrane stress response buffers lethal effects of lipid disequilibrium by reprogramming the protein homeostasis network. Mol Cell **48**:16–27.
45. **Finke K**, **Plath K**, **Panzner S**, **Prehn S**, **Rapoport TA**, **Hartmann E**, **Sommer T**. 1996. A second trimeric complex containing homologs of the Sec61p complex functions in protein transport across the ER membrane of S. cerevisiae. EMBO J **15**:1482–1494.
46. **Biederer T**, **Volkwein C**, **Sommer T**. 1997. Role of Cue1p in ubiquitination and degradation at the ER surface. Science **278**:1806–1809.
47. **Bordallo J**, **Plemper RK**, **Finger A**, **Wolf DH**. 1998. Der3p/Hrd1p is required for endoplasmic reticulum-associated degradation of misfolded lumenal and integral membrane proteins. Mol Biol Cell **9**:209–222.
48. **Hampton RY**, **Gardner RG**, **Rine J**. 1996. Role of 26S proteasome and HRD genes in the degradation of 3-hydroxy-3-methylglutaryl-CoA reductase, an integral endoplasmic reticulum membrane protein. Mol Biol Cell **7**:2029–2044.
49. **Mehnert M**, **Sommer T**, **Jarosch E**. 2014. Der1 promotes movement of misfolded proteins through the endoplasmic reticulum membrane. Nat Cell Biol **16**:77–86.
50. **Travers KJ**, **Patil CK**, **Wodicka L**, **Lockhart DJ**, **Weissman JS**, **Walter P**. 2000. Functional and Genomic Analyses Reveal an Essential Coordination between the Unfolded Protein Response and ER-Associated Degradation. Cell **101**:249–258.
51. **Friedlander R**, **Jarosch E**, **Urban J**, **Volkwein C**, **Sommer T**. 2000. A regulatory link between ER-associated protein degradation and the unfolded-protein response. Nat Cell Biol **2**:379–384.
52. **Richie DL**, **Feng X**, **Hartl L**, **Aimanianda V**, **Krishnan K**, **Powers-Fletcher MV**, **Watson DS**, **Galande AK**, **White SM**, **Willett T**, **Latgé J-P**, **Rhodes JC**, **Askew DS**. 2011. The virulence of the opportunistic fungal pathogen Aspergillus fumigatus requires cooperation between the endoplasmic reticulum-associated degradation pathway (ERAD) and the unfolded protein response (UPR). Virulence **2**:12–21.
53. **Buck TM**, **Jordan R**, **Lyons-Weiler J**, **Adelman JL**, **Needham PG**, **Kleyman TR**, **Brodsky JL**. 2015. Expression of three topologically distinct membrane proteins elicits unique stress response pathways in the yeast Saccharomyces cerevisiae. Physiol Genomics **47**:198–214.
54. **Hazbun TR**, **Malmström L**, **Anderson S**, **Graczyk BJ**, **Fox B**, **Riffle M**, **Sundin BA**, **Aranda JD**, **McDonald WH**, **Chiu C-H**, **Snydsman BE**, **Bradley P**, **Muller EGD**, **Fields S**, **Baker D**, **Yates JR**, **Davis TN**. 2003. Assigning function to yeast proteins by integration of technologies. Mol Cell **12**:1353–1365.
55. **Huh W-K**, **Falvo JV**, **Gerke LC**, **Carroll AS**, **Howson RW**, **Weissman JS**, **O'Shea EK**. 2003. Global analysis of protein localization in budding yeast. Nature **425**:686–691.
56. **Chen F**, **Mackey AJ**, **Stoeckert CJ**, **Roos DS**. 2006. OrthoMCL-DB: querying a comprehensive multi-species collection of ortholog groups. Nucleic Acids Res **34**:D363–368.
57. **Hoppins S**, **Collins SR**, **Cassidy-Stone A**, **Hummel E**, **Devay RM**, **Lackner LL**, **Westermann B**, **Schuldiner M**, **Weissman JS**, **Nunnari J**. 2011. A mitochondrial-focused

genetic interaction map reveals a scaffold-like complex required for inner membrane organization in mitochondria. J Cell Biol **195**:323–340.

Figure legends

Fig. 1: Identification of a compound with broad antifungal activity. **(A)** Selection of a new antifungal, sr7575, through a chemical library screen of *A. fumigatus* growth inhibition was followed by chemogenomic profiling in *S. cerevisiae* to identify a potential mechanism of action. sr7575 inhibited growth of various fungi, including *A. flavus* (48 h, 37°C, RPMI medium, 5 µg/mL) **(B)**; *C. albicans* and *C. neoformans* (24 h, 37°C, SC medium, 2 µg/mL) **(C)**; *S. cerevisiae* (48 h, 30°C, SC medium, 1 µg/mL) **(D)**.

Fig. 2: Chemogenomic profiling reveals an ERAD-enriched signature for sr7575 toxicity. **(A)** Distribution of relative growth values for *S. cerevisiae* mutant strains grown in the presence of sr7575. Colors indicate functional categories from the pooled library with genes annotated as ERAD (violet), protein translocation (grey), ER membrane complex (EMC; pink), and vesicular traffic (green) showing the most sensitivity to sr7575 when mutated. Note: *YML012C-A** overlaps *UBX2* and "#" indicates a DAmP strain; **(B)** Distribution of sensitivity values for deletion strains affected for genes annotated with the GO term 0030433, ERAD; **(C)** Pearson correlation coefficients between results obtained with sr7575 and a published large scale chemogenomics data set identifies chemical 4166 as having a profile that is most similar to sr7575. Only the scores for the top 100 correlated treatments are displayed; **(D)** Same as **(C)** but with the Spearman rank correlation; **(E)** Comparison of the fitness defect scores between sr7575 and chemical 4166; gene names are color coded as in **(A)**.

743 **Fig. 3**: Summary of mutations conferring increased susceptibility to sr7575. **(A)**
744 Heatmap showing the unique ERAD signature of sr7575 compared with published
745 chemogenomic and SGA growth defect profiles; **(B)** Model showing the two main pathways
746 responsible for ERAD in fungi- Doa10 pathway (green) for clearing misfolded proteins with
747 cytosolic lesions, and the Hrd1 pathway (violet), which degrades misfolded proteins with
748 lumenal or transmembrane lesions. Shared components (Ubx2, Ubc7, Cue1, and the Cdc48
749 complex) are denoted in gray or black.

750 **Fig. 4**: Sensitivity to sr7575 depends on EMC and ERAD components. **(A)** Serial 10-
751 fold dilutions of the WT and selected haploid deletion mutants were grown on SC plates in the
752 absence or presence of 0.25 µg/mL sr7575 for 48 h at 30°C; **(B)** Complementation of sr7575
753 sensitivity for the strains shown in panel **(A)** was tested by using single copy plasmids
754 carrying the corresponding genes; **(C)** Strains lacking core UPR components, *HAC1* and *IRE1*
755 were tested for sensitivity against sr7575 at 0.5 µg/mL.

756 **Fig. 5**: The hypersensitivity of ERAD mutants to sr7575 is conserved in *A. fumigatus*.
757 **(a)** Conidia from *A. fumigatus* WT and deletion mutants were recovered in 0.05% Tween-
758 water and serial dilutions were spotted onto sr7575-containing RPMI 1640, pH 7.0. Plates
759 were incubated at 37°C for 72 h; **(B)** Analysis of UPR target gene expression (*bipA* and *tigA*)
760 by qRT-PCR. Cultures were treated with sr7575, DTT, or sr7575 for 1 h followed by DTT.
761 RNA was extracted and analyzed by qRT-PCR, using *tubA* mRNA for normalization. The
762 results of treated vs untreated samples from three independent experiments are shown.

763 **Fig. 6**: Ynl181w is an ER protein conserved in fungi and involved in adaptation to
764 sr7575. **(A)** T-Coffee alignment of the conserved short chain dehydrogenase region within Sc
765 Ynl181w (PFAM 54-187) and its orthologs in pathogenic fungi. Gene annotations with

number range indicate the position of the PFAM domain: *A. fumigatus* (Afu5g10790; 54-205), *C. albicans* (orf19.6233; 58-204), *C. glabrata* (XP_448202; 54-193); **(B)** Scatter plot showing the correlation between sr7575 sensitivity values and the previously published SGA scores for ynl181w-DAmP; **(C)** Spot assays showing the difference in sensitivity to sr7575 and UPR inducer tunicamycin (TM) for *ynl181w*-DAmP as compared with a strain defective for UPR (*hac1*Δ).

Supplementary Data synopsis

Fig. S1: Synthetic pathways for sr7575 and related compounds.

Fig. S2: Growth of *A. fumigatus*, *A. flavus*, *S. cerevisiae*, *C. albicans* and *C. neoformans* cells in liquid medium in the presence of various concentrations of sr7575.

Fig. S3: sr7575 profile shows little correlation with a previously published large-scale chemogenomics dataset.

Fig. S4: Perturbation of PGA3 function shows similarities with the sensitivity profile for sr7575.

Fig. S5: Susceptibility testing of yeast strains against sr7575.

Fig. S6: Susceptibility of multidrug resistant *S. cerevisiae* strains and azole resistant *C. albicans* strains to sr7575.

Table S1: List of 76 compounds from the CERMN chemical library showing 90% or more growth inhibition of *A.fumigatus* at 25 μg/mL.

Table S2: Analogues of sr7575 and MIC_{100} values against *A. fumigatus*.

Table S3: Analogues of sr7576 and MIC_{100} values against *A. fumigatus*.

Table S4: List of strains used in this study.

Table S5: List of oligonucleotides used in this study.

Table S6 (provided as a separate xls file): Sensitivity of *S. cerevisiae* deletion and DAmP strains to 0.125 μg/mL sr7575.

Text S1: Synthesis of sr7575 and related compounds.

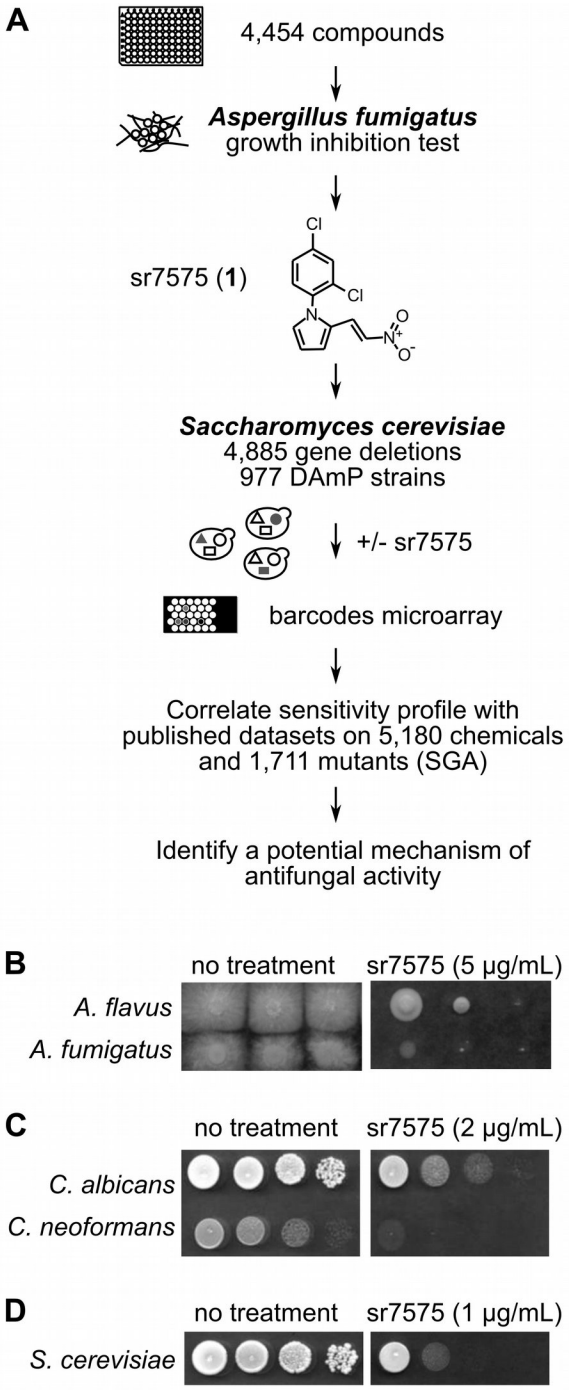

Fig. 1: Identification of a compound with broad antifungal activity. **(A)** Selection of a new antifungal, sr7575, through a chemical library screen of *A. fumigatus* growth inhibition was followed by chemogenomic profiling in *S. cerevisiae* to identify a potential mechanism of action. sr7575 inhibited growth of various fungi, including *A. flavus* (48 h, 37°C, RPMI medium, 5 µg/mL) **(B)**; *C. albicans* and *C. neoformans* (24 h, 37°C, SC medium, 2 µg/mL) **(C)**; *S. cerevisiae* (48 h, 30°C, SC medium, 1 µg/mL) **(D)**.

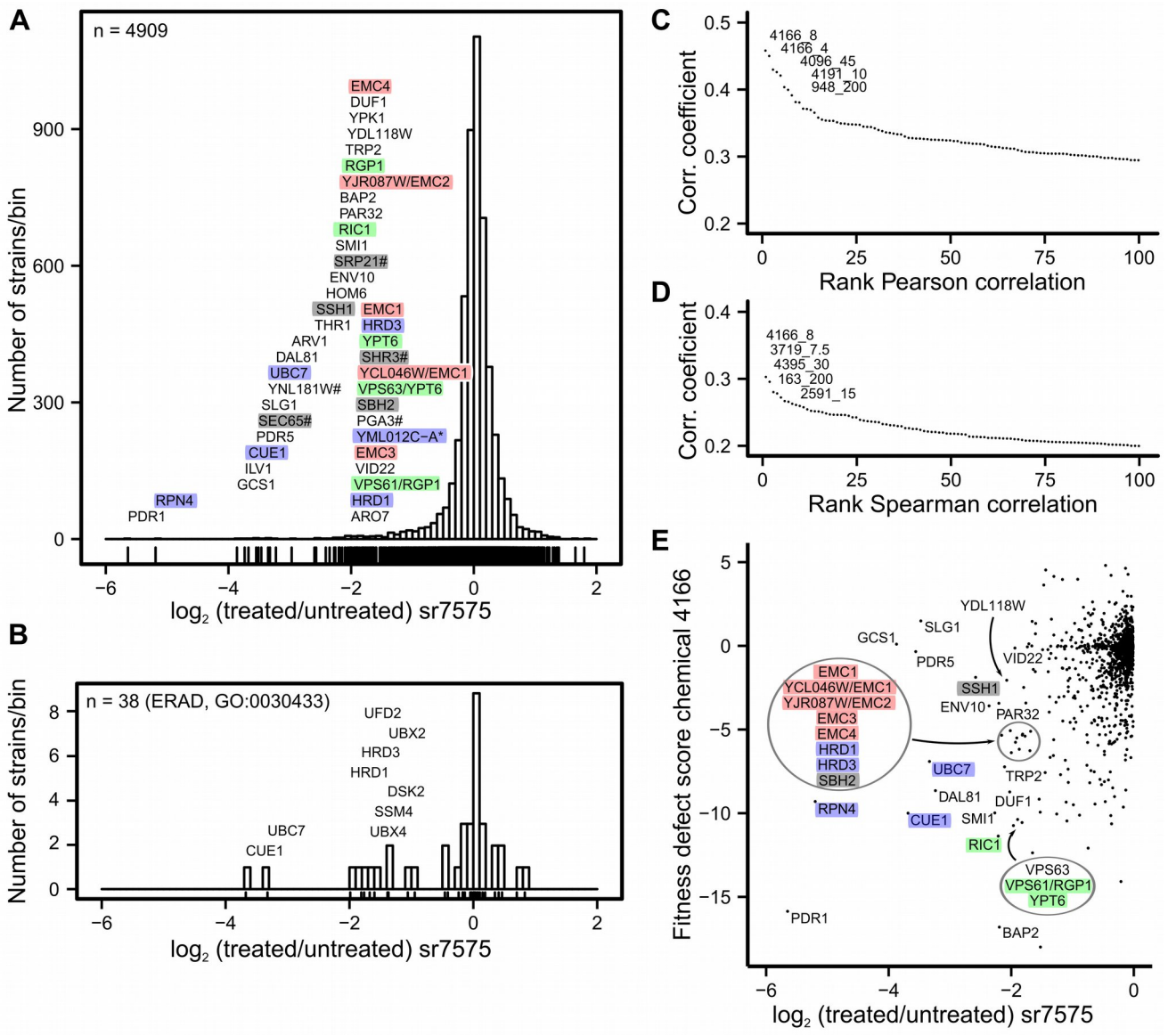

Fig. 2: Chemogenomic profiling reveals an ERAD-enriched signature for sr7575 toxicity. **(A)** Distribution of relative growth values for *S. cerevisiae* mutant strains grown in the presence of sr7575. Colors indicate functional categories from the pooled library with genes annotated as ERAD (violet), protein translocation (grey), ER membrane complex (EMC; pink), and vesicular traffic (green) showing the most sensitivity to sr7575 when mutated. Note: *YML012C-A** overlaps *UBX2* and "#" indicates a DAmP strain; **(B)** Distribution of sensitivity values for deletion strains affected for genes annotated with the GO term 0030433, ERAD; **(C)** Pearson correlation coefficients between results obtained with sr7575 and a published large scale chemogenomics data set identifies chemical 4166 as having a profile that is most similar to sr7575. Only the scores for the top 100 correlated treatments are displayed; **(D)** Same as **(C)** but with the Spearman rank correlation; **(E)** Comparison of the fitness defect scores between sr7575 and chemical 4166; gene names are color coded as in **(A)**.

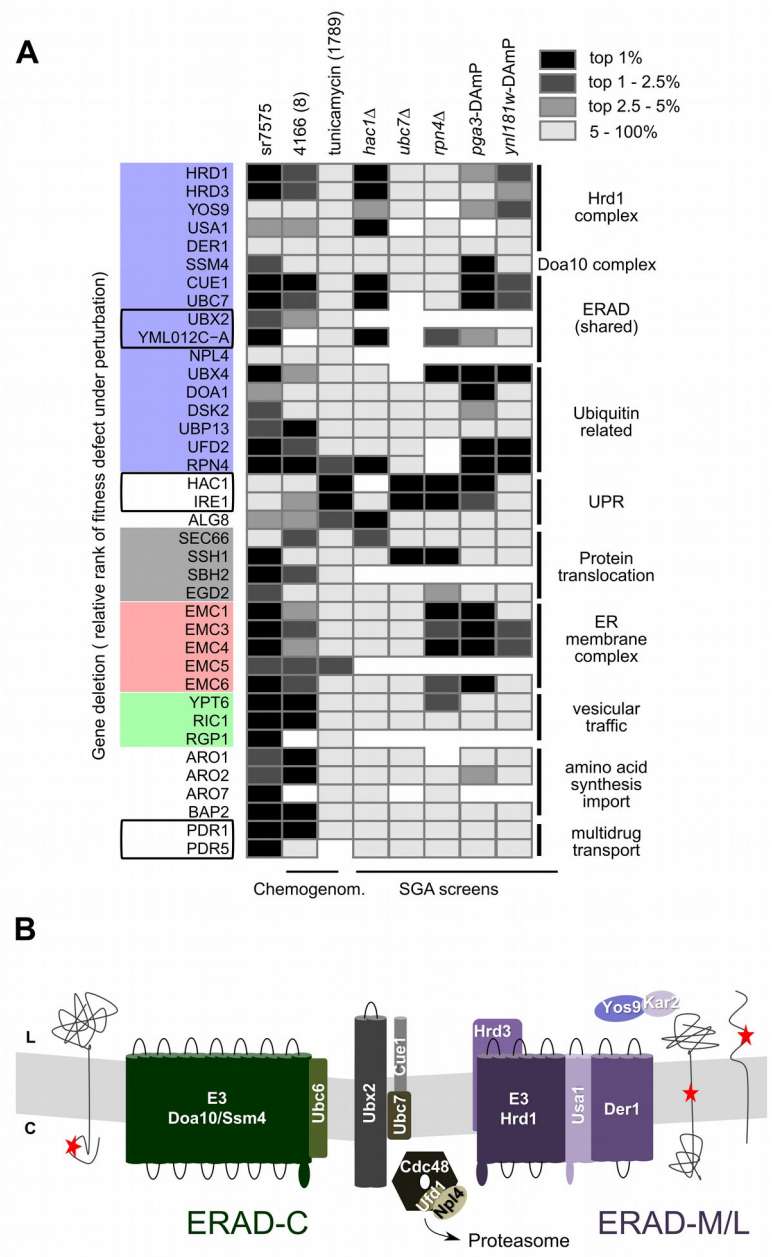

Fig. 3: Summary of mutations conferring increased susceptibility to sr7575. **(A)** Heatmap showing the unique ERAD signature of sr7575 compared with published chemogenomic and SGA growth defect profiles; **(B)** Model showing the two main pathways responsible for ERAD in fungi- Doa10 pathway (green) for clearing misfolded proteins with cytosolic lesions, and the Hrd1 pathway (violet), which degrades misfolded proteins with lumenal or transmembrane lesions. Shared components (Ubx2, Ubc7, Cue1, and the Cdc48 complex) are denoted in gray or black.

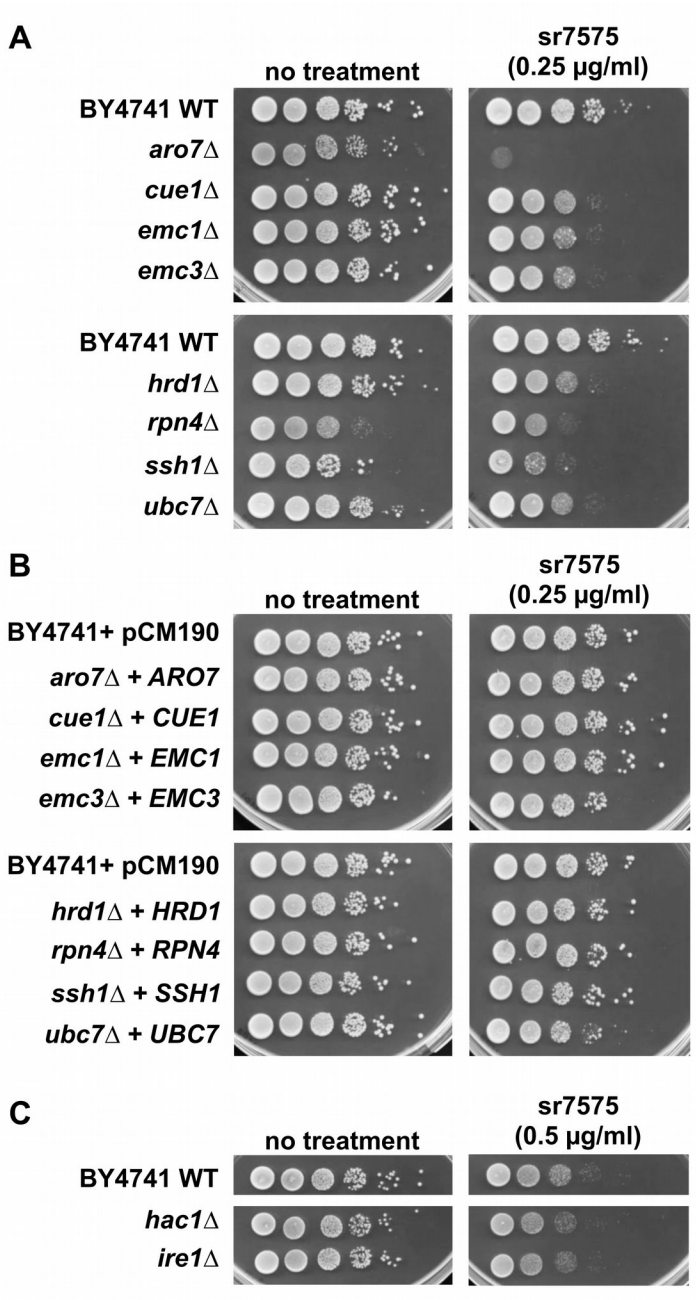

Fig. 4: Sensitivity to sr7575 depends on EMC and ERAD components. **(A)** Serial 10-fold dilutions of the WT and selected haploid deletion mutants were grown on SC plates in the absence or presence of 0.25 µg/mL sr7575 for 48 h at 30°C; **(B)** Complementation of sr7575 sensitivity for the strains shown in panel **(A)** was tested by using single copy plasmids carrying the corresponding genes; **(C)** Strains lacking core UPR components, *HAC1* and *IRE1* were tested for sensitivity against sr7575 at 0.5 µg/mL.

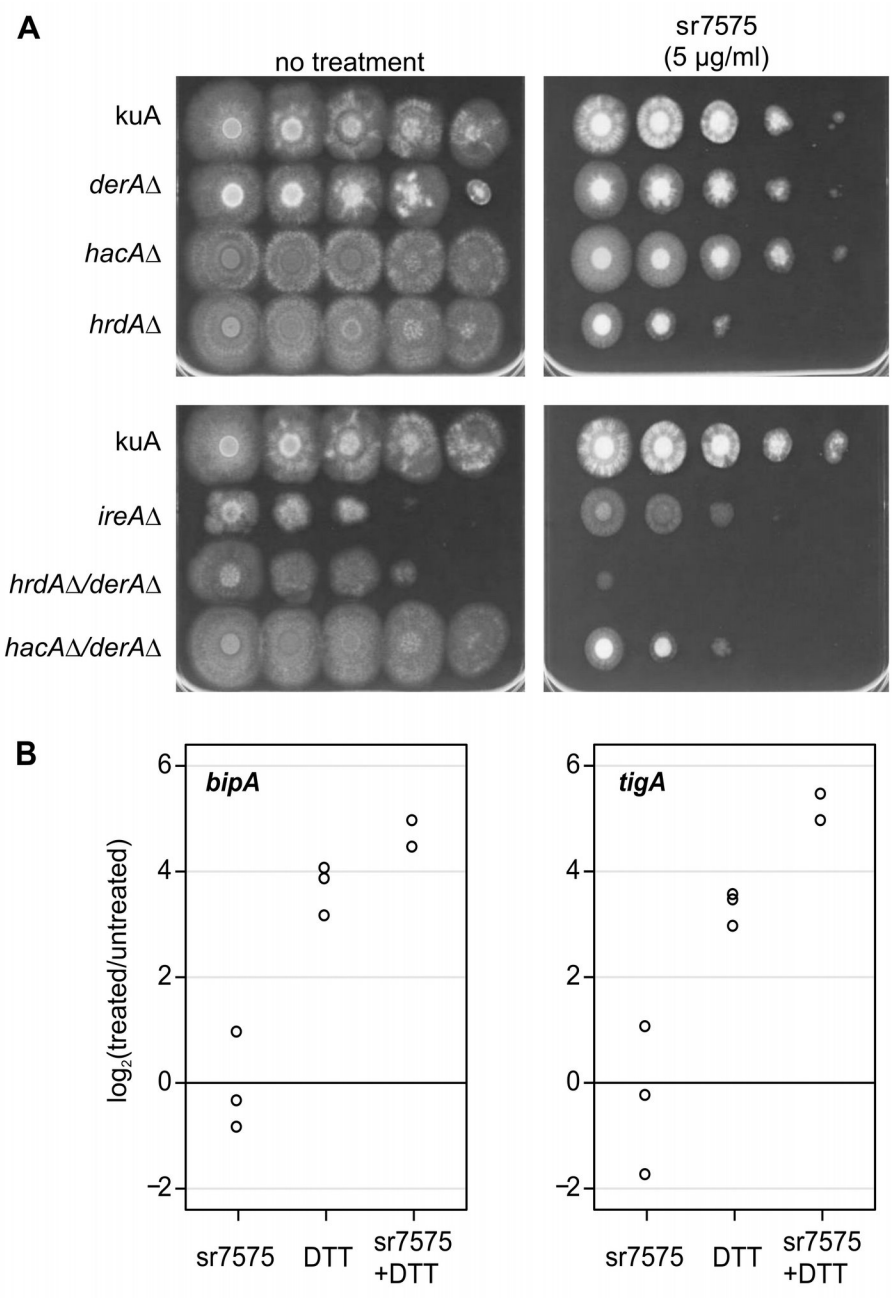

Fig. 5: The hypersensitivity of ERAD mutants to sr7575 is conserved in *A. fumigatus*. **(a)** Conidia from *A. fumigatus* WT and deletion mutants were recovered in 0.05% Tween-water and serial dilutions were spotted onto sr7575-containing RPMI 1640, pH 7.0. Plates were incubated at 37°C for 72 h; **(B)** Analysis of UPR target gene expression (*bipA* and *tigA*) by qRT-PCR. Cultures were treated with sr7575, DTT, or sr7575 for 1 h followed by DTT. RNA was extracted and analyzed by qRT-PCR, using *tubA* mRNA for normalization. The results of treated vs untreated samples from three independent experiments are shown.

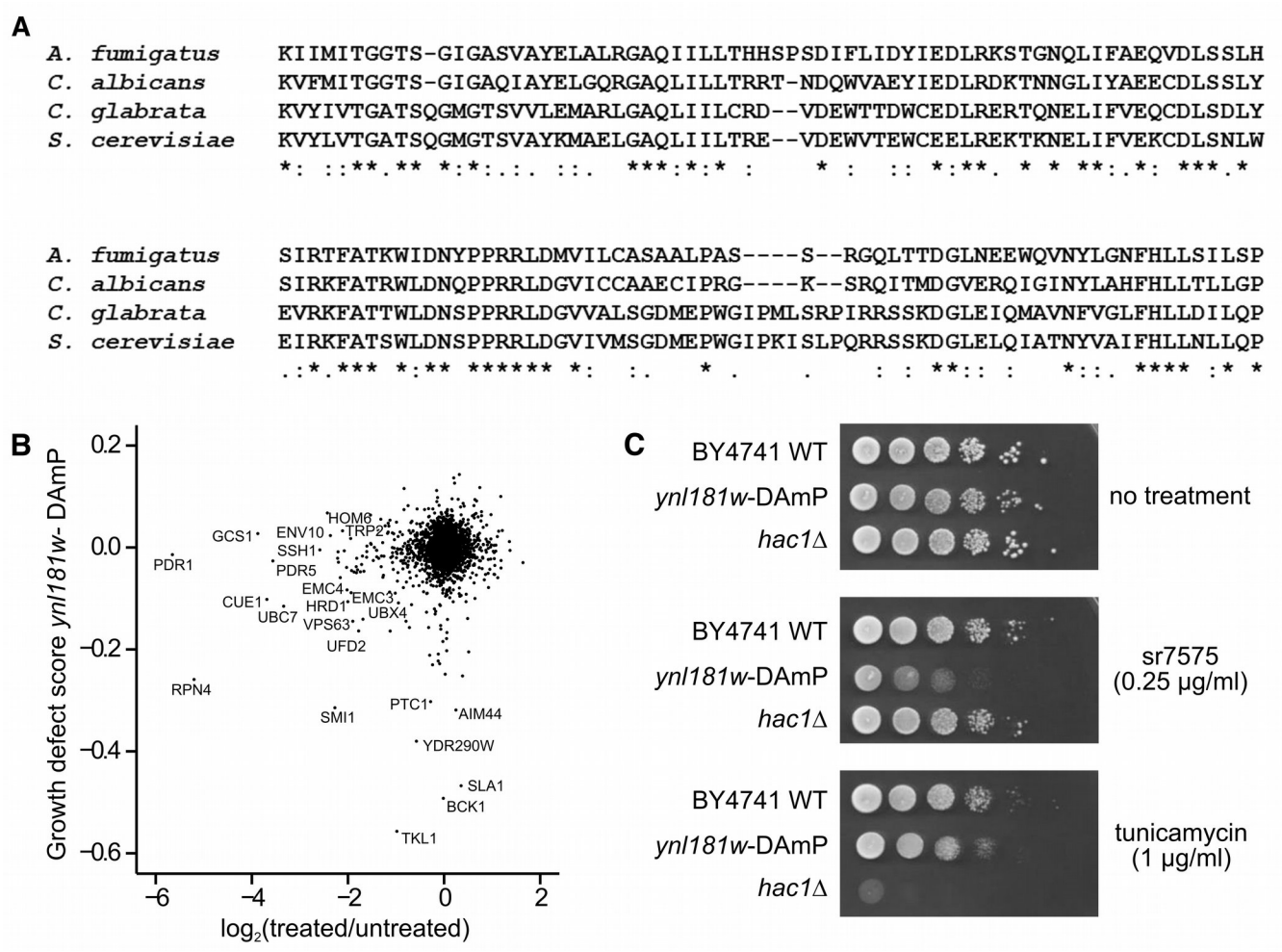

Fig. 6: Ynl181w is an ER protein conserved in fungi and involved in adaptation to sr7575. **(A)** T-Coffee alignment of the conserved short chain dehydrogenase region within Sc Ynl181w (PFAM 54-187) and its orthologs in pathogenic fungi. Gene annotations with number range indicate the position of the PFAM domain: *A. fumigatus* (Afu5g10790; 54-205), *C. albicans* (orf19.6233; 58-204), *C. glabrata* (XP_448202; 54-193); **(B)** Scatter plot showing the correlation between sr7575 sensitivity values and the previously published SGA scores for ynl181w-DAmP; **(C)** Spot assays showing the difference in sensitivity to sr7575 and UPR inducer tunicamycin (TM) for *ynl181w*-DAmP as compared with a strain defective for UPR (*hac1*Δ).

Supplementary Material for Publication of manuscript "Toxicity of a novel antifungal compound is modulated by ERAD components", by Raj et al.

Fig. S1: Synthetic pathways for sr7575 and related compounds.

Fig. S2: Growth of *A. fumigatus*, *A. flavus*, *S. cerevisiae*, *C. albicans* and *C. neoformans* cells in liquid medium in the presence of various concentrations of sr7575.

Fig. S3: sr7575 profile shows little correlation with a previously published large-scale chemogenomics dataset.

Fig. S4: Perturbation of PGA3 function shows similarities with the sensitivity profile for sr7575.

Fig. S5: Susceptibility testing of yeast strains against sr7575.

Fig. S6: Susceptibility of multidrug resistant *S. cerevisiae* strains and azole resistant *C. albicans* strains to sr7575.

Table S1: List of 76 compounds from the CERMN chemical library showing 90% or more growth inhibition of *A.fumigatus* at 25 µg/mL.

Table S2: Analogues of sr7575 and MIC_{100} values against *A. fumigatus*.

Table S3: Analogues of sr7576 and MIC_{100} values against *A. fumigatus*.

Table S4: List of strains and plasmids used in this study.

Table S5: List of oligonucleotides used in this study.

Table S6 (provided as a separate xls file): Sensitivity of *S. cerevisiae* deletion and DAmP strains to 0.125 µg/mL sr7575.

Text S1: Synthesis of sr7575 and related compounds.

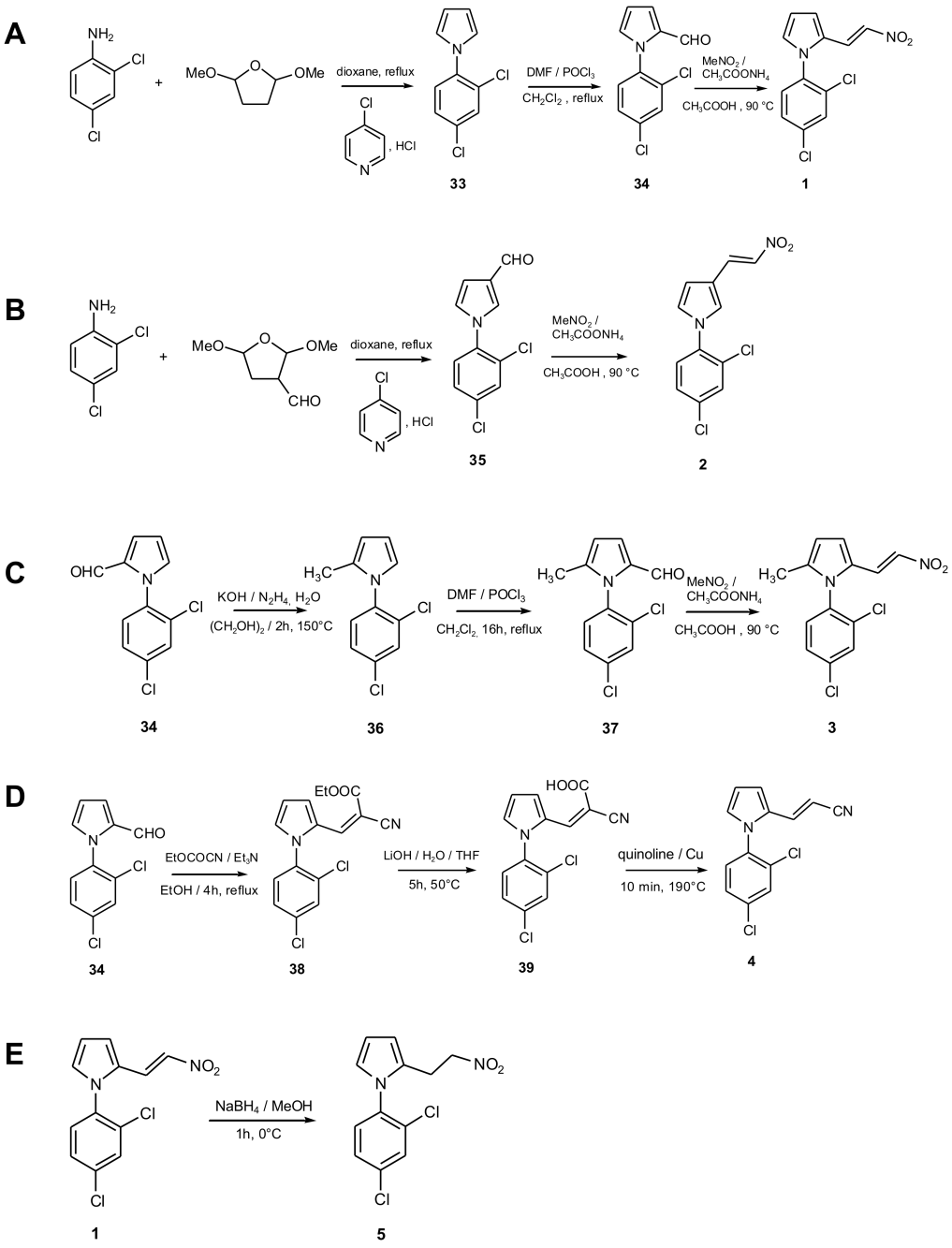

Figure S1. Synthetic pathways for sr7575 and related compounds. Pathways detailing the synthesis of sr7575 and analogues 2-5.

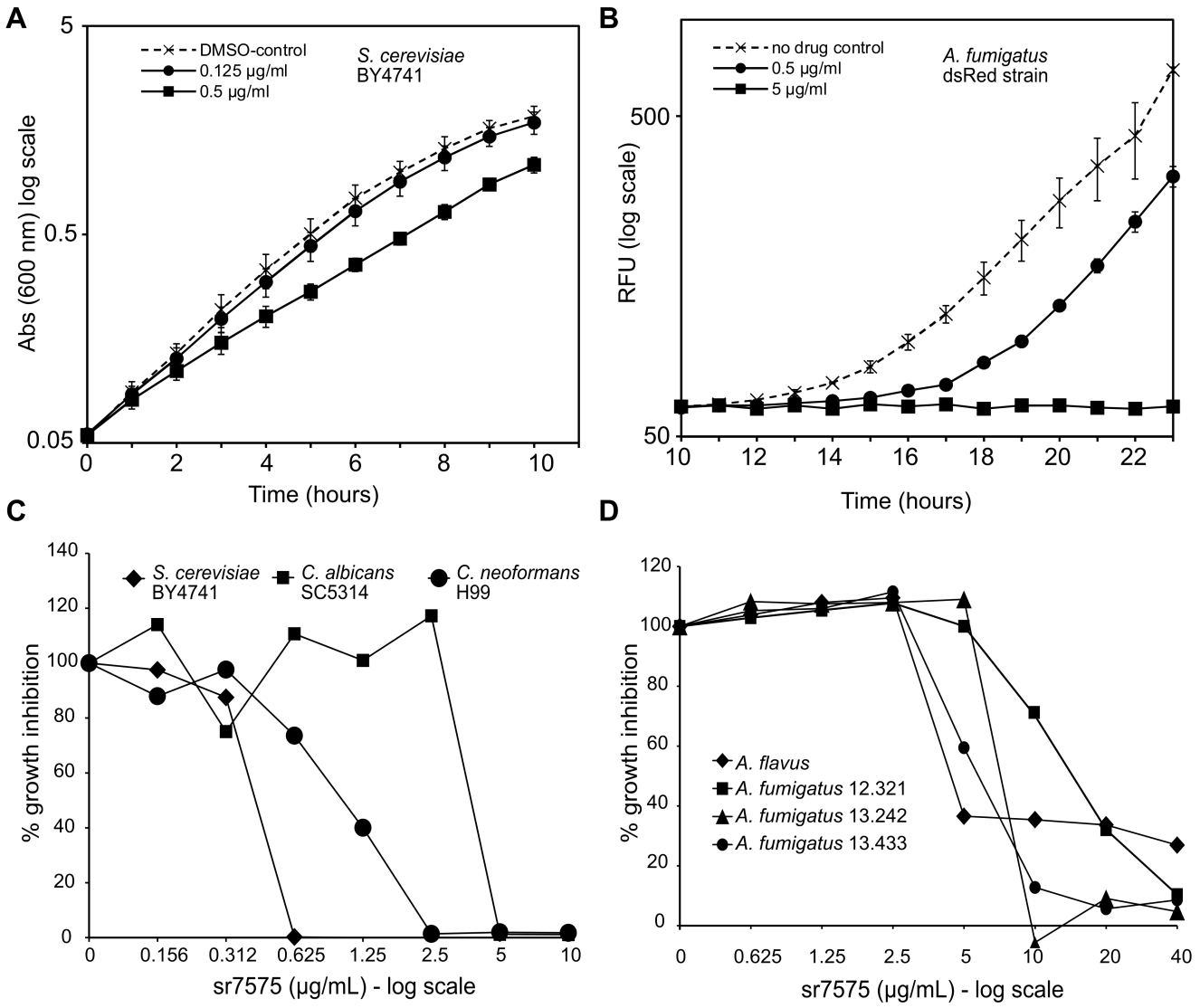

Figure S2. Growth of *A. fumigatus*, *A. flavus*, *S. cerevisiae*, *C. albicans* and *C. neoformans* cells in liquid medium in the presence of various concentrations of sr7575. (A) Log-phase cultures of *S. cerevisiae* WT strain BY4741 were grown in the presence of increasing concentrations of sr7575 with DMSO as vehicle control. The Abs600 was determined every hour for 10 h. (**B**) *A. fumigatus* strain Af293-dsRed was grown for 23 h in RPMI-1640 medium in the presence of increasing concentrations of sr7575. Fluorescence (ex 254 nm/ em 291 nm) was measured and relative fluorescence units (RFU) plotted against time. (**C**) Growth inhibition estimates were obtained at various concentrations of sr7575 by measuring absorbance at 600 nm for *S. cerevisiae* (BY4741, YPD, 30°C, 48 h), *C. albicans* (SC5314, RPMI, 37°C, 48 h) and *C. neoformans* (H99, RPMI, 37°C, 72 h). (**D**) Growth inhibition estimates for *A. flavus* and three *A. fumigatus* clinical isolates (12.321, 13.242, 13.433) were obtained by the resazurin reduction assay in RPMI medium, 37°C, 39 h at concentrations of sr7575 up to 40 µg/ml.

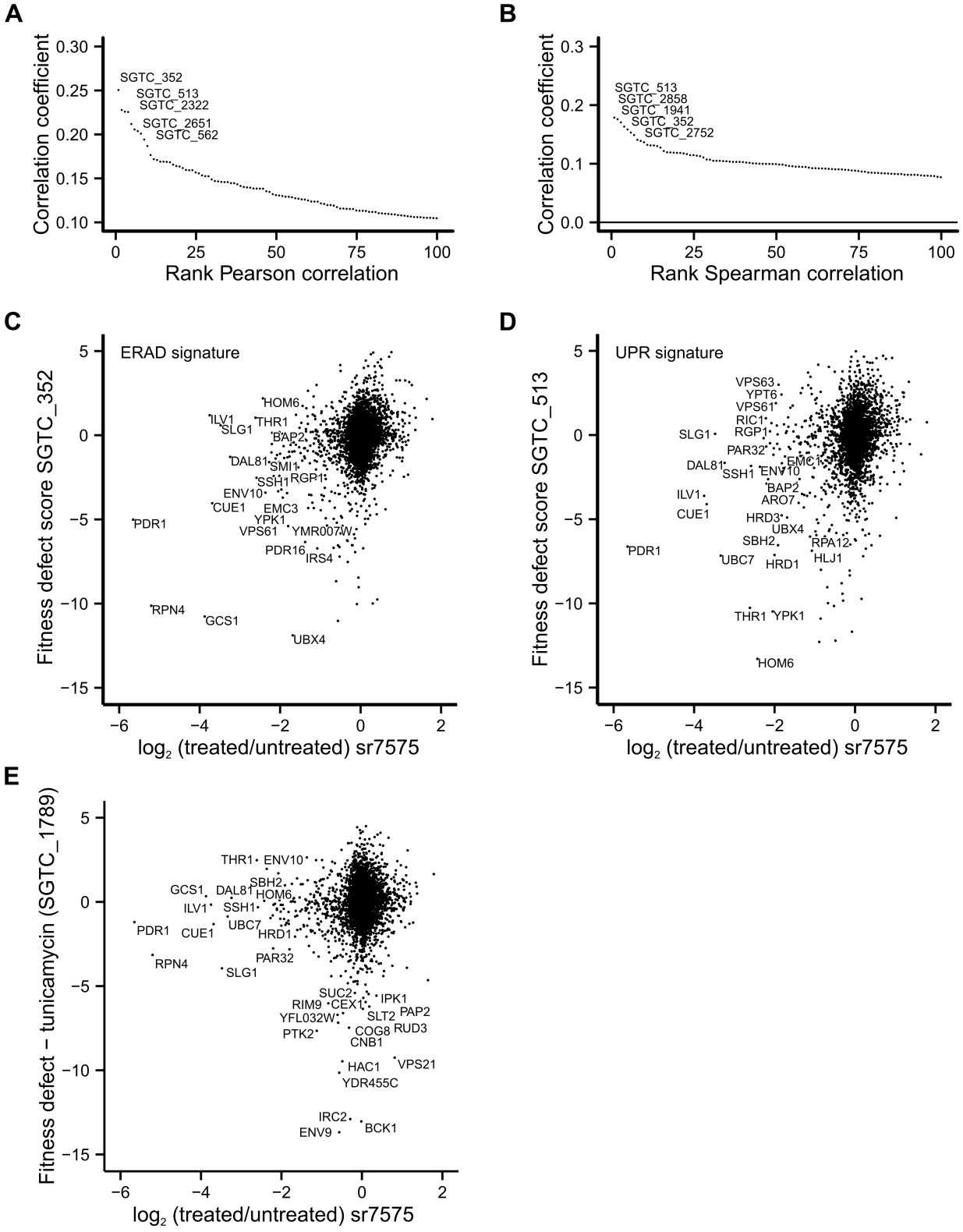

Figure S3. sr7575 profile shows little correlation with a previously published large-scale chemogenomics dataset. Computed Pearson **(A)** and Spearman **(B)** correlation coefficients between sr7575 values and previously published growth scores obtained with 3,356 compounds were ranked in descending order and the top 100 values are indicated. Among the highest correlations, we identified SGTC 352, a drug showing an ERAD signature **(C)** and SGTC 513, a compound with a UPR signature

(D) as being closest to the sr7575 profile. (E) The sr7575 profile showed no correlation with the one published for tunicamycin.

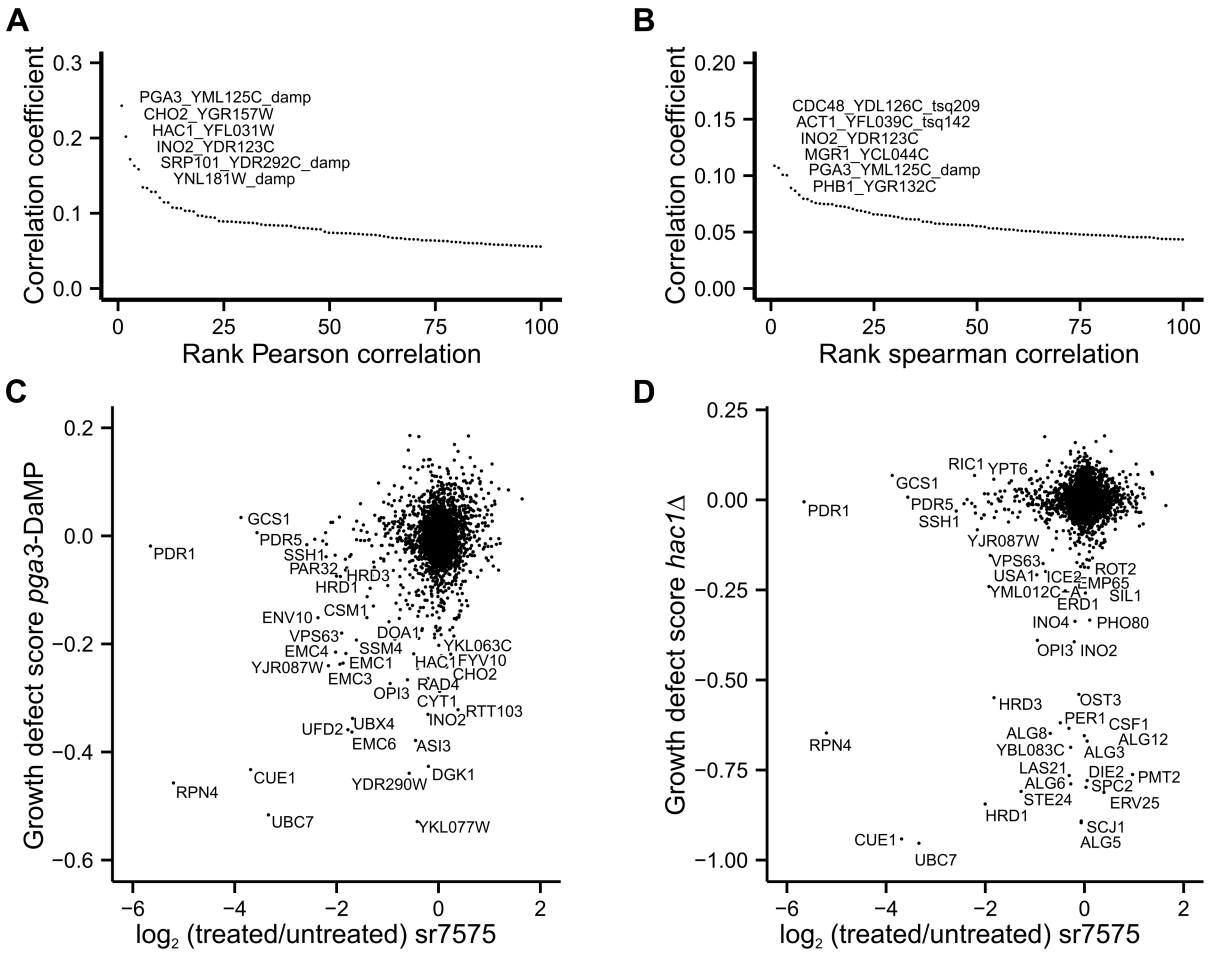

Figure S4. Perturbation of *PGA3* function shows similarities with the sensitivity profile for sr7575. Pearson **(A)** and Spearman **(B)** correlations between the sr7575 profile and 1711 previously published SGA profiles . Fitness defect scores for DAmP modification of *PGA3* are shown in **(C)**, while the interactions of *hac1*Δ and ERAD depleted strains are depicted in **(D)**.

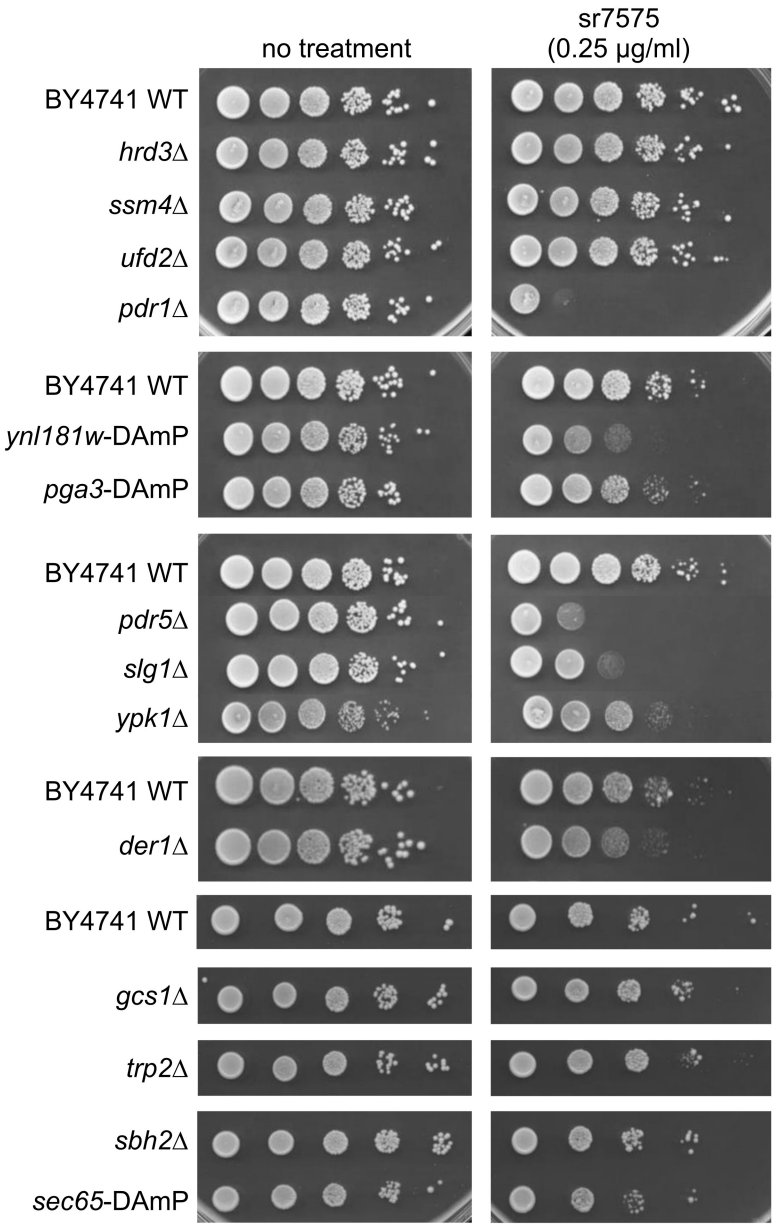

Figure S5. Susceptibility testing of yeast strains against sr7575. Mutants from the haploid deletion background were serially spotted onto SC plates supplemented with sr7575. Plates were incubated at 30°C for 48 h.

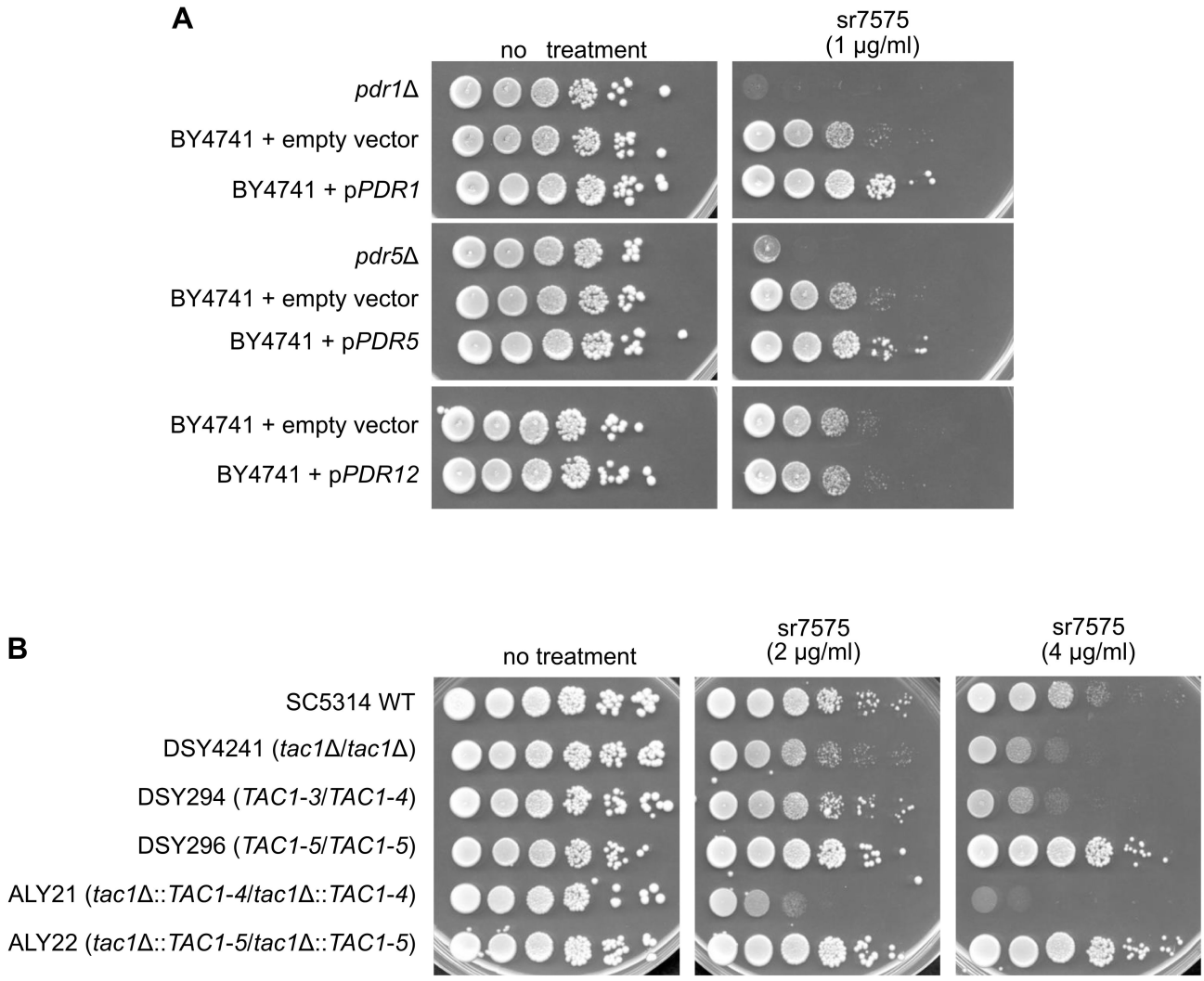

Figure S6. Susceptibility of multidrug resistant *S. cerevisiae* strains and azole resistant *C. albicans* strains to sr7575. (**A**) *S. cerevisiae* strains with deletions of or overexpressing *PDR1*, *PDR5* and *PDR12* were tested for susceptibility to sr7575 (1 µg/mL, SC medium, 30°C, 48 h). (**B**) Comparison of growth inhibition of *C. albicans* strains: WT (SC5314), *TAC1* transcription factor homozygous deletion strain (DSY4241), azole susceptible clinical isolate DSY294, azole resistant clinical isolate DSY296, azole susceptible laboratory generated strain ALY21 and azole resistant laboratory generated strain ALY22 (SC medium in the presence of 2 and 4 µg/mL sr7575, 37°C, 48 h).

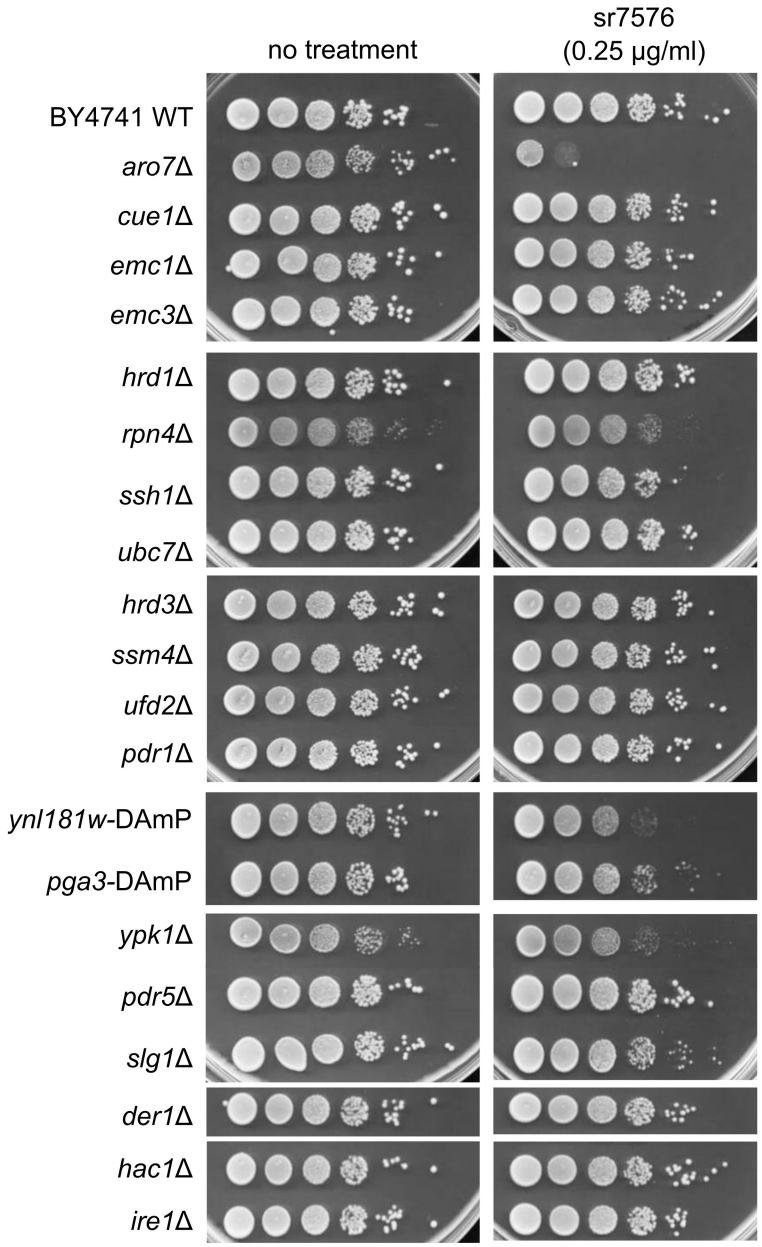

Figure S7. Response of yeast mutants against sr7576. Serial 10-fold dilutions of the WT and haploid deletion mutants were spotted onto SC plates supplemented with sr7576 (0.25 µg/mL). Plates were monitored for growth at 30°C for 48 h.

Supplementary Table S4 - Strains and plasmids used in this study

Strain	Genotype	Reference
BY4741	MATa;*his3*Δ 1;*leu2*Δ 0;*met15*Δ 0;*ura3*Δ 0	Brachmann et al, 1998

(Deletion mutants were generated in the Sc BY4741 background)		Reference
*aro7*Δ	*aro7*::KanMX4	Giaever et al, 2002
*cue1*Δ	*cue1*::KanMX4	
*der1*Δ	*der1*::KanMX4	
*doa10*Δ	*doa10*::KanMX4	
*emc1*Δ	*emc1*::KanMX4	
*emc3*Δ	*emc3*::KanMX4	
*gcs1*Δ	*gcs1*::KanMX4	
*hac1*Δ	*hac1*::KanMX4	
*hrd1*Δ	*hrd1*::KanMX4	
*hrd3*Δ	*hrd3*::KanMX4	
*ire1*Δ	*ire1*::KanMX4	
*pdr1*Δ	*pdr1*::KanMX4	
*pdr5*Δ	*pdr5*::KanMX4	
pga3-DAmP	*pga3*-DAmP (KanMX4)	
*rpn4*Δ	*rpn4*::KanMX4	
*sbh2*Δ	*sbh2*::KanMX4	
sec65-DAMP	*sec65*-DAmP (KanMX4)	
*slg1*Δ	*slg1*::KanMX4	
*ssh1*Δ	*ssh1*::KanMX4	
*trp2*Δ	*trp2*::KanMX4	
*ubc7*Δ	*ubc7*::KanMX4	
*ufd2*Δ	*ufd2*::KanMX4	
ynl181w-DAmP	*ynl181w*-DAmP (KanMX4)	
*ypk1*Δ	*ypk1*::KanMX4	

***A. fumigatus* strains used in this study:**

Strain	Genotype	Reference
kuA	akuA::*ptrA*	Krappmann et al, 2006
*derA*Δ	akuA::ptr*A, derA*::*hph*	Richie DL et al 2011
*hacA*Δ	akuA::*ptrA, hacA*::*hph*	Richie DL et al 2009
*hrdA*Δ	akuA::*ptrA, hrdA*::*hph*	Krishnan K et al 2013
*ireA*Δ	akuA::*ptrA, ireA*::*ble*	Jeng X et al 2011
*derA*Δ/*hacA*Δ	akuA:*ptrA, hacA*::*hph,derA*::*ble*	Richie DL et al 2011
*derA*Δ/*hrdA*Δ	akuA::*ptrA, hrdA*::*hph, derA*::*ble*	Krishnan K et al 2013

Other yeast strains used in this study:

Strain	Genotype	Reference
C. albicans SC5314	wild type	Lohberger et al, 2014
DSY4241	*tac1*Δ::*FRT*/*tac1*Δ::*FRT*	
DSY294	azole susceptible clinical isolate (*TAC1-3/TAC1-4*)	
DSY296	azole resistant clinical isolate (*TAC1-5*/*TAC1-5* ; N977D mutation)	
ALY21	*tac1*Δ::*TAC1-4-FRT*/*tac1*Δ::*TAC1-4-FRT*	
ALY22	*tac1*Δ::*TAC1-5-FRT*/*tac1*Δ::*TAC1-5-FRT*	
C. neoformans H99	wild type	Perfect et al, 1980

MoBY plasmid (library v1.1) complemented *S. cerevisiae* strains:

Strain	Genotype+ MoBY clone identifier	Reference
*aro7*Δ+*ARO7*	*aro7*::KanMX4+ YPR060C::29NP_C9	Ho et al, 2009
*cue1*Δ+*CUE1*	*cue1*::KanMX4+ YMR264W::33NP_H12	
*emc1*Δ+*EMC1*	*emc1*::KanMX4+ YCL045C::41NP_D8	
*emc3*Δ+*EMC3*	*emc3*::KanMX4+ YKL207W::8NP_A12	
*hrd1*Δ+*HRD1*	*hrd1*::KanMX4+ YOL013C::12NP_G12	
*rpn4*Δ+*RPN4*	*rpn4*::KanMX4+ YDL020C::30NP_F2	
*ssh1*Δ+*SSH1*	*ssh1*::KanMX4+ YBR283C::37NP_A11	
*ubc7*Δ+*UBC7*	*ubc7*::KanMX4+ YMR022W::36NP_G3	

YGPM systematic overexpression library in *S. cerevisiae* strains:

Strain	Genotype+ YGPM clone identifier	Reference
Control	BY4741+ YGPM22k06 chrIII:151898...152647	Jones et al, 2008
PDR1	BY4741+ YGPM26h12 chrVII:466658...477209	
PDR5	BY4741+ YGPM33k24 chrXV:619141...631341	
PDR12	BY4741+ YGPM8p07 chrXVI:444386...454435	

References :

Brachmann CB, Davies A, Cost GJ, Caputo E, Li J, Hieter P, Boeke JD. Yeast. 1998 14(2):115-32.
Krappmann S, Sasse C, Braus GH. Eukaryot Cell. 2006 5(1):212-5.
Jones GM, Stalker J, Humphray S, West A, Cox T, Rogers J,
Dunham I, Prelich G. Nature Methods. 2008 5:239-241
Lohberger A, Coste AT, Sanglard D. Eukaryot Cell. 2014 13(1):127-42
Perfect, JR, Lang SDR, and Durack DT. Am. J. Pathol. 1980 101:177-194.

Supplementary Material for Publication of manuscript "Toxicity of a novel antifungal compound is modulated by ERAD components", by Raj et al.

Fig. S1: Synthetic pathways for sr7575 and related compounds.

Fig. S2: Growth of *A. fumigatus*, *A. flavus*, *S. cerevisiae*, *C. albicans* and *C. neoformans* cells in liquid medium in the presence of various concentrations of sr7575.

Fig. S3: sr7575 profile shows little correlation with a previously published large-scale chemogenomics dataset.

Fig. S4: Perturbation of PGA3 function shows similarities with the sensitivity profile for sr7575.

Fig. S5: Susceptibility testing of yeast strains against sr7575.

Fig. S6: Susceptibility of multidrug resistant *S. cerevisiae* strains and azole resistant *C. albicans* strains to sr7575.

Table S1: List of 76 compounds from the CERMN chemical library showing 90% or more growth inhibition of *A.fumigatus* at 25 µg/mL.

Table S2: Analogues of sr7575 and MIC_{100} values against *A. fumigatus*.

Table S3: Analogues of sr7576 and MIC_{100} values against *A. fumigatus*.

Table S4: List of strains and plasmids used in this study.

Table S5: List of oligonucleotides used in this study.

Table S6 (provided as a separate xls file): Sensitivity of *S. cerevisiae* deletion and DAmP strains to 0.125 µg/mL sr7575.

Text S1: Synthesis of sr7575 and related compounds.

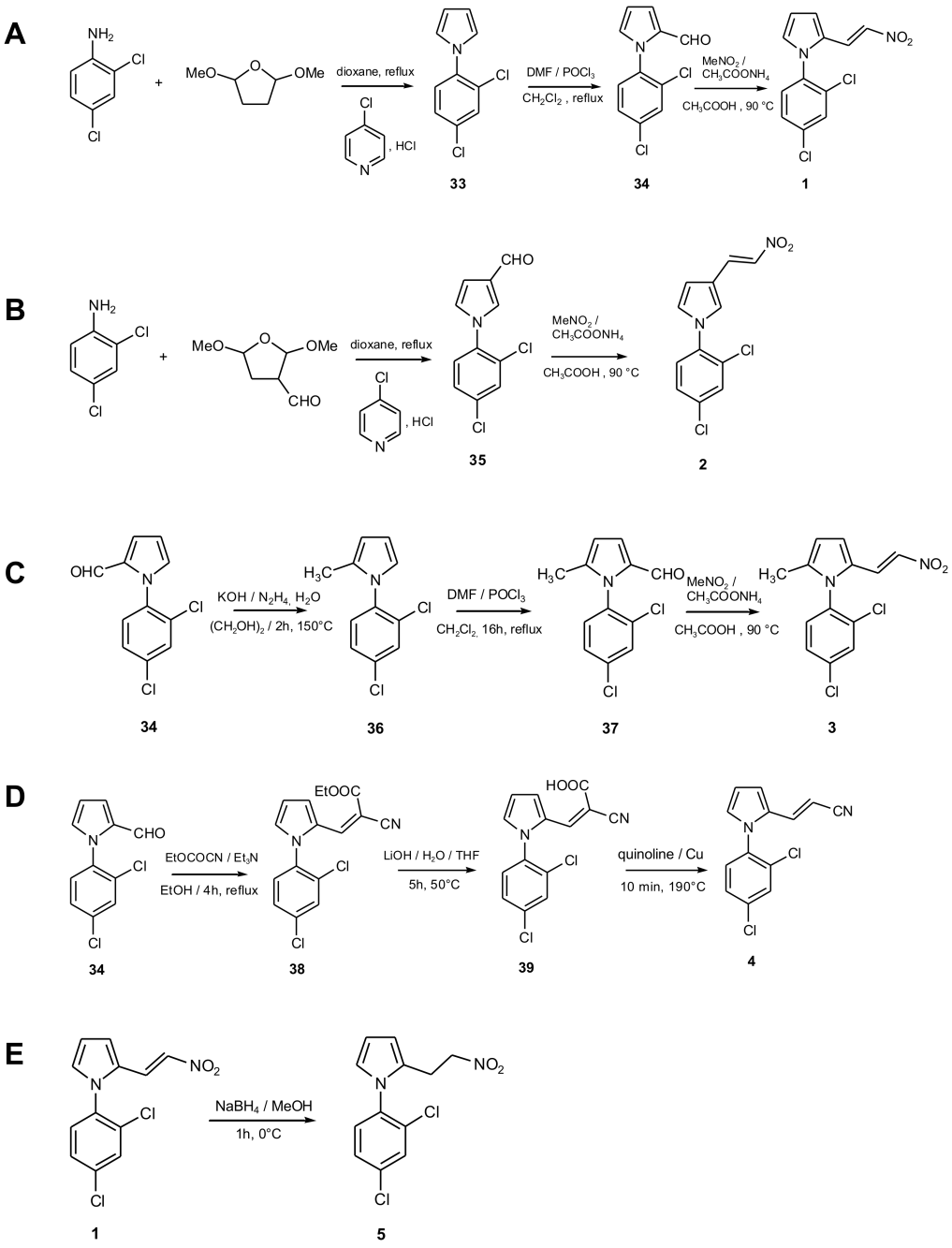

Figure S1. Synthetic pathways for sr7575 and related compounds. Pathways detailing the synthesis of sr7575 and analogues 2-5.

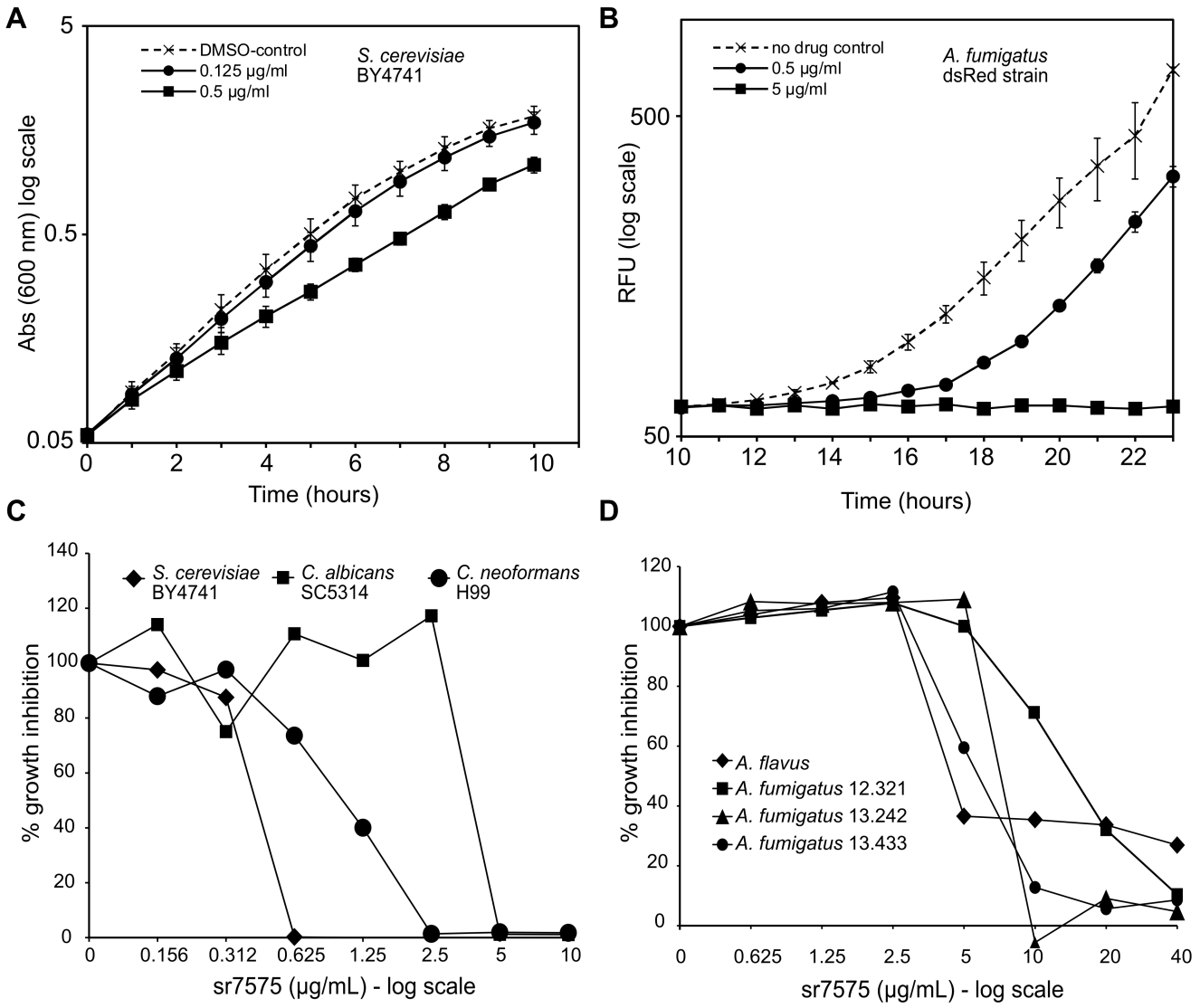

Figure S2. Growth of *A. fumigatus*, *A. flavus*, *S. cerevisiae*, *C. albicans* and *C. neoformans* cells in liquid medium in the presence of various concentrations of sr7575. (A) Log-phase cultures of *S. cerevisiae* WT strain BY4741 were grown in the presence of increasing concentrations of sr7575 with DMSO as vehicle control. The Abs600 was determined every hour for 10 h. (**B**) *A. fumigatus* strain Af293-dsRed was grown for 23 h in RPMI-1640 medium in the presence of increasing concentrations of sr7575. Fluorescence (ex 254 nm/ em 291 nm) was measured and relative fluorescence units (RFU) plotted against time. (**C**) Growth inhibition estimates were obtained at various concentrations of sr7575 by measuring absorbance at 600 nm for *S. cerevisiae* (BY4741, YPD, 30°C, 48 h), *C. albicans* (SC5314, RPMI, 37°C, 48 h) and *C. neoformans* (H99, RPMI, 37°C, 72 h). (**D**) Growth inhibition estimates for *A. flavus* and three *A. fumigatus* clinical isolates (12.321, 13.242, 13.433) were obtained by the resazurin reduction assay in RPMI medium, 37°C, 39 h at concentrations of sr7575 up to 40 µg/ml.

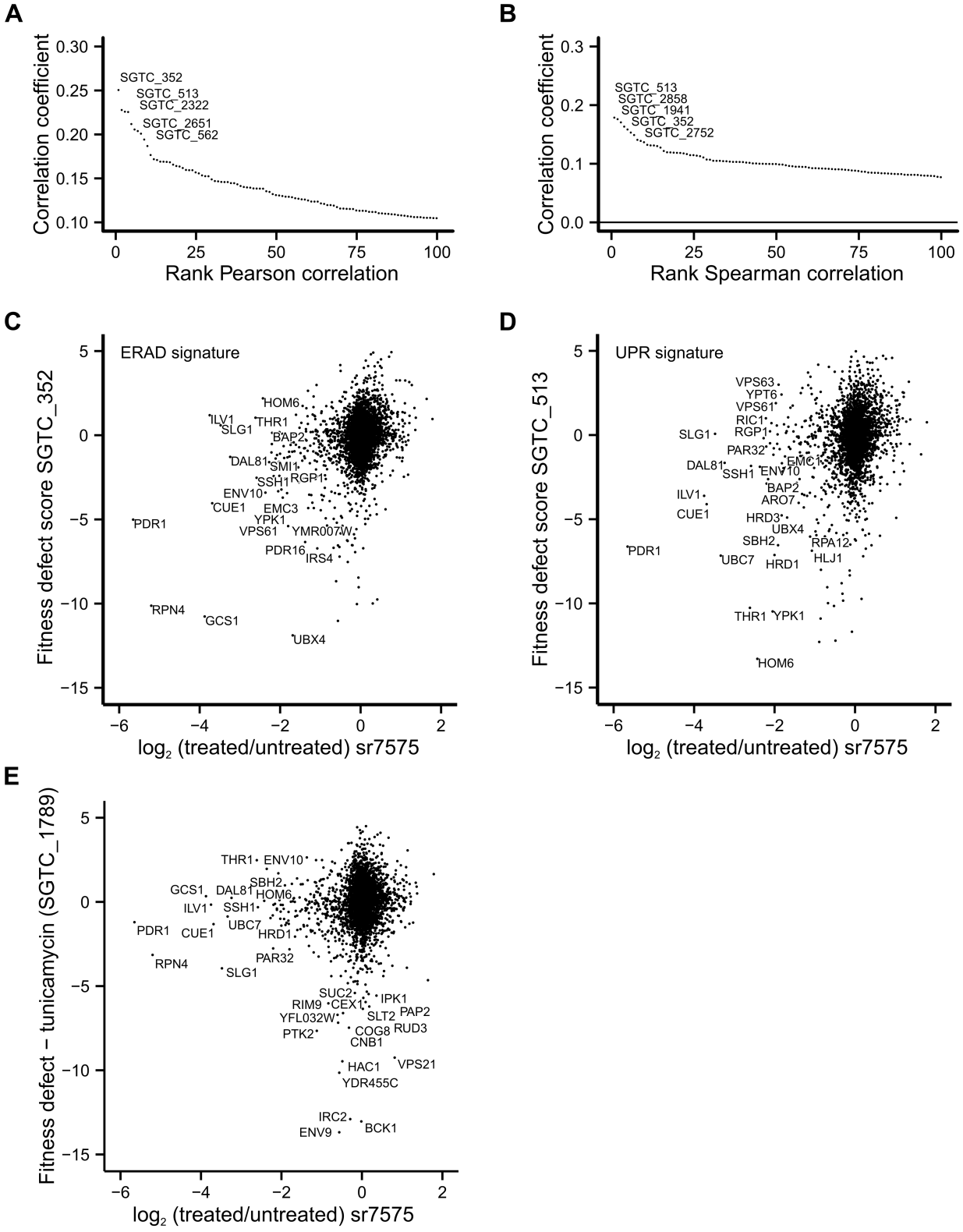

Figure S3. sr7575 profile shows little correlation with a previously published large-scale chemogenomics dataset. Computed Pearson **(A)** and Spearman **(B)** correlation coefficients between sr7575 values and previously published growth scores obtained with 3,356 compounds were ranked in descending order and the top 100 values are indicated. Among the highest correlations, we identified SGTC 352, a drug showing an ERAD signature **(C)** and SGTC 513, a compound with a UPR signature

(D) as being closest to the sr7575 profile. (E) The sr7575 profile showed no correlation with the one published for tunicamycin.

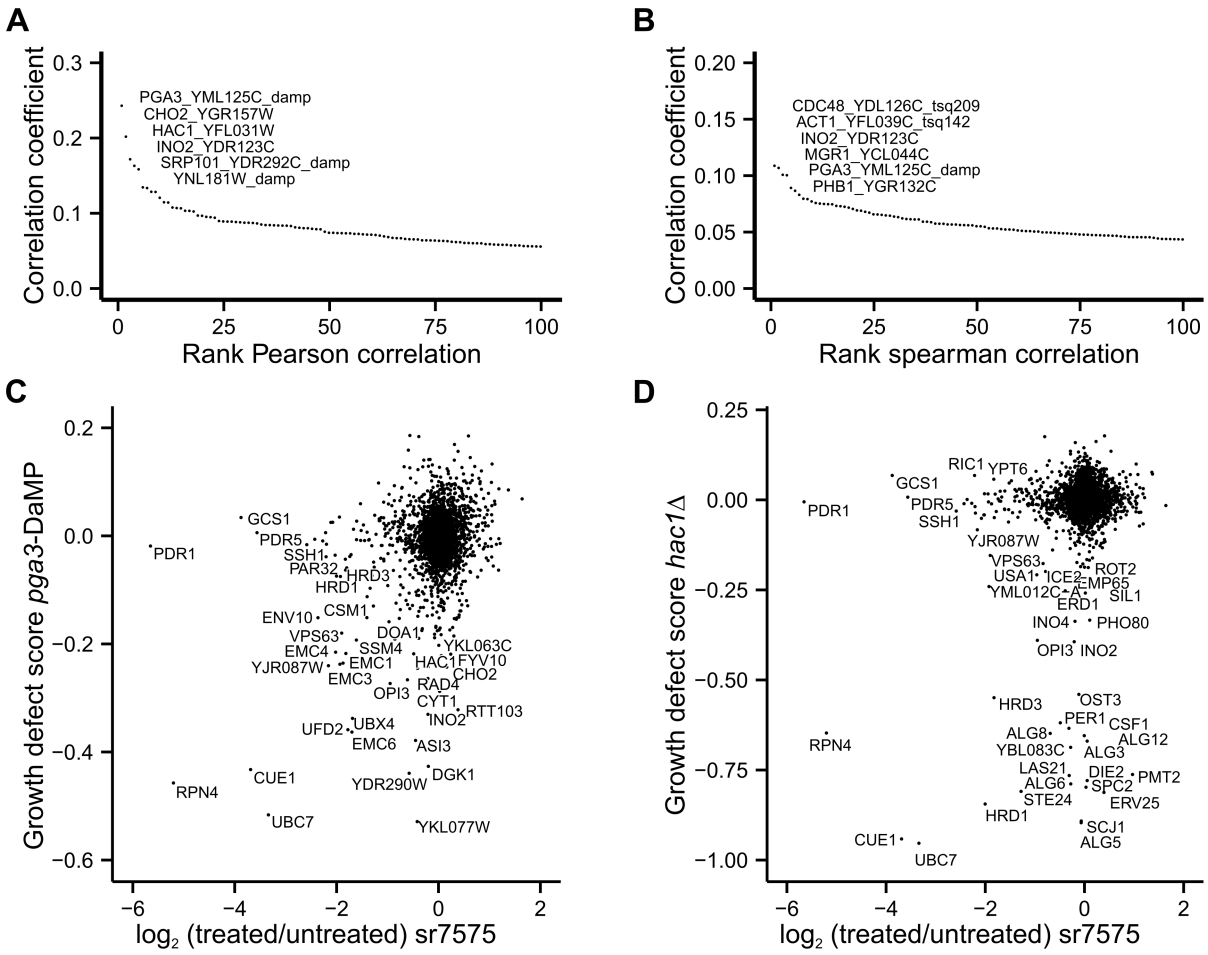

Figure S4. Perturbation of *PGA3* function shows similarities with the sensitivity profile for sr7575. Pearson **(A)** and Spearman **(B)** correlations between the sr7575 profile and 1711 previously published SGA profiles . Fitness defect scores for DAmP modification of *PGA3* are shown in **(C)**, while the interactions of *hac1*Δ and ERAD depleted strains are depicted in **(D)**.

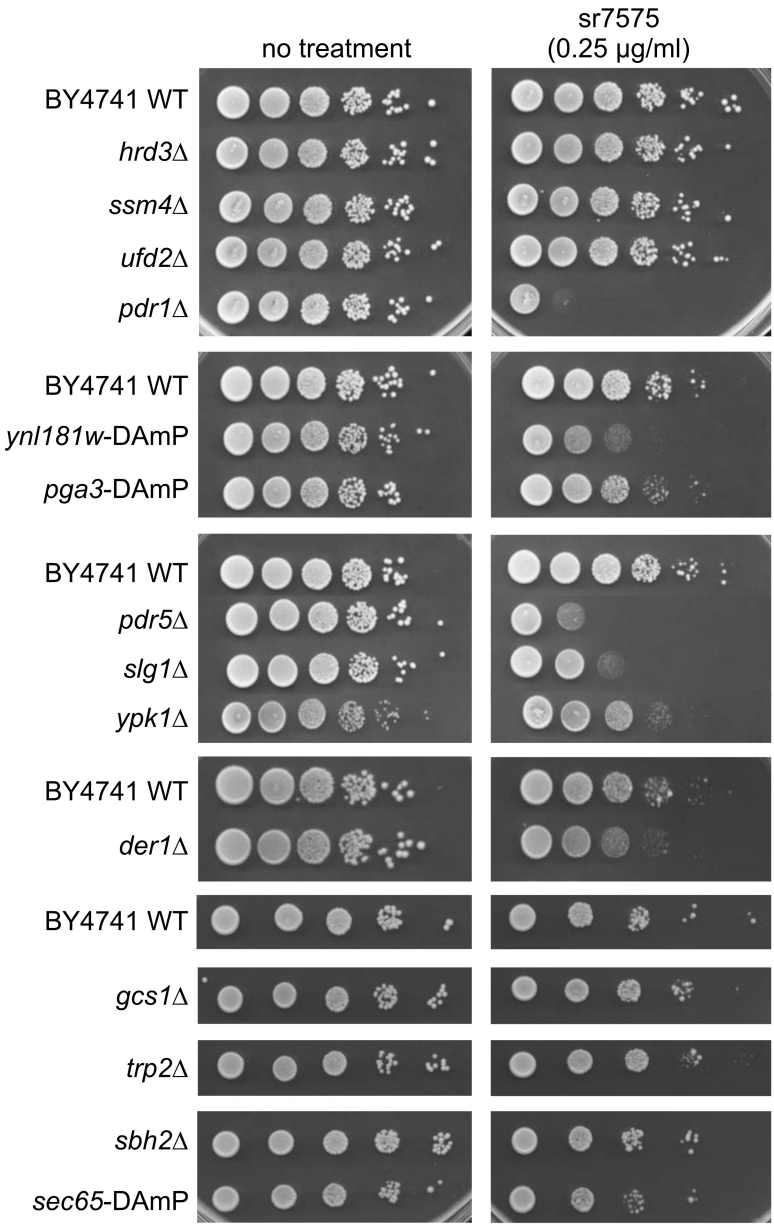

Figure S5. Susceptibility testing of yeast strains against sr7575. Mutants from the haploid deletion background were serially spotted onto SC plates supplemented with sr7575. Plates were incubated at 30°C for 48 h.

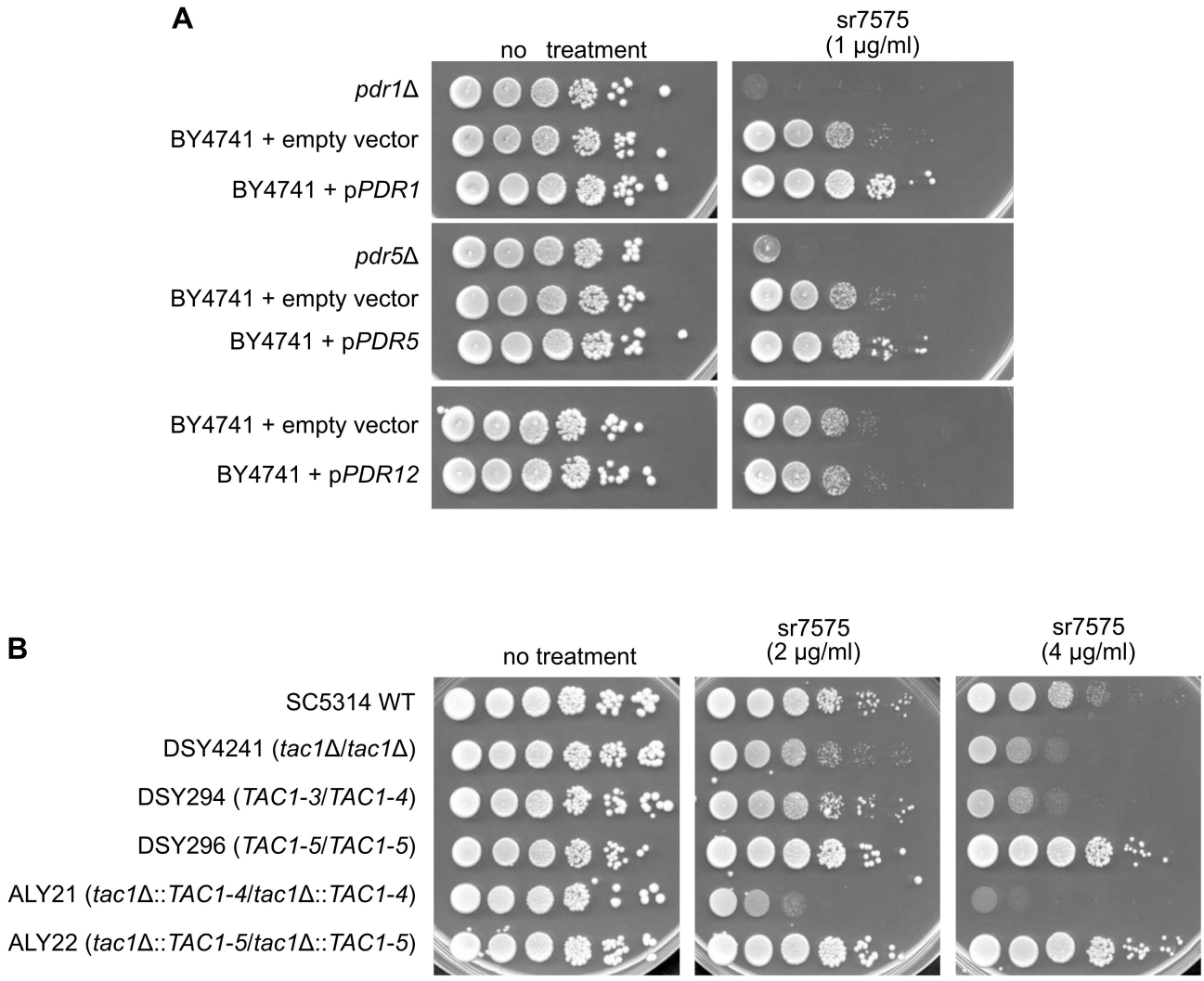

Figure S6. Susceptibility of multidrug resistant *S. cerevisiae* strains and azole resistant *C. albicans* strains to sr7575. (**A**) *S. cerevisiae* strains with deletions of or overexpressing *PDR1*, *PDR5* and *PDR12* were tested for susceptibility to sr7575 (1 µg/mL, SC medium, 30°C, 48 h). (**B**) Comparison of growth inhibition of *C. albicans* strains: WT (SC5314), *TAC1* transcription factor homozygous deletion strain (DSY4241), azole susceptible clinical isolate DSY294, azole resistant clinical isolate DSY296, azole susceptible laboratory generated strain ALY21 and azole resistant laboratory generated strain ALY22 (SC medium in the presence of 2 and 4 µg/mL sr7575, 37°C, 48 h).

Supplementary Table S1 - list of 76 compounds from the CERMN chemical library showing 90% or more growth inhibition of *Aspergillus fumigatus* at 25 µg/mL.

→ Family A:

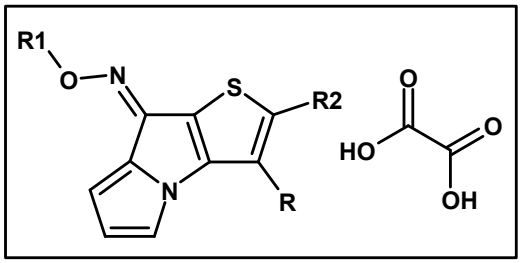

Compound	R	R1	R2	% viability
sr1304[1]	-H	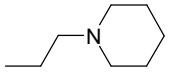	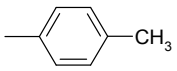	2
sr1308[2]	-H	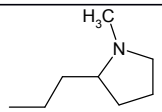	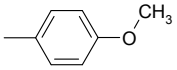	0
sr3163[2]	-H	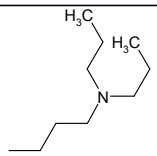	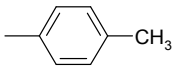	0
sr3164[2]	-H	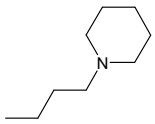	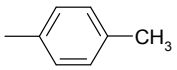	0
sr3168[3]	-H	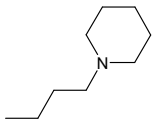	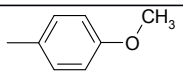	0
sr3169[2]	-H	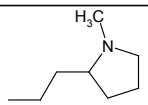	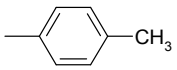	0

1 S. Rault, S. Lemaître, F. Dauphin, A. Kervabon, M. Boulouard, J.-C. Lancelot, PCT Int. Appl., WO2001014381, (2001).

2 Dual Histamine H3R/Serotonin 5-HT4R Ligands with Antiamnesic Properties: Pharmacophore-Based Virtual Screening and Polypharmacology, Lepailleur, Alban; Freret, Thomas; Lemaitre, Stephane; Boulouard, Michel; Dauphin, Francois; Hinschberger, Antoine; Dulin, Fabienne; Lesnard, Aurelien; Bureau, Ronan; Rault, Sylvain; Journal of Chemical Information and Modeling (2014), 54(6), 1773-1784.

sr3172[1]	-H	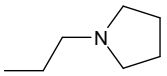	$-OCH_3$	0
sr3174[3]	-H	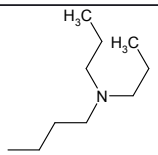	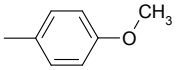	0
sr3179[2]	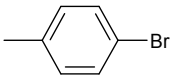	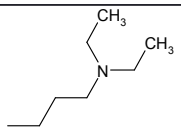	-H	0
sr3180[2]	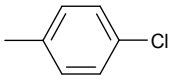	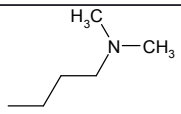	-H	0
sr3181[3]	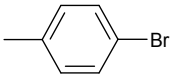	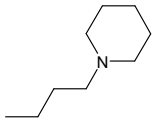	-H	0
sr3182[2]	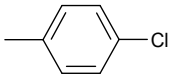	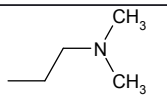	-H	0
sr3185[3]	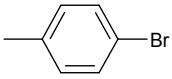	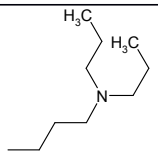	-H	0
sr3186[1]	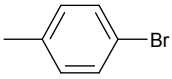	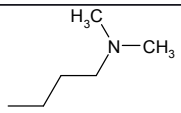	-H	0
sr3188[2]	-H	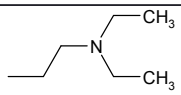	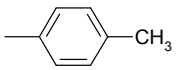	0

→ **Family B:**

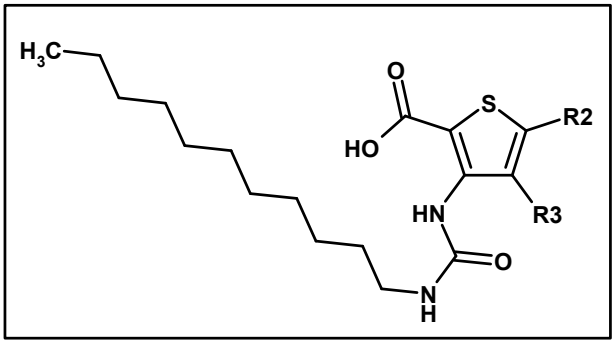

Compound	R2	R3	% viability
sr4045[1]	-H	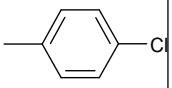	2
sr4046[1]	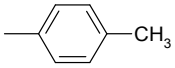	-H	0
sr4049[1]	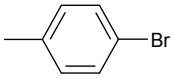	-H	0
sr4050[3]	-H	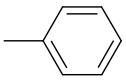	0
sr4051[1]	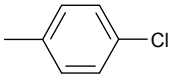	-H	0
sr4052[4]	-H	-H	0

→ **Family C:**_____

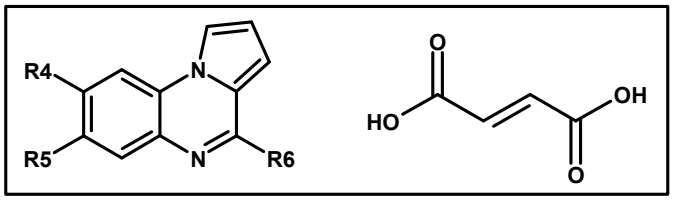

Compound	R4	R5	R6	% viability
mr22450[2]	-H	$-CH_3$	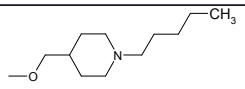	0
mr22442[2]	-H	-Cl	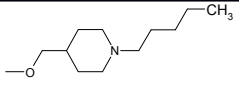	0
mr22455[2]	-H	-Cl	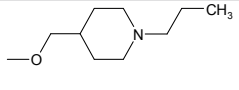	0

3 Solution-phase parallel synthesis of a 1140-member ureidothiophene carboxylic acid library, Le Foulon, Francois-Xavier; Braud, Emmanuelle; Fabis, Frederic; Lancelot, Jean-Charles; Rault, Sylvain, Journal of Combinatorial Chemistry (2005), 7(2), 253-257.

mr22461[2]	-H	-Cl	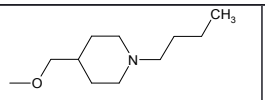	0
mr22478[2]	-H	-Cl	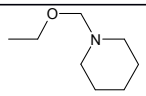	4
mr18993[4]	-Cl	-Cl	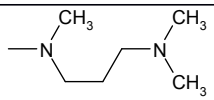	4
mr23269[3]	-H	-H	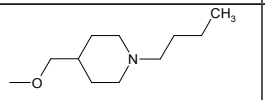	1
mr23270[1]	-H	-F	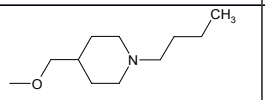	0
mr24316[1]	-H	-Cl	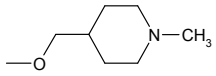	0
mr24344[3]	-H	-H	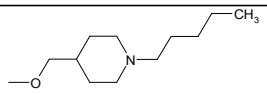	3
sr1832[5]	-H	-H		0
sr2823[1]	-H	-CH3	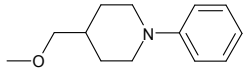	0

→ **Family D:**

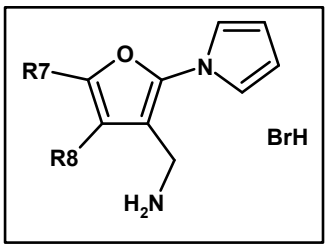

4 Synthesis of new pyrrolo[1,2-a]quinoxalines: potential non-peptide glucagon receptor antagonists, Guillon, Jean; Dallemagne, Patrick; Pfeiffer, Bruno; Renard, Pierre; Manechez, Dominique; Kervran, Alain; Rault, Sylvain, European Journal of Medicinal Chemistry (1998), 33(4), 293-308

5 Novel and Selective Partial Agonists of 5-HT3 Receptors. 2. Synthesis and Biological Evaluation of Piperazinopyridopyrrolopyrazines, Piperazinopyrroloquinoxalines, and PiperazinopyridopyrroloquinoxalinesPrunier, Herve; Rault, Sylvain; Lancelot, Jean-Charles; Robba, Max; Renard, Pierre; Delagrange, Philippe; Pfeiffer, Bruno; Caignard, Daniel-Henri; Misslin, Rene; Guardiola-Lemaitre, Beatrice; et al, Journal of Medicinal Chemistry (1997), 40(12), 1808-1819.

Compound	R7	R8	% viability
sr1457[1]	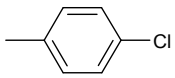	-H	0
sr1460[1]	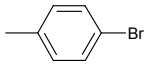	-H	0
sr1462[1]	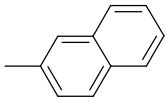	-H	2

→ **Family E:**

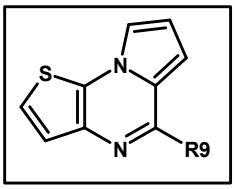

Compound	R9	% viability
sr2845[6]		0
sr3584[7]	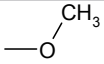	0
mr22410[8]	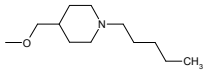	6

6 Novel Selective and Partial Agonists of 5-HT3 Receptors. Part 1. Synthesis and Biological Evaluation of Piperazinopyrrolothienopyrazines, Rault, Sylvain; Lancelot, Jean-Charles; Prunier, Herve; Robba, Max; Renard, Pierre; Delagrange, Philippe; Pfeiffer, Bruno; Caignard, Daniel-Henri; Guardiola-Lemaitre, Beatrice; Hamon, Michel, Journal of Medicinal Chemistry (1996), 39(10), 2068-80.

7 Pyrrolo[1,2-a]thieno[3,2-e]pyrazines, Rault, Sylvain; Cugnon de Sevricourt, Michel; Nguyen-Huy Dung; Robba, Max, Journal of Heterocyclic Chemistry (1981), 18(4), 739-42.

8 Novel antagonists of serotonin-4 receptors: Synthesis and biological evaluation of pyrrolothienopyrazines, Lemaitre, Stephane; Lepailleur, Alban; Bureau, Ronan; Butt-Gueulle, Sabrina; Lelong-Boulouard, Veronique; Duchatelle, Pascal; Boulouard, Michel; Dumuis, Aline; Daveu, Cyril; Lezoualc'h, Frank; et al, Bioorganic & Medicinal Chemistry (2009), 17(6), 2607-2622.

mr22422[1]	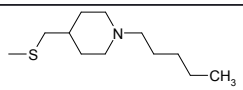	0
mr24356[1]	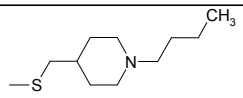	3

→ **Family F:**

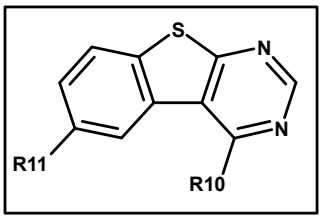

Compound	R10	R11	% viability
sr2205[9]	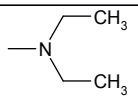	-H	3
sr2210[1]		-H	3
sr2634[1]	-Cl	$-NO_2$	0

→ **Family G:**

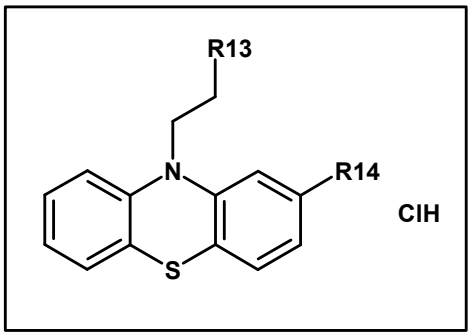

Compound	R13	R14	% viability

9 Scott, William J.; Bierer, Donald E.; Stolle, Andreas, PCT Int. pl. (2003), WO 2003057149

pa2[10]	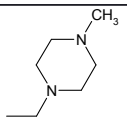	$-CF_3$	0
pa18[11]	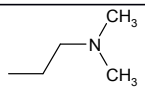	-Cl	0

→ **Singletons:**

Compound	Structure	% viability
mr19807[1]	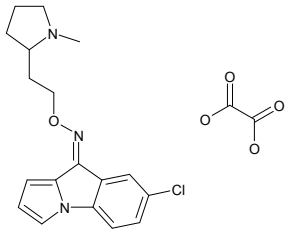	0
mr15010a[1]	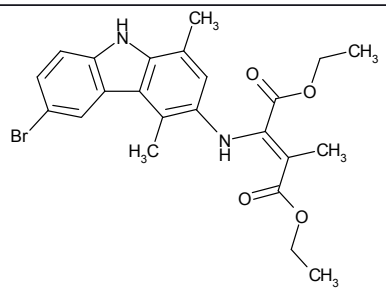	4
mr15059[12]	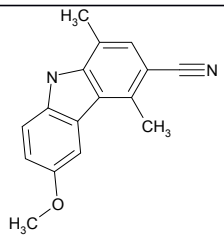	4

10 Trifluoperazine (DCI) dihydrochloride; New (trifluoromethyl)phenothiazine derivatives, Craig, P. N.; Nodiff, E. A.; Lafferty, J. J.; Ullyot, G. E., Journal of Organic Chemistry (1957), 22, 709-11.

11 Chlorpromazine (DCI) hydrochloride; Substituted 10-(dimethylaminopropyl)phenothiazines, Charpentier, Paul; Gailliot, Paul; Jacob, Robert; Gaudechon, Jacques; Buisson, Paul, Compt. rend. (1952), 235, 59-60.

12 Anti-tumor heterocycles. Part 13. The syntheses of two new pyridocarbazoles (ellipticines) and some pyrrolocarbazole analogs, Chunchatprasert, Laddawan; Dharmasena, Priyanthi; Oliveira-Campos, Ana M. F.; Queiroz, Maria J. R. P.; Raposo, Maria M. M.; Shannon, Patrick V. R. Journal of Chemical Research, Synopses (1996), (2), 84-5.

mr22633[13]	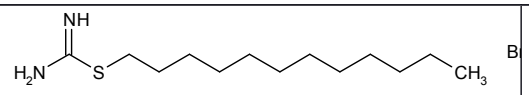	0
mr16310[14]	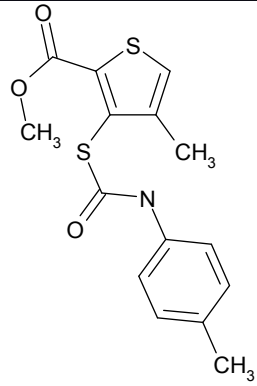	2
mr21034[15]	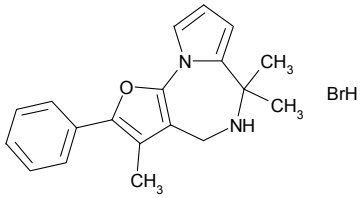	10
mr21018[1]	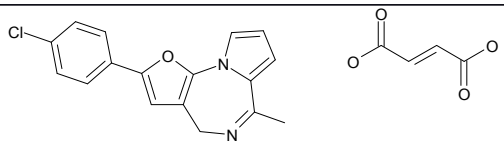	8
mr18499[16]	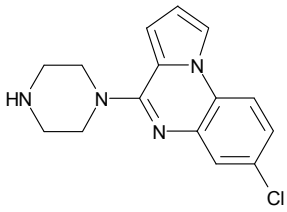	0
sr1429[1]	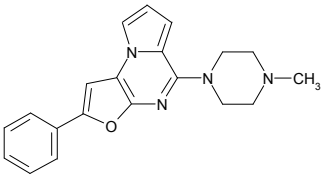	0

13 Comparative effect of a family of substituted thiopseudoureas on protein synthesis by rat liver and Walker carcinoma ribosomes, Carmona, Andres; Gonzalez-Cadavid, Nestor F., Chemico-Biological Interactions (1978), 22(2-3), 309-27.

14 Preparation of 3-mercapto-2-thiophenecarboxylic acid derivatives as intermediates for herbicides, Rault, Sylvain; Lancelot, Jean Charles; Letois, Bertrand; Robba, Max; Labat, Yves Fr. Demande (1993), FR 2689129 A1 19931001.

15 First synthesis of 5,6-dihydro-4H-furo[3,2-f]pyrrolo[1,2-a][1,4]diazepines, Feng, Xiao; Lancelot, Jean-Charles; Gillard, Alain-Claude; Landelle, Henriette; Rault, Sylvain, Journal of Heterocyclic Chemistry (1998), 35(6), 1313-1316.

16 Preparation of pyrrolopyrazines as 5-HT3 ligands, Lancelot, Jean-Charles; Prunier, Herve; Robba, Max; Delagrange, Philippe; Renard, Pierre; Adam, Gerard, Eur. Pat. Appl. (1994), EP 623620 A1 19941109.

sr1461[17]	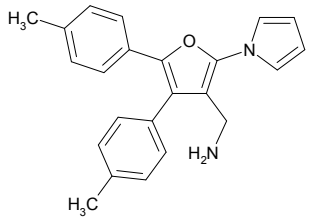	1
sr1475[18]	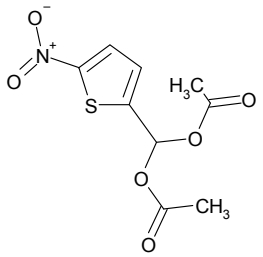	0
sr1810[1]	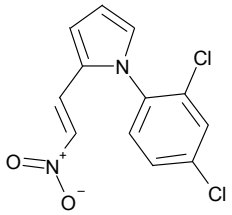	9
sr1821[19]	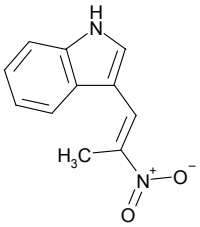	0
sr1922[20]	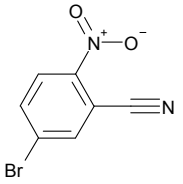	0

17 First synthesis of 4H-furo[3,2-f]pyrrolo[1,2-a][1,4]diazepines, Feng, Xiao; Lancelot, Jean-Charles; Prunier, Herve; Rault, Sylvain, Journal of Heterocyclic Chemistry (1996), 33(6), 2007-2011.

18 Synthesis and in vitro antibacterial evaluation of N-[5-(5-nitro-2-thienyl)-1,3,4-thiadiazol-2-yl] piperazinylquinolones, Foroumadi, Alireza; Mansouri, Shahla; Kiani, Zahra; Rahmani, Afsaneh, European Journal of Medicinal Chemistry (2003), 38(9), 851-854.

19 Alpha-ethyltryptamines as dual dopamine-serotonin releasers, Blough, Bruce E.; Landavazo, Antonio; Partilla, John S.; Decker, Ann M.; Page, Kevin M.; Baumann, Michael H.; Rothman, Richard B., Bioorganic & Medicinal Chemistry Letters (2014), 24(19), 4754-4758.

20 Synthesis of nitrile and benzoyl substituted poly(biphenylene oxide)s via nitro displacement reaction In, Insik; Kim, Sang Youl, Polymer (2006), 47(13), 4549-4556

sr2223	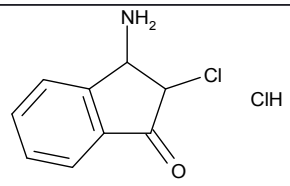	8
sr2323[1]	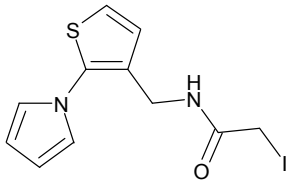	0
sr2565[21]	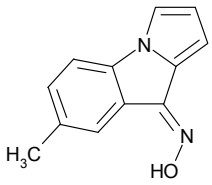	5
sr2627[22]	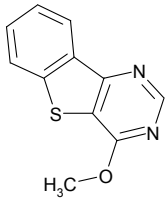	1
sr2970[23]	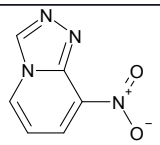	6
sr2809[24]	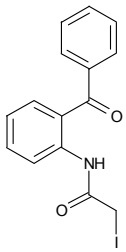	0

21 First tricyclic oximino derivatives as 5-HT3 ligands, Baglin, I.; Daveu, C.; Lancelot, J. C.; Bureau, R.; Dauphin, F.; Pfeiffer, B.; Renard, P.; Delagrange, P.; Rault, S., Bioorganic & Medicinal Chemistry Letters (2001), 11(4), 453-457.

22 [1]Benzothienopyrimidines. I. Study of 3H-benzothieno[3,2-d]pyrimid-4-one, Robba, Max; Touzot, Paulette; El-Kashef, Hussein, Journal of Heterocyclic Chemistry (1980), 17(5), 923-8.

23 Synthesis and physicochemical study of 1,2,4-triazolo[4,3-a]pyridines and of 1,2,4-triazolo[2,3-a]pyridines, Bouteau, Brigitte; Lancelot, Jean Charles; Robba, Max,Journal of Heterocyclic Chemistry (1990), 27(6), 1649-51.

24 Method of producing 2-iodoacetylaminobenzophenones, Mazurov, A. A.; Andronati, S. A.; Yakubovskaya, L. N. U.S.S.R. (1991), SU 1622365 A1 19910123.

sr2967[25]	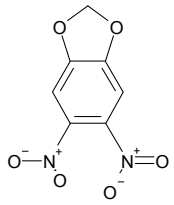	3
mr12044[1]	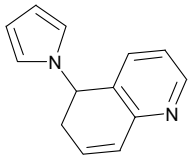	3
sr3184[1]	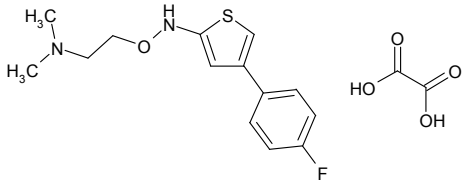	0
sr3456[2]	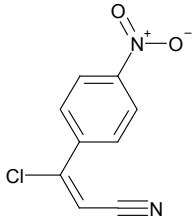	0
sr3355[26]	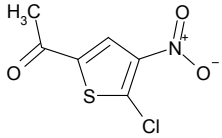	0
sr5443[1]	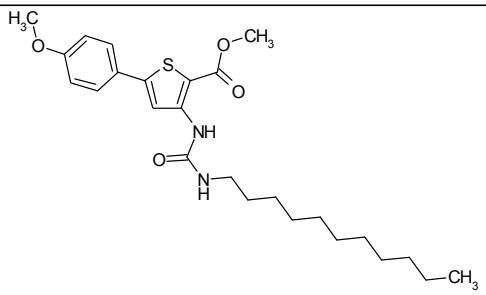	6
sr4274[1]	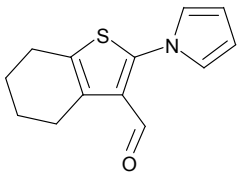	2

25 Synthesis, in vitro cytotoxic and in vivo antitumor activities of new pyrrolo[2,1-c][1,4]benzodiazepines. Part IFoloppe, M. P.; Caballero, E.; Rault, S.; Robba, M., European Journal of Medicinal Chemistry (1992), 27(3), 291-5.

26 Selective Dual Inhibitors of the Cancer-Related Deubiquitylating Proteases USP7 and USP47, Weinstock, Joseph; Wu, Jian; Cao, Ping; Kingsbury, William D.; McDermott, Jeffrey L.; Kodrasov, Matthew P.; McKelvey, Devin M.; Suresh Kumar, K. G.; Goldenberg, Seth J.; Mattern, Michael R.; et al, ACS Medicinal Chemistry Letters (2012), 3(10), 789-792.

sr4080[27]	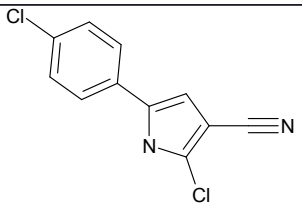	8
sr4211[28]	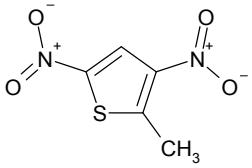	8
mr24355[10]	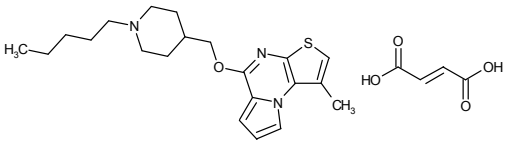	0

27 Insecticidal action and mitochondrial uncoupling activity of AC-303,630 and related halogenated pyrroles, Black, Bruce C.; Hollingworth, Robert M.; Ahammadsahib, Kabeer I.; Kukel, Christine D.; Donovan, Stephen Pesticide Biochemistry and Physiology (1994), 50(2), 115-28.

28 Synthesis of dinitro-substituted furans, thiophenes, and azoles, Katritzky, Alan R.; Vakulenko, Anatoliy V.; Sivapackiam, Jothilingam; Draghici, Bogdan; Damavarapu, Reddy Synthesis (2008), (5), 699-706.

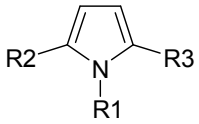

Compound	R1	R2	R3	MIC_{100} (µg/ml)
sr7575 (1)	2,4-dichlorophenyl	H	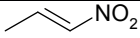	2.4-4.8
3	2,4-dichlorophenyl	CH_3	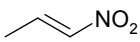	> 26-32
4	2,4-dichlorophenyl	H	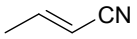	> 26-32
5	2,4-dichlorophenyl	H		> 26-32
6	4-chlorophenyl	H	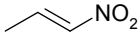	2.4-4.8
7	3-chlorophenyl	H	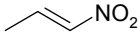	9.6
8	2-chlorophenyl	H	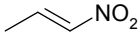	13 - 26
9	3,4-dichlorophenyl	H	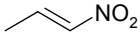	9.6
10	2,3-dichlorophenyl	H	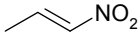	19.2
11	2,5-dichlorophenyl	H	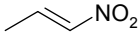	> 38.5
12	3,5-dichlorophenyl	H	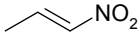	9.6
13	2,6-dichlorophenyl	H	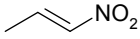	19.2
14	2,4,5-trichlorophenyl	H	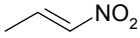	9.6
15	2,4,6-trichlorophenyl	H	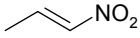	26 - 32
16	2-fluoro-4-chlorophenyl	H	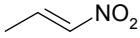	13 - 26
17	2-chloro-4-fluorophenyl	H	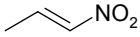	13
18	2,4-dibromophenyl	H	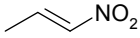	13 - 26
19	2-bromo-4-chlorophenyl	H	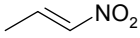	13 - 26
20	2-chloro-4-bromophenyl	H	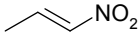	13
21	2-iodo-4-chlorophenyl	H	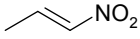	26
22	2-chloro-4-iodophenyl	H	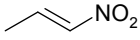	26

Supplementary Table S2: Analogues of sr7575 and MIC values against *A. fumigatus*.

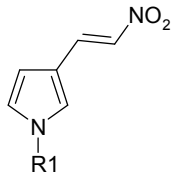

Compound	R1	MIC_{100} (µg/ml)
sr7576 (2)	2,4-dichlorophenyl	> 38.5
23	3-chlorophenyl	26 - 32
24	3,4-dichlorophenyl	26 - 32
25	3,5-dichlorophenyl	26 - 32
26	2,6-dichlorophenyl	38.5
27	2,4,6-trichlorophenyl	38.5
28	2-bromo-4-chlorophenyl	> 26 - 32
29	2-chloro-4-bromophenyl	> 26 - 32
30	2,4-dibromorophenyl	> 26 - 32
31	2-iodo-4-chlorophenyl	> 26 - 32
32	2-chloro-4-iodophenyl	>26 - 32

Supplementary Table S3: Analogues of sr7576 and MIC values against *A. fumigatus*.

Supplementary Table S4 - Strains and plasmids used in this study

Strain	Genotype	Reference
BY4741	MATa;*his3*Δ 1;*leu2*Δ 0;*met15*Δ 0;*ura3*Δ 0	Brachmann et al, 1998

(Deletion mutants were generated in the Sc BY4741 background)		Reference
*aro7*Δ	*aro7*::KanMX4	Giaever et al, 2002
*cue1*Δ	*cue1*::KanMX4	
*der1*Δ	*der1*::KanMX4	
*doa10*Δ	*doa10*::KanMX4	
*emc1*Δ	*emc1*::KanMX4	
*emc3*Δ	*emc3*::KanMX4	
*gcs1*Δ	*gcs1*::KanMX4	
*hac1*Δ	*hac1*::KanMX4	
*hrd1*Δ	*hrd1*::KanMX4	
*hrd3*Δ	*hrd3*::KanMX4	
*ire1*Δ	*ire1*::KanMX4	
*pdr1*Δ	*pdr1*::KanMX4	
*pdr5*Δ	*pdr5*::KanMX4	
pga3-DAmP	*pga3*-DAmP (KanMX4)	
*rpn4*Δ	*rpn4*::KanMX4	
*sbh2*Δ	*sbh2*::KanMX4	
sec65-DAMP	*sec65*-DAmP (KanMX4)	
*slg1*Δ	*slg1*::KanMX4	
*ssh1*Δ	*ssh1*::KanMX4	
*trp2*Δ	*trp2*::KanMX4	
*ubc7*Δ	*ubc7*::KanMX4	
*ufd2*Δ	*ufd2*::KanMX4	
ynl181w-DAmP	*ynl181w*-DAmP (KanMX4)	
*ypk1*Δ	*ypk1*::KanMX4	

***A. fumigatus* strains used in this study:**

Strain	Genotype	Reference
kuA	akuA::*ptrA*	Krappmann et al, 2006
*derA*Δ	akuA::ptr*A, derA*::*hph*	Richie DL et al 2011
*hacA*Δ	akuA::*ptrA, hacA*::*hph*	Richie DL et al 2009
*hrdA*Δ	akuA::*ptrA, hrdA*::*hph*	Krishnan K et al 2013
*ireA*Δ	akuA::*ptrA, ireA*::*ble*	Jeng X et al 2011
*derA*Δ/*hacA*Δ	akuA:*ptrA, hacA*::*hph,derA*::*ble*	Richie DL et al 2011
*derA*Δ/*hrdA*Δ	akuA::*ptrA, hrdA*::*hph, derA*::*ble*	Krishnan K et al 2013

Other yeast strains used in this study:

Strain	Genotype	Reference
C. albicans SC5314	wild type	Lohberger et al, 2014
DSY4241	*tac1*Δ::*FRT*/*tac1*Δ::*FRT*	
DSY294	azole susceptible clinical isolate (*TAC1-3/TAC1-4*)	
DSY296	azole resistant clinical isolate (*TAC1-5*/*TAC1-5* ; N977D mutation)	
ALY21	*tac1*Δ::*TAC1-4-FRT*/*tac1*Δ::*TAC1-4-FRT*	
ALY22	*tac1*Δ::*TAC1-5-FRT*/*tac1*Δ::*TAC1-5-FRT*	
C. neoformans H99	wild type	Perfect et al, 1980

MoBY plasmid (library v1.1) complemented *S. cerevisiae* strains:

Strain	Genotype+ MoBY clone identifier	Reference
*aro7*Δ+*ARO7*	*aro7*::KanMX4+ YPR060C::29NP_C9	Ho et al, 2009
*cue1*Δ+*CUE1*	*cue1*::KanMX4+ YMR264W::33NP_H12	
*emc1*Δ+*EMC1*	*emc1*::KanMX4+ YCL045C::41NP_D8	
*emc3*Δ+*EMC3*	*emc3*::KanMX4+ YKL207W::8NP_A12	
*hrd1*Δ+*HRD1*	*hrd1*::KanMX4+ YOL013C::12NP_G12	
*rpn4*Δ+*RPN4*	*rpn4*::KanMX4+ YDL020C::30NP_F2	
*ssh1*Δ+*SSH1*	*ssh1*::KanMX4+ YBR283C::37NP_A11	
*ubc7*Δ+*UBC7*	*ubc7*::KanMX4+ YMR022W::36NP_G3	

YGPM systematic overexpression library in *S. cerevisiae* strains:

Strain	Genotype+ YGPM clone identifier	Reference
Control	BY4741+ YGPM22k06 chrIII:151898...152647	Jones et al, 2008
PDR1	BY4741+ YGPM26h12 chrVII:466658...477209	
PDR5	BY4741+ YGPM33k24 chrXV:619141...631341	
PDR12	BY4741+ YGPM8p07 chrXVI:444386...454435	

References :

Brachmann CB, Davies A, Cost GJ, Caputo E, Li J, Hieter P, Boeke JD. Yeast. 1998 14(2):115-32.
Krappmann S, Sasse C, Braus GH. Eukaryot Cell. 2006 5(1):212-5.
Jones GM, Stalker J, Humphray S, West A, Cox T, Rogers J,
Dunham I, Prelich G. Nature Methods. 2008 5:239-241
Lohberger A, Coste AT, Sanglard D. Eukaryot Cell. 2014 13(1):127-42
Perfect, JR, Lang SDR, and Durack DT. Am. J. Pathol. 1980 101:177-194.

Supplementary Table S5 - list of oligonucleotides used in this study

List of oligonucleotides to screen deletion/DAmP mutants:

Gene	Primer name	Sequence
Kanamycin	KANMX-FW	5'-AGATGCGAAGTTAAGTGCGC-3'
ARO7	ARO7dR	5'-GAGAGAAGGTCATGGATGTG-3'
CUE1	CUE1dR	5'-GTAAGGGGAGAAGAACGTTC-3'
DER1	DER1dR	5'-TCTGCAAACGGACACCAAGT-3'
EMC1	EMC1dR	5'-GCACATCATTTCCAGACGAG-3'
EMC3	EMC3dR	5'-GCGAGGACTTTTTGCCATAC-3'
GCS1	GCS1dR	5'-GTGGTAGTTCTCTCTCCTTG-3'
HAC1	HAC1dR	5'-AGAGCCGTGAGAGTGAGAGT-3'
HRD1	HRD1dR	5'-TATGTCACCTTCCTATGCCG-3'
HRD3	HRD3dR	5'-ATGAACGGCAATTTGAGACC-3'
IRE1	IRE1dR	5'-TCTTGCACTTTTCGCCATGC-3'
PDR1	PDR1dR	5'-TGGCAACTATGTGGTGCAAT-3'
PDR5	PDR5dR	5'-GCATCTTGCTCTTTCCTCTC-3'
RPN4	RPN4dR	5'-CTGGGTACGAATTCAAGGAG-3'
SBH2	SBH2dR	5'-CATGCACCCTTAACATCGTC-3'
SEC65	SEC65-DAmP	5'-GGAAGTTGTGAGTACTGACG-3'
SLG1	SLG1dR	5'-TATATCGTCTTTCAACGCGG-3'
SSH1	SSH1dR	5'-CCACGAAGCAAGGTAACAAG-3'
SSM4	SSM4dR	5'-GACGAGGGCTAAGCAGTTTG-3'
TRP2	TRP2dR	5'-CCAAACCACATTGGTCTAGG-3'
UBC7	UBC7dR	5'-TACTGTACGGCTTGGAAGAG-3'
UFD2	UFD2dR	5'-ACCGTCATCAACGAACAACA-3'
YPK1	YPK1dR	5'-CCGTTCGTGGTTAAGGTAAG-3'

List of oligonucleotides to screen MoBY plasmids:

Gene	Primer name	Sequence
ARO7	ARO7iF	5'-TCGCCACATGTCCTTCAGTT-3'
	ARO7iR	5'-GCAAGTATTCCACCTCAACTTCC-3'
CUE1	CUE1iF	5'-ATGGAGGATTCGAGATTGCTT-3'
	CUE1iR	5'-CTGGCTTGCCAAACCAACAA-3'
EMC1	EMC1iF	5'-TGCCCCTTCTACGACCATTT-3'
	EMC1iR	5'-TGCCATTCGTGTCATGCTCT-3'
EMC3	EMC3iF	5'-ACCAGCTGAAGTATTGGGTCC-3'
	EMC3iR	5'-TATCCCGGCCTGAATACCCA-3'
HRD1	HRD1iF	5'-TGCGTGTATTCAGCCACCAA-3'
	HRD1iR	5'-GCCAAGATATCCCACACCACA-3'
RPN4	RPN4iF	5'-GCGAAACCCCATTGCAGAAG-3'
	RPN4iR	5'-TGGTGATGCAGTCGAAGGTT-3'
SSH1	SSH1iF	5'-TTGGTCGGTGCTGGCATATT-3'
	SSH1iR	5'-GGATGCACCCGTAACAGCT-3'
UBC7	UBC7iF	5'-CGAAAACCGCTCAGAAACGT-3'
	UBC7iR	5'-GCATCAATGTTGGCACCACT-3'

Supporting information (S1) - Synthesis of sr7575-related compounds.

General Methods

All chemical reagents and solvents were purchased from commercial sources and used without further purification. Thin-layer chromatography (TLC) was performed on silica gel plates. Silica gel 0.06−0.2 mm, 60 Å was used for all column chromatography. Melting points were determined on a Kofler melting point apparatus. NMR spectra were recorded on a BRUKER AVANCE III 400 MHz (^{1}H NMR at 399.8 MHz and ^{13}C NMR at 100 MHz) with the solvents indicated. Chemical shifts are reported in parts per million (ppm) on the δ scale and referenced to the appropriate solvent peak. High-resolution mass spectral (HRMS) were performed on a BRUKER maxis mass spectrometer by the "fédération de Recherche" ICOA / CBM (FR2708) platform. LC-MS Analysis was performed on a Waters alliance 2695 using the following gradient: A (95%)/B (5%) to A (5%)/B (95%) in 4 min. This ratio was held for 1.5 min before returning to initial conditions in 0.5 min. Initial conditions were then maintained for 2 min (A, H $_2$O; B, MeCN; each containing 0.1% HCOOH; column, C18 Xbridge 4.6 x 50 mm / 2.5 µm). MS detection was performed with a SQDetector.

Compound sr1810: Mixture of (*E*) 1-(2,4-Dichlorophenyl)-2-(2-nitrovinyl)-1*H*-pyrrole [75%] and (*E*) 1-(2,4-Dichlorophenyl)-3-(2-nitrovinyl)-1H-pyrrole [25%].

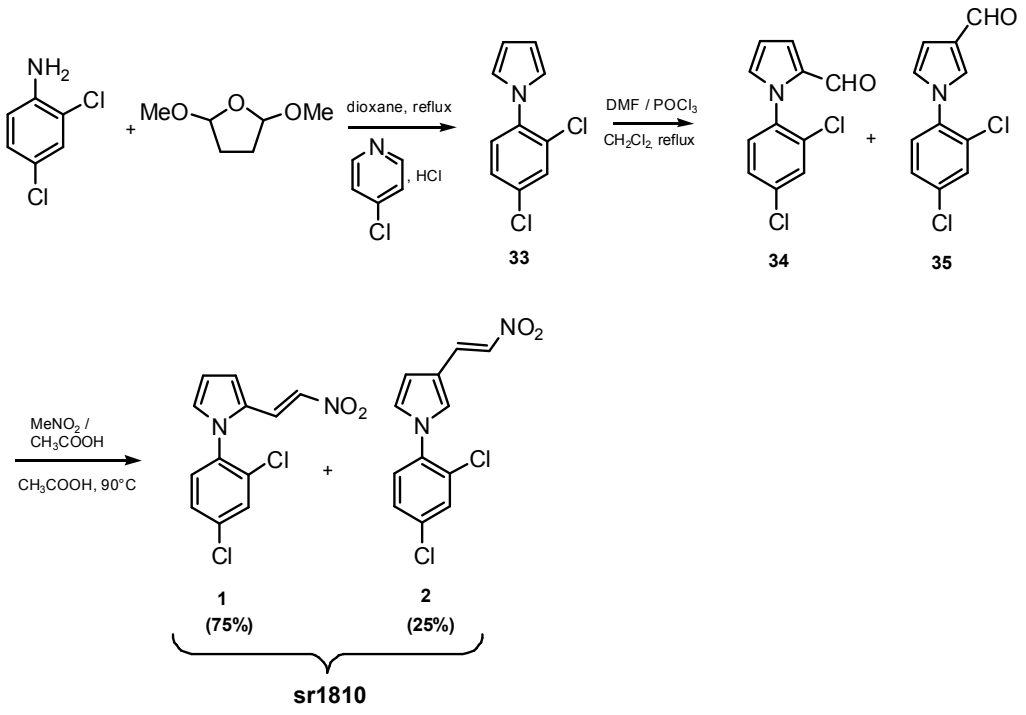

1-(2,4-Dichlorophenyl)-1*H*-pyrrole (**33**).[1] 4-chloropyridine, hydrochloride (9.25 g, 0.0617 mol) and 2,5-dimethoxytetrahydrofuran (8.15 g, 0.0617 mol) were stirred in 150 mL of dioxane at room temperature for 30 min. 2,4-dichloroaniline (10 g, 0.0617 mol) was then added and the mixture was stirred at reflux for 4 h. The reaction was cooled down to room temperature and concentrated under vacuum. 150 mL of water were added to the residue, followed by 200 mL of Et $_2$O. The aqueous layer was extracted with Et $_2$O (2x 100 mL). The

[1] Azizi, N. *et al.* Iron-catalyzed inexpensive and practical synthesis of N-substituted pyrroles in water. *Synlett*, **14**, 2245-2248 (2009).

combined organic layers were washed with HCl 1N (200 mL) and water (2x 200 mL), dried over $MgSO_4$ and concentrated under vacuum. The resulting residue was purified by chromatography on silica gel using CH_2Cl_2 as eluant to give compound **33** as a brown oil (11.4 g, 87%). ^{1}H NMR (400 MHz, $CDCl_3$) δ 7.56 (d, *J* = 2.2 Hz, 1H), 7.35 (dd, *J* = 8.7 and 2.3 Hz, 1H), 7.31 (d, *J* = 8.6 Hz, 1H), 6.92 (t, *J* = 2.1 Hz, 2H), 6.39 (t, *J* = 1.9 Hz, 2H). ^{13}C NMR (100 MHz, $CDCl_3$) δ 137.5, 133.3, 130.5, 130.4, 128.5, 127.9, 122.1, 109.7.

Mixture of 1-(2,4-Dichlorophenyl)-1*H*-pyrrole-2-carbaldehyde (**34**) and 1-(2,4-Dichlorophenyl)-1*H*-pyrrole-3-carbaldehyde (**35**). Dimethylformamide (2.20 mL, 0.0283 mol) was stirred at 0°C. Phosphorus oxychloride (2.7 mL, 0.0283 mol) was then added dropwise and the white solid obtained was stayed cold for 30 min. After this time, a solution of compound **33** (6 g, 0.0283 mol) in 120 mL of CH_2Cl_2 was slowly added dropwise to the reaction mixture. The reaction was refluxed for 20 h. After cooling, 120 mL of water were added and the mixture was stirred at room temperature for 30 min. Then, the layers were separated and the aqueous layer was alkalized with 20% sodium hydroxide solution. This aqueous layer was extracted with Et_2O (2x 120 mL). The combined organic layers were dried over $MgSO_4$ and concentrated under vacuum. The mixture of compound **34** and **35** was engaged in the next tape without further purification and was obtained as brown solid (4.4 g, 65%). LC-MS (ESI): t_R = 4.66 and 4.79 min; $[M+H]^+$ 240.35. HRMS for $C_{11}H_8Cl_2NO$ $[M+H]^+$ calculated mass: 239.9977 , measured: 239.9974.
Compound **34**: ^{1}H NMR (400 MHz, $CDCl_3$) δ 9.44 (s, 1H), 7.44 (d, *J* = 2.3 Hz, 1H), 7.26 (dd, *J* = 8.6 and 2.0 Hz, 1H), 7.20 (d, *J* = 8.4 Hz, 1H), 7.04 (dd, *J* = 1.4 and 4.0 Hz, 1H), 6.86 (m, 1H), 6.37 (dd, *J* = 4.0 and 2.8 Hz, 1H). ^{13}C NMR (100 MHz, $CDCl_3$) δ 178.5, 136.0, 135.2, 132.9, 132.9, 131.1, 130.0, 129.6, 127.7, 123.2, 111.2.
Compound **35**: ^{1}H NMR (400 MHz, $CDCl_3$) δ 9.79 (s, 1H), 7.50 (d, *J* = 2.3 Hz, 1H), 7.40 (t, *J* = 1.7 Hz, 1H), 7.31 (dd, *J* = 8.5 and 2.3 Hz, 1H), 7.25 (d, *J* = 8.4 Hz, 1H), 6.80 (t, *J*= 2.8 Hz, 1H), 6.73 (m, 1H). ^{13}C NMR (100 MHz, $CDCl_3$) δ 185.4, 136.1, 135.0, 130.8, 130.7, 130.0, 128.4, 128.2, 127.8, 124.8, 108.8.

sr1810: Mixture of (*E*) 1-(2,4-Dichlorophenyl)-2-(2-nitrovinyl)-1*H*-pyrrole (**1**) and (*E*) 1-(2,4-Dichlorophenyl)-3-(2-nitrovinyl)-1*H*-pyrrole (**2**). Nitromethane (54 mL, 1 mol) and ammonium acetate (15.4 g, 0.2 mol) were stirred in 100 mL of acetic acid at 30°C for 30 min. Then, the mixture of compounds **34** and **35** (12 g, 0.05 mol) was added and the solution was heated at 90°C for 24 h. Then, the reaction was concentrated under vacuum. A saturated solution of sodium hydrogenocarbonate (100 mL) was added to the residue. This aqueous layer was extracted with EtOAc (2x 100mL). The organic layers were washed with water (2x 100 mL), dried over $MgSO_4$ and concentrated under vacuum. The mixture of compound **1** and **2** was obtained as a yellow solid (8.7 g, 61%). Mp: 114 °C. LC-MS (ESI): t_R = 5.22 and 5.32 min; $[M+H]^+$ 283.31. HRMS for $C_{12}H_9Cl_2N_2O_2$ $[M+H]^+$ calculated mass: 283.0035, measured: 283.0035.
Compound **1**: ^{1}H NMR (400 MHz, $CDCl_3$) δ 7.62 (d, *J* = 2.3 Hz, 1H), 7.56 (d, *J* = 13.3 Hz, 1H), 7.45 (dd, *J* = 8.4 and 2.3 Hz, 1H), 7.33 (d, *J* = 8.4 Hz, 1H), 7.17 (d, *J* = 13.4 Hz, 1H), 7.00 (m, 1H), 6.95 (m, 1H), 6.49 (m, 1H). ^{13}C NMR (100 MHz, $CDCl_3$) δ 136.4, 134.3, 133.4, 132.6, 130.8, 130.3, 130.0, 128.4, 127.4, 125.8, 116.7, 112.3.
Compound **2**: ^{1}H NMR (400 MHz, $CDCl_3$) δ 8.04 (d, *J* = 13.4 Hz, 1H), 7.58 (d, *J* = 2.3 Hz, 1H), 7.47 (d, *J* = 13.2 Hz, 1H), 7.39 (dd, *J* = 8.4 and 2.3 Hz, 1H), 7.30-7.26 (m, 2H), 6.92 (m, 1H), 6.56 (m, 1H). ^{13}C NMR (100 MHz, $CDCl_3$) δ 136.0, 134.9, 134.2, 133.2, 130.9, 130.8, 128.3, 128.2, 127.9, 125.5, 116.8, 108.3.

(*E*) 1-(2,4-Dichlorophenyl)-2-(2-nitrovinyl)-1*H*-pyrrole (1 or sr7575**)**. See **Supplementary Fig.1a**.

1-(2,4-Dichlorophenyl)-1*H*-pyrrole-2-carbaldehyde (**34**). Dimethylformamide (2.20 mL, 0.0283 mol) was stirred at 0°C. Phosphorus oxychloride (2.7 mL, 0.0283mol) was then added dropwise and the white solid obtained was cooled for 30 min. After this time, a solution of compound **33** (6 g, 0.0283 mol) in 120 mL of CH_2Cl_2 was added dropwise to the reaction mixture. The reaction was refluxed for 20 h. After cooling to room temperature, 120 mL of water were added and the mixture was stirred at room temperature for 30 min. Then, the layers were separated and the aqueous layer was alkalized with 20% sodium hydroxide solution. This aqueous layer was extracted with Et_2O (2x 120 mL) and the organic layers were dried over $MgSO_4$ and concentrated under vacuum. The residue was purified by chromatography on silica gel using cyclohexane and CH_2Cl_2 as eluants (50/50) to afford compound **34** as a beige solid (2.1 g, 30%). ^{1}H NMR (400 MHz, $CDCl_3$) δ 9.44 (s, 1H), 7.44 (d, J = 2.3 Hz, 1H), 7.26 (dd, J = 8.6 and 2.0 Hz, 1H), 7.20 (d, J = 8.4 Hz, 1H), 7.04 (dd, J = 4.0 and 1.4 Hz, 1H), 6.86 (m, 1H), 6.37 (dd, J = 4.0 and 2.8 Hz, 1H). ^{13}C NMR (100 MHz, $CDCl_3$) δ 178.5, 136.0, 135.2, 132.9, 132.9, 131.1, 130.0, 129.6, 127.7, 123.2, 111.2. LC-MS (ESI): t_R = 4.79 min; $[M+H]^+$ 240.35. HRMS for $C_{11}H_8Cl_2NO$ $[M+H]^+$ calculated mass: 239.9977 , measured: 239.9974.

(*E*) 1-(2,4-Dichlorophenyl)-2-(2-nitrovinyl)-1*H*-pyrrole **(1)**. Nitromethane (54 mL, 1 mol) and ammonium acetate (15.4 g, 0.2 mol) were stirred in 100 mL of acetic acid at 30°C for 30 min. Then, 1-(2,4-dichlorophenyl)-1*H*-pyrrole-2-carbaldehyde (12 g, 0.05 mol) was added and the mixture was heated at 90°C for 24 h. Then, the reaction was concentrated under vacuum. A saturated solution of sodium hydrogenocarbonate (100 mL) was added to the residue. The aqueous layer was extracted with EtOAc (2x 100mL). The combined organic layers were washed with water (2x 100 mL), dried over $MgSO_4$ and concentrated under vacuum. The resulting residue was purified by chromatography on silica gel using cyclohexane and CH_2Cl_2 as eluant (50/50) to obtain compound **1** as a yellow solid (6.6 g, 47%). Mp: 118°C. ^{1}H NMR (400 MHz, $CDCl_3$) δ 7.62 (d, J = 2.3 Hz, 1H), 7.56 (d, J = 13.3 Hz, 1H), 7.45 (dd, J = 2.3 and 8.3 Hz, 1H), 7.33 (d, J = 8.4 Hz, 1H), 7.17 (d, J = 13.4 Hz, 1H), 7.00 (m, 1H), 6.95 (m, 1H), 6.49 (m, 1H). ^{13}C NMR (100 MHz, $CDCl_3$) δ 136.4, 134.3, 133.4, 132.6, 130.8, 130.3, 130.0, 128.4, 127.4, 125.8, 116.7, 112.3. LC-MS (ESI): t_R= 5.20 min; $[M+H]^+$ 283.44. HRMS for $C_{12}H_9Cl_2N_2O_2$ $[M+H]^+$ calculated mass: 283.0035, measured: 283.0036.

(*E*) 1-(2,4-Dichlorophenyl)-3-(2-nitrovinyl)-1*H*-pyrrole (2 or sr7576**)**. See **Supplementary Fig.1b**.

1-(2,4-Dichlorophenyl)-1*H*-pyrrole-3-carbaldehyde (**35**).[2] 4-chloropyridine, hydrochloride (9.88 g, 0.0617 mol) and 2,5-Dimethoxy-3-tetrahydrofurancarboxaldehyde (8.15 g, 0.0617 mol) were stirred in 150 mL of dioxane at room temperature for 30 min. 2,4-dichloroaniline (10 g, 0.0617 mol) was then added and the mixture was stirred at reflux for 4 h. The reaction was cooled to room temperature and concentrated under vacuum. 150 mL of water were added to the residue, followed by 200 mL of Et_2O. The aqueous layer was extracted with Et_2O (2x 100 mL). The combined organic layers were washed with 1N HCl (200 mL) and water (2x 200 mL), dried over $MgSO_4$ and concentrated under vacuum. The resulting residue was purified by chromatography on silica gel using CH_2Cl_2 as eluant to afford compound **35** as a

[2] Dallemagne, P. *et al*. A convenient rearrangement of 1-phenylpyrrole-2-carboxaldehydes into their 3-isomers. *Synthetic Communications*. **13**, 1855-1857 (1994).

beige solid (5.2 g, 35%). Mp: 186°C. ^{1}H NMR (400 MHz, $CDCl_3$) δ 9.79 (s, 1H), 7.50 (d, *J* = 2.3 Hz, 1H), 7.40 (t, *J* = 1.7 Hz, 1H), 7.31 (dd, *J* = 8.5 and 2.3 Hz, 1H), 7.25 (d, *J* = 8.4 Hz, 1H), 6.80 (t, *J* = 2.8 Hz, 1H), 6.73 (m, 1H). ^{13}C NMR (100 MHz, $CDCl_3$) δ 185.4, 136.1, 135.0, 130.8, 130.7, 130.0, 128.4, 128.2, 127.8, 124.8, 108.8. LC-MS (ESI): t_R= 4.66 min; $[M+H]^+$ 240.35.

(*E*) 1-(2,4-Dichlorophenyl)-3-(2-nitrovinyl)-1*H*-pyrrole (**2**). Nitromethane (54 mL, 1 mol) and ammonium acetate (15.4 g, 0.2 mol) were stirred in 100 mL of acetic acid at 30°C for 30 minutes. Then, 1-(2,4-dichloro-phenyl)-1 *H*-pyrrole-2-carbaldehyde (12 g, 0.05 mol) was added and the mixture was heated at 90°C for 24 h. The reaction was concentrated under vacuum. A saturated solution of sodium hydrogenocarbonate (100 mL) was added to the residue. This aqueous layer was extracted with EtOAc (2x 100 mL). The organic layers were washed with water (2x 100 mL), dried over $MgSO_4$ and concentrated under vacuum. The solid resulting residue was purified by chromatography on silica gel using cyclohexane and CH_2Cl_2 as eluant (50/50) to give compound **2** as a yellow solid (6.1 g, 43%). Mp: 186 °C. ^{1}H NMR (400 MHz, DMSO-d_6) δ 8.11 (d, *J* = 13.3 Hz, 1H), 7.95 (d, *J* = 13.3 Hz, 1H), 7.90 (d, *J* = 2.3 Hz, 1H), 7.78 (m, 1H), 7.60 (dd, *J* = 6.4 and 8.5 Hz, 1H), 7.58 (d, *J* = 8.7 Hz, 1H), 7.19 (m, 1H), 6.86 (m, 1H). ^{13}C NMR (100 MHz, DMSO- d_6) δ 136.5, 134.8, 134.6, 134.0, 130.6, 130.2, 130.0, 129.7, 129.0, 126.3, 117.5, 109.3. LC-MS (ESI): t_R= 5.34 min; $[M+H]^+$ 283.40. HRMS for $C_{12}H_9Cl_2N_2O_2$ $[M+H]^+$calculated mass: 283.0035, measured: 283.0036.

(*E*) 1-(2,4-dichlorophenyl)-2-methyl-5-(2-nitrovinyl)-1*H*-pyrrole (**3**). See **Supplementary Fig.1c**.

1-(2,4-Dichlorophenyl)-2-methyl-1*H*-pyrrole (**36**). A mixture of 1-(2,4-Dichlorophenyl)-1 *H*-pyrrole-2-carbaldehyde (**34**) (1g, 0.02 mol), potassium hydroxide (0.7g, 0.06 mol) and hydrazine monohydrate (0.61 ml, 0.06 mol) in ethylene glycol (20 ml) was stirred at room temperature for 30 min, then slowly heated to 150°C and maintained for 2 h. The reaction mixture was allowed to cool to room temperature, poured into ice-water and extracted with Et_2O (2x 20 ml). The combined organic layers were washed with water, brine, dried over $MgSO_4$, filtered and concentrated under vacuum. The crude compound was purified by chromatography on silica gel using cyclohexane and CH_2Cl_2 as eluant (90/10) to afford compound **36** as an orange oil (0.78 g, 70%). ^{1}H NMR (400 MHz, $CDCl_3$) δ 7.53 (d, *J* = 2.2 Hz, 1H), 7.33 (dd, *J* = 8.5 and 2.3 Hz, 1H), 7.26 (d, *J* = 8.3 Hz, 1H), 6.60 (dd, *J* = 2.8 and 1.9 Hz, 1H), 6.22 (t, *J* = 3.0 Hz, 1H), 6.04 (m, 1H), 2.04 (s, 3H). ^{13}C NMR (100 MHz, $CDCl_3$) δ 136.7, 134.6, 133.7, 130.5, 130.1, 130.0, 127.7, 121.3, 108.5, 107.4, 12.1. HRMS for $C_{11}H_{10}Cl_2N$ $[M+H]^+$calculated mass: 226.0184, measured: 226.0185.

Synthetic procedure for the compound (**3**) is the similar as that described for the compound (**1**) and spectra data are shown below.

1-(2,4-Dichlorophenyl)-5-methyl-1*H*-pyrrole-2-carbaldehyde (**37**). Yellow oil (61%). ^{1}H NMR (400 MHz, $CDCl_3$) δ 9.37 (s, 1H), 7.55 (d, *J* = 2.4 Hz, 1H), 7.38 (dd, *J* = 8.5 and 2.4 Hz, 1H), 7.25 (d, *J* = 8.5 Hz, 1H), 7.03 (d, *J* = 3.9 Hz, 1H), 6.22 (d, *J* = 3.9 Hz, 1H), 2.04 (s, 3H). ^{13}C NMR (100 MHz, $CDCl_3$) δ 177.6, 140.1, 135.4, 134.8, 133.7, 132.7, 130.4, 130.1, 128.0, 123.8, 110.4, 12.1. LC-MS (ESI): t_R= 4.52 min; $[M+H]^+$ 254.37. HRMS for $C_{12}H_{10}Cl_2NO$ $[M+H]^+$calculated mass: 254.0133, measured: 254.0133.

(E) 1-(2,4-Dichlorophenyl)-2-methyl-5-(2-nitrovinyl)-1 *H*-pyrrole (**3**). Orange solid (50%). Mp: 90°C. ^{1}H NMR (400 MHz, $CDCl_3$) δ 7.65 (d, *J* = 2.4 Hz, 1H), 7.47 (m, 2H), 7.28 (m,

1H), 6.99 (d, *J* = 13.4 Hz, 1H), 6.90 (d, *J* = 4.0 Hz, 1H), 6.27 (d, *J* = 4.0 Hz, 1H), 2.06 (s, 3H). ^{13}C NMR (100 MHz, $CDCl_3$) δ 139.8, 136.8, 134.5, 133.1, 131.1, 130.9, 130.6, 128.7, 127.7, 125.3, 118.0, 111.7, 12.8. LC-MS (ESI): t_R = 5.35 min; $[M+H]^+$ 297.42. HRMS for $C_{13}H_{11}Cl_2N_2O_2$ $[M+H]^+$ calculated mass: 297.0192, measured: 297.0193.

(*E*) 3-[1-(2,4-Dichlorophenyl)-1*H*-pyrrol-2-yl]-acrylonitrile (4). See **Supplementary Fig.1d**.

2-Cyano-3-(1-(2,4-dichlorophenyl)-1*H*-pyrrol-2-yl)-acrylic acid ethyl ester (**38**). To a solution of 1-(2,4-dichlorophenyl)-1*H*-pyrrole-2-carbaldehyde (**34**) (1g, 4.16 mmol) in ethanol (10 ml), were added ethylcyanoacetate (0.49 ml, 4.58 mmol) and triethylamine (0.58 ml, 4.16 mmol). The mixture was refluxed for 4 h. After removal of the solvent under vacuum, CH_2Cl_2 was added to the residue and the organic layer was washed with water, dried over $MgSO_4$, filtered and concentrated in vacuo. The crude compound was purified by chromatography on silica gel using CH_2Cl_2 as eluant to obtain compound **34** as a yellow solid (1.2 g, 86%). Mp: 138 °C. ^{1}H NMR (400 MHz, $CDCl_3$) δ 7.86 (d, *J* = 4.2 Hz, 1H), 7.59 (d, *J* = 1.6 Hz, 1H), 7.52 (s, 1H), 7.41 (dd, *J* = 8.3 and 1.5 Hz, 1H), 7.28 (d, *J* = 8.5 Hz, 1H), 7.07 (m, 1H), 6.59 (m, 1H), 4.26 (q, *J* = 7.1 Hz, 2H), 1.32 (t, *J* = 7.1 Hz, 3H). ^{13}C NMR (100 MHz, $CDCl_3$) δ 163.5, 140.1, 136.5, 133.6, 133.5, 130.7, 130.7, 130.6, 128.3, 128.3, 119.4, 116.6, 113.3, 95.2, 62.2, 14.2. HRMS for $C_{16}H_{13}Cl_2N_2O_2$ $[M+H]^+$calculated mass: 335.0348, measured: 335.0346.

2-Cyano-3-(1-(2,4-dichlorophenyl)-1*H*-pyrrol-2-yl)-acrylic acid (**39**). To a solution of lithium hydroxyde (340 mg, 0.014 mol) in water (50 ml) was added a solution of 2-cyano-3-(1-(2,4-dichlorophenyl)-1*H*-pyrrol-2-yl)-acrylic acid ethyl ester (**38**) (3.2 g, 9.54 mmol) in THF (50 ml) and the mixture was heated at 50°C for 5h. After removing THF under vacuum, the aqueous layer was acidified with 6N HCl and then extracted with EtOAc (2x 50 mL). The organic layers were washed with water (2x 50 mL), dried over $MgSO_4$ and concentrated in vacuo. The product was purified by recrystallization in CH_2Cl_2 to obtain compound **39** as a yellow solid (1.1 g, 37%). Mp: 110°C. ^{1}H NMR (400 MHz, $CDCl_3$) δ 7.95 (d, *J* = 4.1 Hz, 1H), 7.64 (d, *J* = 2.2 Hz, 1H), 7.56 (s, 1H), 7.46 (dd, *J* = 8.3 and 2.2 Hz, 1H), 7.31 (d, *J* = 8.3 Hz, 1H), 7.15 (m, 1H), 6.65 (m, 1H). ^{13}C NMR (100 MHz, $CDCl_3$) δ 168.8, 141.2, 136.7, 133.5, 133.2, 131.8, 130.8, 130.6, 128.4, 128.3 120.7, 116.0, 113.8, 93.8. LC-MS (ESI): t_R = 4.55 min; $[M+H]^+$ 307.32. HRMS for $C_{14}H_9Cl_2N_2O_2$ $[M+H]^+$calculated 307.0035, measured: 307.0034.

3-(1-(2,4-Dichlorophenyl)-1*H*-pyrrol-2-yl)-acrylonitrile (**4**). To a solution of copper (155 mg, 2.44 mmol) in quinoleine (10 ml), heated at 190°C, was added 2-cyano-3-(1-(2,4-dichlorophenyl)-1*H*-pyrrol-2-yl)-acrylic acid (**39**) (500 mg, 1.62 mmol). The mixture was stirred vigorously. After the carbon dioxide evolution stopped and TLC indicated complete consumption of the starting material, the reaction was cooled to room temperature and 1N HCl (10 ml) was added. The aqueous layer was extracted with CH_2Cl_2 (2x 15 mL). The combined organic layers were washed with water (2x 20 mL), dried over $MgSO_4$ and concentrated under vacuum. The resulting residue was purified by chromatography on silica gel using cyclohexane and CH_2Cl_2 as eluant (50/50 to 30/70) to obtain compound **4** as a white solid (150 mg, 36%). Mp: 108 °C. ^{1}H NMR (400 MHz, $CDCl_3$) δ 7.58 (d, *J* = 2.3 Hz, 1H), 7.53 (m, 1H), 7.39 (dd, *J* = 8.4 and 2.3 Hz, 1H), 7.28 (d, *J* = 8.5 Hz, 1H), 6.86 (m, 1H), 6.49 (t, *J* = 3.2 Hz, 1H), 6.44 (d, *J* = 12.1 Hz, 1H), 5.01 (d, *J* = 12.1 Hz, 1H). ^{13}C NMR (100 MHz, $CDCl_3$) δ 135.8 135.1, 134.5, 133.7, 130.8, 130.4, 129.3, 128.1, 126.4, 118.2, 114.3, 111.6,

88.7. LC-MS (ESI): t_R = 5.18 min; $[M+H]^+$ 263.51. HRMS for $C_{13}H_9Cl_2N_2$ $[M+H]^+$calculated mass: 263.0137, measured: 263.0136.

1-(2,4-Dichlorophenyl)-2-(2-nitroethyl)-1*H*-pyrrole (5). See **Supplementary Fig.1e**. 1-(2,4-Dichlorophenyl)-2-(2-nitroethyl)-1*H*-pyrrole (**5**). To a solution of (*E*) 1-(2,4-Dichlorophenyl)-2-(2-nitrovinyl)-1*H*-pyrrole **(1)** (200 mg, 0.70 mmol) in methanol (7 ml) was added portionwise sodium borohydride (53 mg, 1.41 mmol) at 0°C. After the addition, the reaction mixture was stirred at 0°C for 1 h. Then a mixture of ice / water (10 ml) was added and the aqueous layer was extracted with EtOAc (2x 20 ml). The combined organic layers were washed with water (2x 30 ml), dried over $MgSO_4$, filtered and concentrated under vacuum to give compound **5** as a brown oil (0.1 g, 50%). ^{1}H NMR (400 MHz, $CDCl_3$) δ 7.57 (d, *J* = 2.4 Hz, 1H), 7.39 (dd, *J* = 8.4 and 2.3 Hz, 1H), 7.30 (d, *J* = 8.5 Hz, 1H), 6.64 (dd, *J* = 2.9 and 1.7 Hz, 1H), 6.27 (t, *J* = 3.2 Hz, 1H), 6.13 (m, 1H), 4.48 (dd, *J* = 15.2 and 7.7 Hz, 2H), 3.09 (dd, *J* = 15.4 and 7.5 Hz, 2H). ^{13}C NMR (100 MHz, $CDCl_3$) δ 135.7, 135.4, 133.7, 130.6, 130.3, 128.1, 127.6, 122.8, 109.2, 108.0, 74.1, 24.3. HRMS for $C_{12}H_{11}Cl_2N_2O_2$ $[M+H]^+$calculated mass: 285.0192, measured: 285.0189.

(*E*) 1-(4-Chlorophenyl)-2-(2-nitrovinyl)-1*H*-pyrrole (6).

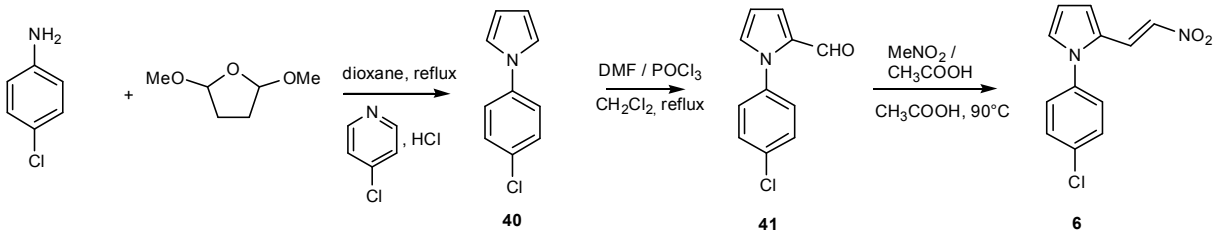

Synthetic procedure for compound (**6**) is similar as that described for compound (**1**) and spectra data are shown below.

1-(4-chlorophenyl)-1*H*-pyrrole (**40**).[3] Beige solid (85%). Mp: 90 °C. ^{1}H NMR (400 MHz, $CDCl_3$) δ 7.28 (d, *J* = 9.2 Hz, 2H), 7.21 (d, *J* = 9.1 Hz, 2H), 6.94 (t, *J* = 2.2 Hz, 2H), 6.35 (t, *J* = 2.2 Hz, 2H). ^{13}C NMR (100 MHz, $CDCl_3$) δ 139.4, 131.1, 129.8, 121.6, 119.3, 110.8.

1-(4-chlorophenyl)-1*H*-pyrrole-2-carbaldehyde (**41**).[4] Orange solid (30%). Mp: 98°C. ^{1}H NMR (400 MHz, $CDCl_3$) δ 9.49 (s, 1H), 7.35 (d, *J* = 8.8 Hz, 2H), 7.21 (d, *J* = 8.7 Hz, 2H), 7.07 (dd, *J* = 4.0 and 1.7 Hz, 1H), 6.97 (m, 1H), 6.34 (dd, *J* = 4.1 and 2.7 Hz, 1H). ^{13}C NMR (100 MHz, $CDCl_3$) δ 178.7, 137.5, 134.1, 132.4, 131.3, 129.2, 127.2, 123.7, 111.1. LC-MS (ESI): t_R= 4.52 min; $[M+H]^+$ 206.39.

(*E*) 1-(4-chlorophenyl)-2-(2-nitrovinyl)-1 *H*-pyrrole (**6**).Yellow solid (54%). Mp: 124 °C. ^{1}H NMR (400 MHz, $CDCl_3$) δ 7.74 (d, *J* = 13.3 Hz, 1H), 7.49 (d, *J* = 8.6 Hz, 2H), 7.24 (d, *J* =

[3] Das, B. *et al*. Novel approach for the synthesis of N-substituted pyrroles starting directly from nitro compounds in water. *Synthetic Communications*. **4**, 548-553 (2012)

[4] Pina, M. *et al* . Synthesis and spectral data of 1-aryl-2-formylpyrroles. *Khimiya Geterotsiklicheskikh Soedinenii*. **2**, 180-184, (1989).

13.4 Hz, 1H), 7.22 (d, *J* = 8.6 Hz, 2H), 7.07 (m, 1H), 6.91 (d, *J* = 3.8 Hz, 1H), 6.42 (t, *J* = 3.6 Hz, 1H). ^{13}C NMR (100 MHz, $CDCl_3$) δ 136.5, 134.9, 132.8, 130.0, 129.9, 127.8, 127.6, 125.2, 116.5, 112.1. LC-MS (ESI): t_R= 5.07 min; $[M+H]^+$ 249.44. HRMS for $C_{12}H_{10}ClN_2O_2$ $[M+H]^+$ calculated mass: 249.0425, measured: 249.0425.

(*E*) 1-(3-Chlorophenyl)-2-(2-nitrovinyl)-1*H*-pyrrole (7).

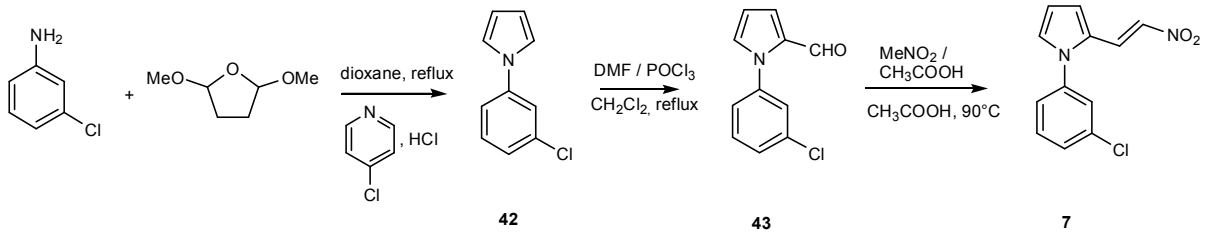

42 43 7

Synthetic procedure for compound (**7**) is similar as that described for compound (**1**) and spectra data are shown below.

1-(3-chlorophenyl)-1*H*-pyrrole (**42**).[5] Brown solid (90%). Mp: 54 °C. ^{1}H NMR (400 MHz, $CDCl_3$) δ 7.30 (t, *J* = 2.0 Hz, 1H), 7.22 (d, *J* = 7.9 Hz, 1H), 7.18 (ddd, *J* = 8.1, 2.1 and 1.2 Hz, 1H), 7.11 (ddd, *J* = 7.9, 2.0 and 1.2 Hz, 1H), 6.97 (t, *J* = 2.2 Hz, 2H), 6.26 (t, *J* = 2.2 Hz, 2H). ^{13}C NMR (100 MHz, $CDCl_3$) δ 141.8, 135.2, 130.6, 125.6, 120.6, 119.2, 118.4, 111.1.

1-(3-chlorophenyl)-1*H*-pyrrole-2-carbaldehyde (**43**).[4] Brown solid (50%). Mp: 68°C. ^{1}H NMR (400 MHz, $CDCl_3$) δ 9.49 (s, 1H), 7.31-7.27 (m, 3H), 7.18-7.15 (m, 1H), 7.06 (dd, *J* = 4.0 and 1.7 Hz, 1H), 6.97 (m, 1H), 6.33 (dd, *J* = 3.9 and 2.7 Hz, 1H). ^{13}C NMR (100 MHz, $CDCl_3$) δ 178.7, 140.0, 134.6, 132.4, 131.2, 130.0, 128.4, 126.3, 124.4, 123.5, 111,2. LC-MS (ESI): t_R = 4.42 min; $[M+H]^+$ 206.34.

(*E*) 1-(3-Chlorophenyl)-2-(2-nitrovinyl)-1*H*-pyrrole (**7**)**.** Red oil (50%). ^{1}H NMR (400 MHz, $CDCl_3$) δ 7.78 (d, *J* = 13.3 Hz, 1H), 7.50-7.48 (m, 2H), 7.35 (m, 1H), 7.32 (d, *J* = 13.3 Hz, 1H), 7.20-7.23 (m, 1H), 7.12 (dd, *J* = 2.6 and 1.1 Hz, 1H), 6.95 (dd, *J* = 4.0 and 2.6 Hz, 1H), 6.45 (dd, *J*= 3.8 and 0.9 Hz, 1H). ^{13}C NMR (100 MHz, $CDCl_3$) δ 139.1, 135.5, 132.9, 130.7, 129.8, 129.1, 127.7, 126.6, 125.2, 124.7, 116.5, 112.2. LC-MS (ESI): t_R = 5.06 min; $[M+H]^+$ 249.40. HRMS for $C_{12}H_{10}ClN_2O_2$ $[M+H]^+$ calculated mass: 249.0425, measured: 249.0425.

(*E*) 1-(2-Chlorophenyl)-2-(2-nitrovinyl)-1*H*-pyrrole (8).

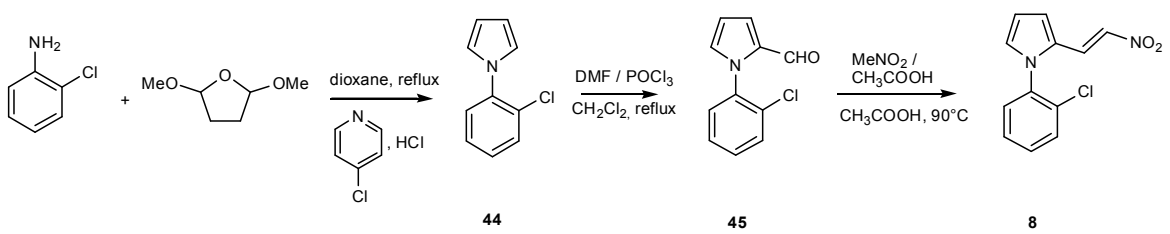

44 45 8

[5] Corsi, C. *et al*. Preparation of pyrrole derivatives as plant growth regulators. PCT Int. Appl., 2010069879, 24 Jun 2010.

Synthetic procedure for compound (**8**) is similar as that described for compound (**1**) and spectra data are shown below.

1-(2-Chlorophenyl)-1*H*-pyrrole (**44**)[1]**.** Brown oil (87%). ^{1}H NMR (400 MHz, $CDCl_3$) δ 7.47 (m , 1H), 7.32-7.22 (m, 3H), 6.88 (t, *J* = 2.2 Hz, 2H), 6.31 (t, *J* = 2.2 Hz, 2H). ^{13}C NMR (100 MHz, $CDCl_3$) δ 138.8, 130.7, 129.7, 128.3, 127.9, 127.6, 122.2, 109.3.

1-(2-Chlorophenyl)-1*H*-pyrrole-2-carbaldehyde (**45**).[4] Beige solid (29%). Mp: 94°C. ^{1}H NMR (400 MHz, $CDCl_3$) δ 9.42 (d, *J* = 0.5 Hz, 1H), 7.44 (m, 1H), 7.35-7.27 (m, 2H), 7.05 (dd, *J* = 4.0 and 1.7 Hz, 1H), 7.07 (dd, *J* = 4.0 and 1.8 Hz, 1H), 6.89 (m, 1H), 6.37 (dd, *J* = 4.0 and 2.5 Hz, 1H). ^{13}C NMR (100 MHz, $CDCl_3$) δ 178.6, 137.1, 133.0, 132.0, 131.0, 130.2, 130.0, 129.0, 127.4, 122.2, 110.9. LC-MS (ESI): t_R = 4.38 min; $[M+H]^+$ 206.39.

(*E*) 1-(2-Chlorophenyl)-2-(2-nitrovinyl)-1 *H*-pyrrole (**8**)**.** Brown oil (50%). ^{1}H NMR (400 MHz, $CDCl_3$) δ 7.62-7.57 (m, 2H), 7.51 (dt, *J* = 7.5 and 1.7 Hz, 1H), 7.46 (dt, *J* = 7.6 and 1.5 Hz, 1H), 7.38 (dd, *J* = 7.6 and 1.7 Hz, 1H), 7.09 (d, *J* =13.3 Hz, 1H), 7.04 (dd, *J* = 2.5 and 0.9 Hz, 1H), 6.95 (dd, *J* = 2.6 and 1.1 Hz, 1H), 6.49 (dd, *J* = 2.7 and 0.9 Hz, 1H). ^{13}C NMR (100 MHz, $CDCl_3$) δ 135.7, 132.5, 132.3, 131.0, 130.9, 130.3, 129.6, 128.0, 127.8, 125.8, 116.9, 112.0. LC-MS (ESI): t_R = 4.95 min; $[M+H]^+$ 249.44. HRMS for $C_{12}H_{10}ClN_2O_2$ $[M+H]^+$ calculated mass: 249.0425, measured: 249.0425.

(*E*) 1-(3,4-Dichlorophenyl)-2-(2-nitrovinyl)-1*H*-pyrrole (9).

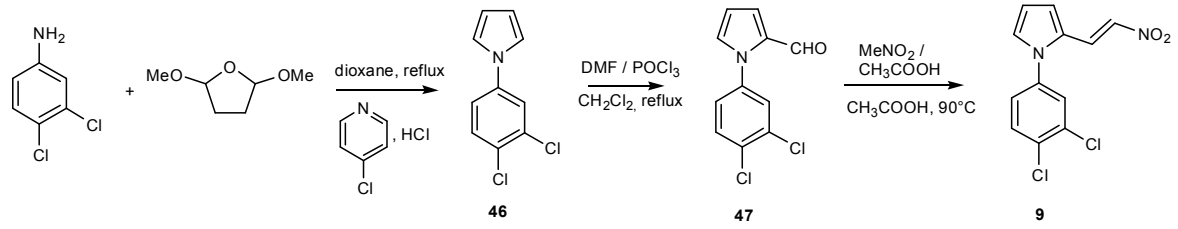

Synthetic procedure for compound (**9**) is similar as that described for compound **(1**) and spectra data are shown below.

1-(3,4-Dichlorophenyl)-1*H*-pyrrole (**46**)**.** Brown solid (77%). Mp: 56 °C. ^{1}H NMR (400 MHz, $CDCl_3$) δ 7.51-7.48 (m, 2H), 7.24 (dd, *J* = 8.7 and 2.6 Hz, 1H), 7.05 (t, *J* = 2.1 Hz, 2H), 6.39 (t, *J* = 2.2 Hz, 2H). ^{13}C NMR (100 MHz, $CDCl_3$) δ 140.0, 133.5, 131.2, 129.2, 122.1, 119.4, 119.2, 111.4.

1-(3,4-Dichlorophenyl)-1*H*-pyrrole-2-carbaldehyde (**47**)**.** Brown solid (40%). Mp: 104°C. ^{1}H NMR (400 MHz, $CDCl_3$) δ 9.50 (d, *J* = 0.7 Hz, 1H), 7.44 (d, *J* = 8.4 Hz, 1H), 7.39 (d, *J* = 2.5 Hz, 1H), 7.14 (dd, *J* = 8.5 and 2.5 Hz, 1H), 7.07 (dd, *J* = 4.0 and 1.8 Hz, 1H), 6.97 (m, 1H), 6.35 (dd, *J* = 4.0 and 2.6 Hz, 1H). ^{13}C NMR (100 MHz, $CDCl_3$) δ 178.6, 138.3, 132.9, 132.5, 132.2, 131.6, 130.6, 127.8, 125.5, 124.6, 111,4. LC-MS (ESI): t_R = 4.81 min; $[M+H]^+$ 240.30. HRMS for $C_{11}H_8Cl_2NO$ $[M+H]^+$ calculated mass: 239.9977, measured: 239.9975.

(*E*) 1-(3,4-Dichlorophenyl)-2-(2-nitrovinyl)-1*H*-pyrrole (**9**) : yellow solid (65%). Mp: 128 °C. ^{1}H NMR (400 MHz, $CDCl_3$) δ 7.75 (d, *J* = 13.3 Hz, 1H), 7.64 (d, *J* = 8.5 Hz, 1H), 7.46 (d, *J* = 2.4 Hz, 1H), 7.34 (d, *J* = 13.3 Hz, 1H), 7.17 (dd, *J* = 8.5 and 2.4 Hz, 1H), 7.10 (dd, *J* = 2.6 and 1.1 Hz, 1H), 6.95 (dd, *J* = 4.0 and 1.3 Hz, 1H), 6.49 (dd, *J* = 3.9 and 2.8 Hz, 1H). ^{13}C NMR (100 MHz, $CDCl_3$) δ 135.7, 132.5, 132.3, 131.0, 130.9, 130.3, 129.6, 128.0, 127.8, 125.8, 116.9, 112.0. LC-MS (ESI): t_R = 5.29 min; $[M+H]^+$ 283.44. HRMS for $C_{12}H_9Cl_2N_2O_2$ $[M+H]^+$ calculated mass: 283.0035, measured: 283.0035.

(*E*) 1-(2,3-Dichlorophenyl)-2-(2-nitrovinyl)-1*H*-pyrrole (10).

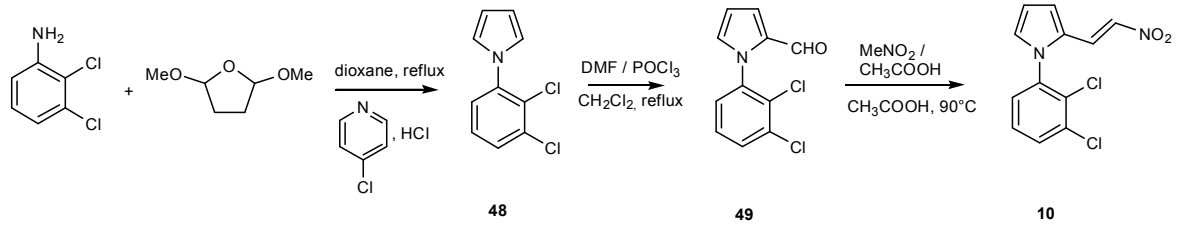

Synthetic procedure for compound (**10)** is similar as that described for compound (**1**) and spectra data are shown below.

1-(2,3-Dichlorophenyl)-1*H*-pyrrole (**48**).[3] Pink oil (78%). ^{1}H NMR (400 MHz, $CDCl_3$) δ 7.49-7.47 (m, 1H), 7.27 (m, 2H), 6.90 (t, *J* = 2.1 Hz, 2H), 6.36 (t, *J* = 2.1 Hz, 2H). ^{13}C NMR (100 MHz, $CDCl_3$) δ 140.5, 134.4, 129.2, 129.0, 127.5, 126.2, 122.2, 109.6.
1-(2,3-Dichlorophenyl)-1*H*-pyrrole-2-carbaldehyde (**49**). Yellow solid (32%). Mp: 92°C. ^{1}H NMR (400 MHz, $CDCl_3$) δ 9.54 (s, 1H), 7.59 (dd, *J* = 7.6 and 2.1 Hz, 1H), 7.35-7.28 (m, 2H), 7.15 (dd, *J* = 4.0 and 1.6 Hz, 1H), 6.98 (m, 1H), 6.48 (dd, *J* = 4.1 and 2.5 Hz, 1H). ^{13}C NMR (100 MHz, $CDCl_3$) δ 178.5, 139.0, 134.0, 132.9, 131.3, 131.0, 130.8, 127.3, 127.2, 122.9, 111,1. LC-MS (ESI): t_R = 4.69 min; $[M+H]^+$ 240.30. HRMS for $C_{11}H_8Cl_2NO$ $[M+H]^+$ calculated mass: 239.9977, measured: 239.9975.

(*E*) 1-(2,3-Dichlorophenyl)-2-(2-nitrovinyl)-1 *H*-pyrrole (**10**). Yellow solid (53%). Mp: 122 °C. ^{1}H NMR (400 MHz, $CDCl_3$) δ 7.69 (dd, *J* = 8.1 and 1.5 Hz, 1H), 7.56 (d, *J* = 13.3 Hz, 1H), 7.40 (t, *J* = 8.0 Hz, 1H), 7.32 (dd, *J* = 7.9 and 1.5 Hz, 1H), 7.17 (d, *J* = 13.3 Hz, 1H), 7.03 (dd, *J* = 2.5 and 1.5 Hz, 1H), 6.96 (m, 1H), 6.50 (m, 1H). ^{13}C NMR (100 MHz, $CDCl_3$) δ 137.3, 134.8, 132.6, 131.9, 131.8, 130.0, 128.0, 127.9, 127.4, 125.7, 116.7, 112.3. LC-MS (ESI): t_R = 5.11 min; $[M+H]^+$ 283.44. HRMS for $C_{12}H_9Cl_2N_2O_2$ $[M+H]^+$ calculated mass: 283.0035, measured: 283.0035.

(*E*) 1-(2,5-Dichlorophenyl)-2-(2-nitrovinyl)-1*H*-pyrrole (11).

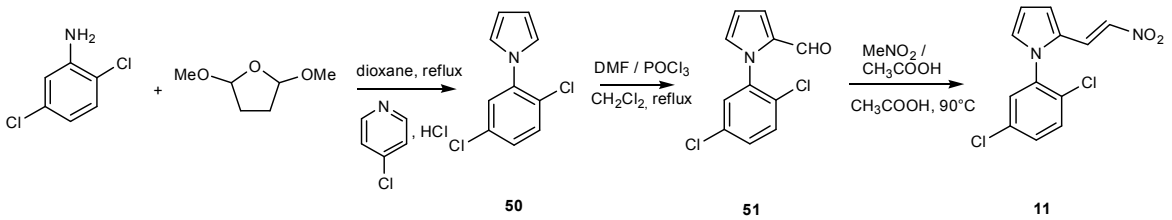

Synthetic procedure for compound (**11)** is similar as that described for compound (**1**) and spectra data are shown below.

1-(2,5-Dichlorophenyl)-1*H*-pyrrole (**50).** Brown oil (79%). ^{1}H NMR (400 MHz, $CDCl_3$) δ 7.35 (d, *J* = 8.4 Hz, 1H), 7.27 (d, *J* = 2.4 Hz, 1H), 7.17 (dd, *J* = 8.6 and 2.4 Hz, 1H), 6.82 (t, *J* = 2.2 Hz, 2H), 6.26 (t, *J* = 2.2 Hz, 2H). ^{13}C NMR (100 MHz, $CDCl_3$) δ 139.5, 133.1, 131.6, 128.1, 127.8, 127.7, 122.0, 109.9. HRMS for $C_{10}H_9Cl_2N$ $[M+H]^+$ calculated mass: 212.0028, measured: 212.0030.

1-(2,5-Dichlorophenyl)-1*H*-pyrrole-2-carbaldehyde (**51**)**.** Orange solid (45%). Mp: 126°C. ^{1}H NMR (400 MHz, $CDCl_3$) δ 9.54 (s, 1H), 7.45 (d, *J* = 8.5 Hz, 1H), 7.40 (m, 1H), 7.37 (m, 1H), 7.13 (dd, *J* = 4.0 and 1.8 Hz, 1H), 6.95 (m, 1H), 6.46 (dd, *J* = 3.9 and 2.6 Hz, 1H). ^{13}C NMR (100 MHz, $CDCl_3$) δ 178.5, 138.2, 132.9, 132.8, 130.9, 130.8, 130.6, 130.0, 129.0, 123.1, 111.2. LC-MS (ESI): t_R = 4.72 min; $[M+H]^+$ 240.35. HRMS for $C_{11}H_8Cl_2NO$ $[M+H]^+$ calculated mass: 239.9977, measured: 239.9972.

(*E*) 1-(2,5-Dichlorophenyl)-2-(2-nitrovinyl)-1*H*-pyrrole (**11**) Yellow solid (59%). Mp: 124 °C. ^{1}H NMR (400 MHz, $CDCl_3$) δ 7.55 (d, *J* = 13.2 Hz, 1H), 7.53 (s, 1H), 7.51 (d, *J* = 2.4 Hz, 1H), 7.41 (d, *J* = 2.3 Hz, 1H), 7.16 (d, *J* = 13.4 Hz, 1H), 7.01 (dd, *J* = 2.7 and 1.5 Hz, 1H), 6.95 (dd, *J* = 4.0 and 1.3 Hz, 1H), 6.50 (m, 1H). ^{13}C NMR (100 MHz, $CDCl_3$) δ 136.6, 133.7, 132.8, 131.6, 131.2, 131.1, 129.9, 129.8, 127.4, 125.8, 116.8, 112.5. LC-MS (ESI): t_R= 5.13 min; $[M+H]^+$ 283.49. HRMS for $C_{12}H_9Cl_2N_2O_2$ $[M+H]^+$ calculated mass: 283.0035, measured: 283.0035.

(*E*) 1-(3,5-Dichlorophenyl)-2-(2-nitrovinyl)-1*H*-pyrrole (12).

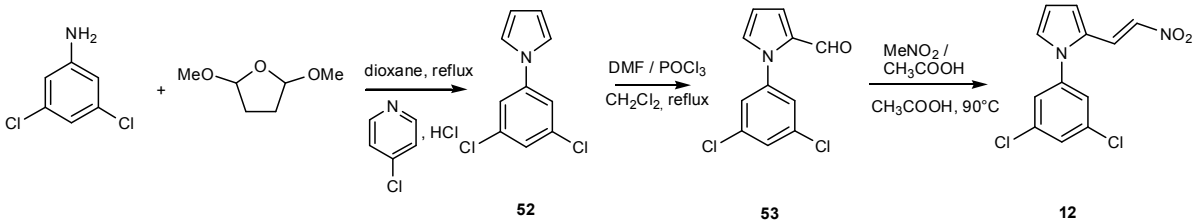

Synthetic procedure for compound (**12**) is similar as that described for compound (**1**) and spectra data are shown below.

1-(3,5-Dichlorophenyl)-1*H*-pyrrole (**52**)**.** Brown solid (79%). Mp: 60 °C. ^{1}H NMR (400 MHz, $CDCl_3$) δ 7.29 (d, *J* = 1.8 Hz, 2H), 7.23 (t, *J* = 1.8 Hz, 1H), 7.05 (t, *J* = 2.2 Hz, 2H), 6.38 (t, *J* = 2.2 Hz, 2H). ^{13}C NMR (100 MHz, $CDCl_3$) δ 142.2, 135.9, 125.4, 119.1, 118.7, 111.6. HRMS for $C_{10}H_8Cl_2N$ $[M+H]^+$ calculated mass: 212.0028, measured: 212.0032.

1-(3,5-Dichlorophenyl)-1*H*-pyrrole-2-carbaldehyde (**53**). Yellow solid (50%). Mp: 144°C. ^{1}H NMR (400 MHz, $CDCl_3$) δ 9.52 (s, 1H), 7.34 (t, *J* = 1.8 Hz, 1H), 7.20 (d, *J* = 1.8 Hz, 2H), 7.07 (dd, *J* = 3.9 and 1.6 Hz, 1H), 6.98 (m, 1H), 6.35 (dd, *J* = 3.9 and 2.7 Hz, 1H). ^{13}C NMR (100 MHz, $CDCl_3$) δ 178.5, 140.7, 135.1, 132.2, 131.3, 128.4, 124.8, 124.6, 111.5. LC-MS (ESI): t_R = 4.69 min; $[M+H]^+$ 240.26. HRMS for $C_{11}H_8Cl_2NO$ $[M+H]^+$ calculated mass: 239.9975, measured: 239.9977.

(*E*) 1-(3,5-Dichlorophenyl)-2-(2-nitrovinyl)-1*H*-pyrrole (**12**). Orange solid (65%). Mp: 120°C. ^{1}H NMR (400 MHz, $CDCl_3$) δ 7.76 (d, *J* = 13.3 Hz, 1H), 7.52 (t, *J* = 1.8 Hz, 1H), 7.46 (d, *J* = 2.4 Hz, 1H), 7.34 (d, *J* = 13.3 Hz, 1H), 7.25 (d, *J* = 1.8 Hz, 1H), 7.10 (dd, *J* = 2.6 and 1.5 Hz, 1H), 6.95 (dd, *J* = 4.0 and 1.3 Hz, 1H), 6.46 (m, 1H). ^{13}C NMR (100 MHz, $CDCl_3$) δ 139.8, 136.2, 133.4, 129.6, 129.2, 127.2, 125.2, 125.1, 116.7, 112.5. LC-MS (ESI): t_R = 5.33 min; $[M+H]^+$ 283.44. HRMS for $C_{12}H_9Cl_2N_2O_2$ $[M+H]^+$ calculated mass: 283.0035, measured: 283.0036.

(*E*) 1-(2,6-Dichlorophenyl)-2-(2-nitrovinyl)-1*H*-pyrrole (13)

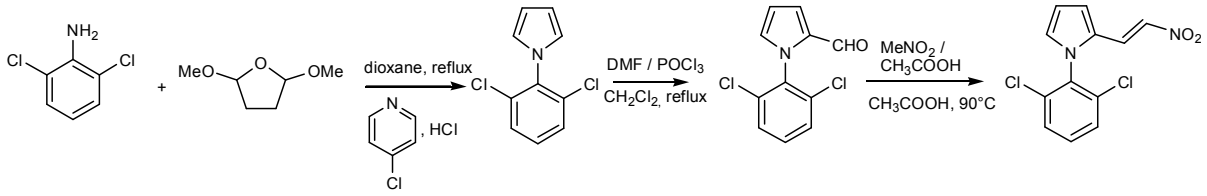

Synthetic procedure for compound (**13**) is similar as that described for compound (**1**) and spectra data are shown below.

1-(2,6-Dichlorophenyl)-1*H*-pyrrole (**54**).[6] Orange solid (83%). Mp: 90 °C. ^{1}H NMR (400 MHz, $CDCl_3$) δ 7.47 (m, 2H), 7.33-7.29 (m, 1H), 6.76 (t, *J* = 2.3 Hz, 2H), 6.43 (t, *J* = 2.2 Hz, 2H). ^{13}C NMR (100 MHz, $CDCl_3$) δ 137.0, 134.5, 129.6, 128.7, 121.9, 109.4.

1-(2,6-Dichlorophenyl)-1*H*-pyrrole-2-carbaldehyde (**55**).[6] Orange solid (45%). Mp: 94°C. ^{1}H NMR (400 MHz, $CDCl_3$) δ 9.53 (s, 1H), 7.45 (m, 2H), 7.34 (dd, *J* = 9.0 and 7.3 Hz, 1H), 7.16 (dd, *J* = 3.8 and 1.6 Hz, 1H), 6.92 (m, 1H), 6.52 (dd, *J* = 3.9 and 2.7 Hz, 1H). ^{13}C NMR (100 MHz, $CDCl_3$) δ 178.4, 135.6, 134.2, 132.3, 130.4, 130.2, 128.4, 123.1, 111,4. LC-MS (ESI): t_R = 4.61 min; $[M+H]^+$ 240.35.

(*E*) 1-(2,6-Dichlorophenyl)-2-(2-nitrovinyl)-1*H*-pyrrole (**13**). Orange solid (60%). Mp: 120°C. ^{1}H NMR (400 MHz, $CDCl_3$) δ 7.54 (m, 2H), 7.53 (d, *J* = 12.9 Hz, 1H), 7.46 (m, 1H), 7.03-7.01 (d, *J* = 13.1 Hz, 1H), 6.99 (dd, *J* = 4.0 and 1.4 Hz, 1H), 6.96 (dd, *J* = 2.7 and 1.4 Hz, 1H), 6.55 (dd, *J* = 3.9 and 2.8 Hz, 1H). ^{13}C NMR (100 MHz, $CDCl_3$) δ 135.1, 133.8, 132.3, 131.4, 129.5, 129.1, 127.2, 125.1, 117.5, 112.7. LC-MS (ESI): t_R = 5.05 min; $[M+H]^+$ 283.40. HRMS for $C_{12}H_9Cl_2N_2O_2$ $[M+H]^+$ calculated mass: 283.0035 , measured: 283.0035.

(*E*) 1-(2,4,5-Trichlorophenyl)- 2-(2-nitrovinyl)-1*H*-pyrrole (14).

---

[6] Ikegami, H. *et al*. Hydrazide compound and their preparation, formulation and pesticidal use. PCT Int. Appl., 2007043677, 19 Apr 2007

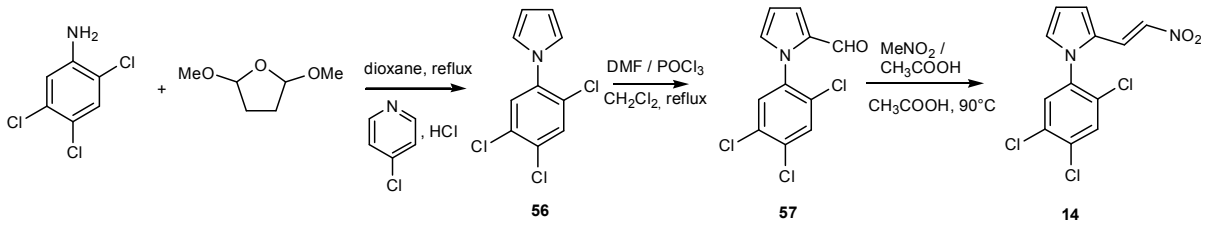

Synthetic procedure for compound (**14**) is similar as that described for compound (**1**) and spectra data are shown below.

1-(2,4,5-Trichlorophenyl)-1*H*-pyrrole (**56**).[7] Brown solid (79%). Mp: 102 °C. ^{1}H NMR (400 MHz, $CDCl_3$) δ 7.54 (s, 1H), 7.38 (s, 1H), 6.80 (t, *J* = 2.2 Hz, 2H), 6.27 (t, *J* = 2.2 Hz, 2H). ^{13}C NMR (100 MHz, $CDCl_3$) δ 138.0, 131.7, 131.7, 131.6, 128.8, 128.2, 122.0, 110.2.

1-(2,4,5-Trichlorophenyl)-1*H*-pyrrole-2-carbaldehyde (**57**)**.** Beige solid (32%). Mp: 96°C. ^{1}H NMR (400 MHz, $CDCl_3$) δ 9.55 (s, 1H), 7.62 (s, 1H), 7.46 (s, 1H), 7.13 (dd, *J* = 4.0 and 1.5 Hz, 1H), 6.94 (m, 1H), 6.47 (dd, *J* = 3.9 and 2.5 Hz, 1H). ^{13}C NMR (100 MHz, $CDCl_3$) δ 178.5, 136.7, 133.7, 132.9, 131.4, 131.1, 131.0, 130.9, 130.0, 123.7, 111.4. LC-MS (ESI): t_R = 5.07 min; $[M+H]^+$ 274.26. HRMS for $C_{11}H_7Cl_3NO$ $[M+H]^+$ calculated mass: 273.9587, measured: 273.9587.

(*E*) 1-(2,4,5-Trichlorophenyl)- 2-(2-nitrovinyl)-1*H*-pyrrole (**14**)**.** Yellow solid (62%). Mp: 166 °C.^{1}H NMR (400 MHz, $CDCl_3$) δ 7.65 (s, 1H), 7.46-7.43 (m, 2H), 7.14 (d, *J* = 13.3 Hz, 1H), 6.91 (dd, *J* = 2.7 and 1.5 Hz, 1H), 6.88 (dd, *J* = 4.0 and 1.3 Hz 1H), 6.42 (dd, *J* = 3.8 and 2.8 Hz, 1H). ^{13}C NMR (100 MHz, $CDCl_3$) δ 135.1, 134.9, 133.0, 132.3, 131.8, 131.5, 130.8 129.7, 127.1, 125.8, 116.6, 112.7. LC-MS (ESI): t_R = 5.42 min; $[M+H]^+$ 317.27. HRMS for $C_{12}H_8Cl_3N_2O_2$ $[M+H]^+$ calculated mass: 316.9645, measured: 316.9645.

(*E*) 1-(2,4,6-Trichlorophenyl)- 2-(2-nitrovinyl)-1*H*-pyrrole (15).

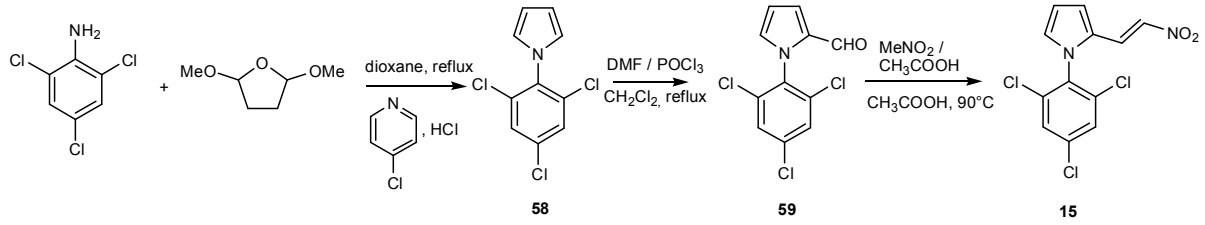

Synthetic procedure for compound (**15**) is similar as that described for compound (**1**) and spectra data are shown below.

1-(2,4,6-Trichlorophenyl)-1*H*-pyrrole (**58**). Beige solid (88%). Mp: 90 °C. ^{1}H NMR (400 MHz, $CDCl_3$) δ 7.37 (s, 2H), 6.60 (t, *J* = 2.2 Hz, 2H), 6.30 (t, *J* = 2.2 Hz, 2H). ^{13}C NMR (100 MHz, $CDCl_3$) δ 135.8, 135.1, 134.6, 128.6, 121.8, 109.7. HRMS for $C_{10}H_7Cl_3N$ $[M+H]^+$ calculated mass: 245.9638, measured: 245.9642.

---

[7] Ma, F *et al* . A recyclable magnetic nanoparticles supported antimony catalyst for the synthesis of N-substituted pyrroles in water. *Applied Catalysis* , *A: General* , **457**, 34-41 (2013)

1-(2,4,6-Trichlorophenyl)-1*H*-pyrrole-2-carbaldehyde (**59**). Yellow solid (30%). Mp: 100 °C. ^{1}H NMR (400 MHz, $CDCl_3$) δ 9.54 (s, 1H), 7.46 (s, 2H), 7.15 (dd, *J* = 4.0 and 1.5 Hz, 1H), 6.89 (m, 1H), 6.52 (dd, *J* = 4.0 and 2.8 Hz, 1H). ^{13}C NMR (100 MHz, $CDCl_3$) δ 178.4, 135.3, 134.8, 134.6, 132.2, 130.4, 128.5, 123.6, 111,7. LC-MS (ESI): t_R = 4.97 min; $[M+H]^+$ 274.31. HRMS for $C_{11}H_7Cl_3NO$ $[M+H]^+$ calculated mass: 273.9587, measured: 273.9587.

(*E*) 1-(2,4,6-Trichlorophenyl)- 2-(2-nitrovinyl)-1 *H*-pyrrole (**15**). Light brown solid (50%). Mp: 114 °C. ^{1}H NMR (400 MHz, $CDCl_3$) δ 7.56 (s, 2H), 7.47 (d, *J* = 13.3 Hz, 1H), 7.10 (d, *J* = 13.3 Hz, 1H), 6.98 (dd, *J* = 4.0 and 1.3 Hz, 1H), 6.92 (dd, *J* = 2.7 and 1.4 Hz 1H), 6.55 (dd, *J* = 3.8 and 2.9 Hz, 1H). ^{13}C NMR (100 MHz, $CDCl_3$) δ 136.8, 135.7, 132.7, 132.6, 129.3, 129.2, 126.8, 125.1, 117.3, 113.0. LC-MS (ESI): t_R = 5.32 min; $[M+H]^+$ 317.32. HRMS for $C_{12}H_8Cl_3N_2O_2$ $[M+H]^+$ calculated mass: 316.9645, measured: 316.9645.

(*E*) 1-(2-Chloro-4-fluorophenyl)-2-(2-nitrovinyl)-1*H*-pyrrole (16).

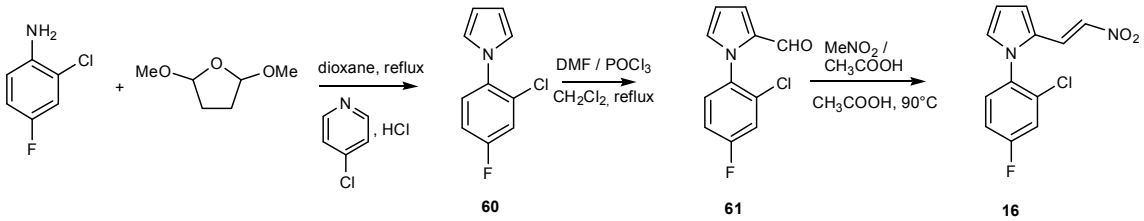

Synthetic procedure for compound (**16**) is similar as that described for compound (**1**) and spectra data are shown below.

1-(2-Chloro-4-fluorophenyl)-1*H*-pyrrole (**60**). Orange oil (80%). ^{1}H NMR (400 MHz, $CDCl_3$) δ 7.47 (d, *J* = 8.0 Hz, 2H), 7.31 (dd, *J* = 8.6 and 7.6 Hz, 1H), 6.76 (t, *J* = 2.3 Hz, 2H), 6.43 (t, *J* = 2.2 Hz, 2H). ^{13}C NMR (100 MHz, $CDCl_3$) δ 161.1 (d, *J* = 250.7 Hz), 135.3 (d, *J* = 3.9 Hz), 131.0 (d, *J* = 10.7 Hz), 129.0 (d, *J* = 10.7 Hz), 122.3 (s), 117.7 (d, *J* = 25.8 Hz), 114.6 (d, *J* = 21.9 Hz), 109.5 (s). HRMS for $C_{10}H_8ClFN$ $[M+H]^+$ calculated mass: 196.0323, measured: 196.0326.

1-(2-Chloro-4-fluorophenyl)-1*H*-pyrrole-2-carbaldehyde (**61**)**.** White solid (61%). Mp: 104°C. ^{1}H NMR (400 MHz, $CDCl_3$) δ 9.43 (s, 1H), 7.25 (dd, *J* = 8.7 and 5.4 Hz, 1H), 7.18 (dd, *J* = 8.0 and 2.8 Hz, 1H), 7.04 (dd, *J* = 4.0 and 1.6 Hz, 1H), 7.02-6.97 (m, 1H), 6.86 (m, 1H), 6.37 (dd, *J* = 4.0 and 2.6 Hz, 1H). ^{13}C NMR (100 MHz, $CDCl_3$) δ 178.6 (s), 162.1 (d, *J* = 250.9 Hz), 133.6 (d, *J* = 3.7 Hz), 133.1 (d, *J* = 10.5 Hz), 133.0 (s), 131.2 (s), 129.9 (d, *J* = 9.2 Hz), 123.0 (bs), 117.5 (d, *J* = 25.9 Hz), 114,6 (d, *J* = 21.6 Hz), 111.0 (s). LC-MS (ESI): t_R = 4.49 min; $[M+H]^+$ 224.40. HRMS for $C_{11}H_8ClFNO$ $[M+H]^+$ calculated mass: 224.0272, measured: 224.0272.

(*E*) 1-(2-Chloro-4-fluorophenyl)-2-(2-nitrovinyl)-1 *H*-pyrrole (**16**). Orange solid (55%). Mp: 102 °C. ^{1}H NMR (400 MHz, $CDCl_3$) δ 7.54 (d, *J* = 13.4 Hz, 1H), 7.40-7.34 (m, 2H), 7.20-7.15 (m, 1H), 7.12 (d, *J* = 13.3 Hz, 1H), 7.01 (dd, *J* = 2.6 and 1.5 Hz, 1H), 6.95 (dd, *J* = 4.0 and 1.3 Hz, 1H), 6.49 (dd, *J* = 3.8 and 2.8 Hz, 1H). ^{13}C NMR (100 MHz, $CDCl_3$) δ 162.6 (d, *J* = 257.9 Hz), 133.9 (d, *J* = 10.9 Hz), 132.5 (s), 132.0 (d, *J*= 3.7 Hz), 130.8 (d, *J* = 9.5 Hz), 130.3 (s), 127.5 (s), 125.9 (s), 118.3 (d, *J* = 25.7 Hz), 116.8 (s), 115.4 (d, *J* = 22.3 Hz), 112.3 (s). LC-MS (ESI): t_R = 4.95 min; $[M+H]^+$ 267.41. HRMS for $C_{12}H_9ClFN_2O_2$ $[M+H]^+$ calculated mass: 267.0331, measured: 267.0329.

(*E*) 1-(4-Chloro-2-fluorophenyl)-2-(2-nitrovinyl)-1*H*-pyrrole (17).

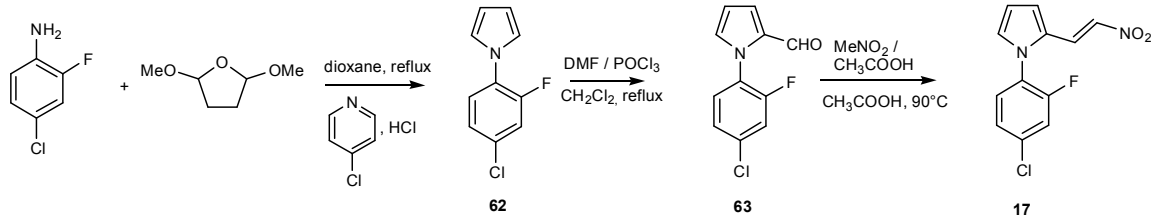

Synthetic procedure for compound (**17**) is similar as that described for compound (**1**) and spectra data are shown below.

1-(4-Chloro-2-fluorophenyl)-1*H*-pyrrole (**62**). Orange oil (75%). ^{1}H NMR (400 MHz, $CDCl_3$) δ 7.34 (t, *J* = 8.5 Hz, 1H), 7.27 (m, 1H), 7.21 (ddd, *J* = 8.4, 2.2 and 1.2 Hz, 1H), 7.03 (q, *J* = 2.1 Hz, 2H), 6.38 (t, *J* = 2.2 Hz, 2H). ^{13}C NMR (100 MHz, $CDCl_3$) δ 154.7 (d, *J* = 255.7 Hz), 131.9 (d, *J* = 9.8 Hz), 127.8 (d, *J* = 10.5 Hz), 125.5 (d, *J* = 2.0 Hz), 125.1 (d, *J* = 4.1 Hz), 121.2 (d, *J* = 4.8 Hz), 117.8 (d, *J* = 23.7 Hz), 110.3 (s). HRMS for $C_{10}H_8ClFN$ $[M+H]^+$ calculated mass: 196.0323, measured: 196.0329.

1-(4-Chloro-2-fluorophenyl)-1*H*-pyrrole-2-carbaldehyde (**63**)**.** White solid (60%). Mp: 82°C. ^{1}H NMR (400 MHz, $CDCl_3$) δ 9.58 (s, 1H), 7.32-7.23 (m, 3H), 7.15 (m, 1H), 7.01 (m, 1H), 6.47 (m, 1H). ^{13}C NMR (100 MHz, $CDCl_3$) δ 178.6 (s), 156.9 (d, *J* = 253.8 Hz), 135.0 (d, *J* = 9.2 Hz), 132.8 (s), 131.5 (s), 128.9 (s), 126.3 (d, *J* = 12.9 Hz), 124.7 (d, *J* = 3.7 Hz), 124,0 (bs), 117,2 (d, *J* = 22.8 Hz), 111.3 (s). LC-MS (ESI): t_R = 4.55 min; $[M+H]^+$ 224.35. HRMS for $C_{11}H_8ClFNO$ $[M+H]^+$ calculated mass: 224.0272, measured: 224.0272.

(*E*) 1-(4-Chloro-2-fluorophenyl)-2-(2-nitrovinyl)-1 *H*-pyrrole (**17**). Yellow solid (60%). Mp: 134 °C. ^{1}H NMR (400 MHz, $CDCl_3$) δ 7.60 (dt, *J* = 13.4 and 0.6 Hz, 1H), 7.34 (dd, *J* = 1.9 and 0.5 Hz, 1H), 7.32 (m, 1H), 7.29 (m, 1H), 7.26-7.23 (m, 1H), 7.03 (m, 1H), 6.94 (dd, *J* = 4.0 and 1.4 Hz, 1H), 6.49 (dd, *J* = 3.8 and 2.8 Hz, 1H). ^{13}C NMR (100 MHz, $CDCl_3$) δ 156.9 (d, *J* = 257.9 Hz), 136.2 (d, *J* = 9.6 Hz), 133.0 (s), 130.2 (s), 129.7 (s), 127.3 (s), 125.8 (s), 125.7 (d, *J* = 3.7 Hz), 124.6 (d, *J* = 12.3 Hz), 118.1 (d, *J* = 22.7 Hz), 116.5 (s), 112.5 (s). LC-MS (ESI): t_R = 5.02 min; $[M+H]^+$ 267.45. HRMS for $C_{12}H_9ClFN_2O_2$ $[M+H]^+$ calculated mass: 267.0331, measured: 267.0330.

(*E*) 1-(2,4-Dibromophenyl)-2-(2-nitrovinyl)-1*H*-pyrrole (18).

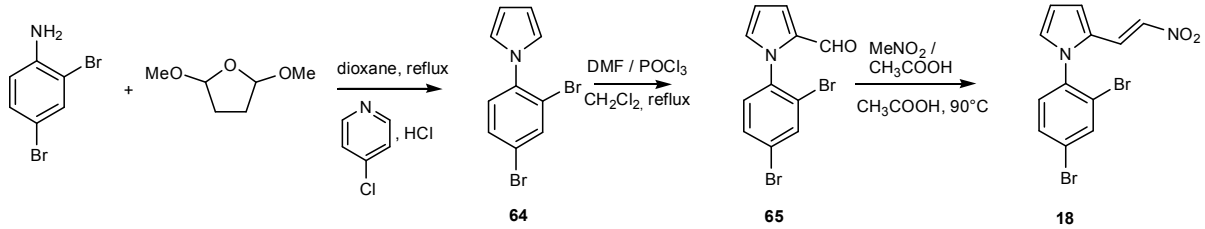

Synthetic procedure for compound (**18**) is similar as that described for compound (**1**) and spectra data are shown below.

1-(2,4-Dibromophenyl)-1*H*-pyrrole (**64**). Orange oil (94%). ^{1}H NMR (400 MHz, $CDCl_3$) δ 7.86 (d, *J* = 2.2 Hz, 1H), 7.52 (dd, *J* = 8.1 and 1.9 Hz, 1H), 7.21 (d, *J* = 8.3 Hz, 1H), 6.85 (t, *J* = 2.4 Hz, 2H), 6.35 (t, *J* = 2.3 Hz, 2H). ^{13}C NMR (100 MHz, $CDCl_3$) δ 139.6, 136.1, 131.3, 129.2, 122.1, 121.4, 120.6, 109.6. HRMS for $C_{10}H_8Br_2N$ $[M+H]^+$ calculated mass: 299.9018, measured: 299.9017.

1-(2,4-Dibromophenyl)-1*H*-pyrrole-2-carbaldehyde (**65**)**.** White solid (30%). Mp: 88 °C. ^{1}H NMR (400 MHz, $CDCl_3$) δ 9.52 (s, 1H), 7.55 (d, *J* = 2.3 Hz, 1H), 7.54 (dd, *J* = 8.4 and 2.3 Hz, 1H), 7.22 (d, *J* = 8.5 Hz, 1H), 7.12 (dd, *J* = 3.9 and 1.7 Hz, 1H), 6.93 (m, 1H), 6.45 (dd, *J* = 3.8 and 2.5 Hz, 1H). ^{13}C NMR (100 MHz, $CDCl_3$) δ 178.2, 138.1, 135.7, 132.7, 131.3, 130.9, 130.0, 123.2, 123.0, 122.9, 111.1. LC-MS (ESI): t_R = 4.92 min; $[M+H]^+$ 328.25. HRMS for $C_{11}H_8Br_2NO$ $[M+H]^+$ calculated mass: 327.8967, measured: 327.8963.

(*E*) 1-(2,4-Dibromophenyl)-2-(2-nitrovinyl)-1 *H*-pyrrole (**18**). Orange solid (60%). Mp: 122 °C. ^{1}H NMR (400 MHz, $CDCl_3$) δ 7.93 (d, *J* = 2.1 Hz, 1H), 7.63 (dd, *J* = 8.4 and 2.2 Hz, 1H), 7.53 (d, *J* = 13.4 Hz, 1H), 7.26 (d, *J* = 8.3 Hz, 1H), 7.13 (d, *J* = 13.5 Hz, 1H), 7.00 (dd, *J* = 2.7 and 1.5 Hz, 1H), 6.95 (dd, *J* = 4.0 and 1.4 Hz, 1H), 6.49 (m, 1H). ^{13}C NMR (100 MHz, $CDCl_3$) δ 136.4, 134.3, 133.4, 132.6, 130.8, 130.3, 130.0, 128.4, 127.4, 125.8, 116.7, 112.3. LC-MS (ESI): t_R = 5.30 min; $[M+H]^+$ 371.30. HRMS for $C_{12}H_9Br_2N_2O_2$ $[M+H]^+$ calculated mass: 370.9025, measured: 370.9023.

(*E*) 1-(2-Bromo-4-chlorophenyl)-2-(2-nitrovinyl)-1*H*-pyrrole (19).

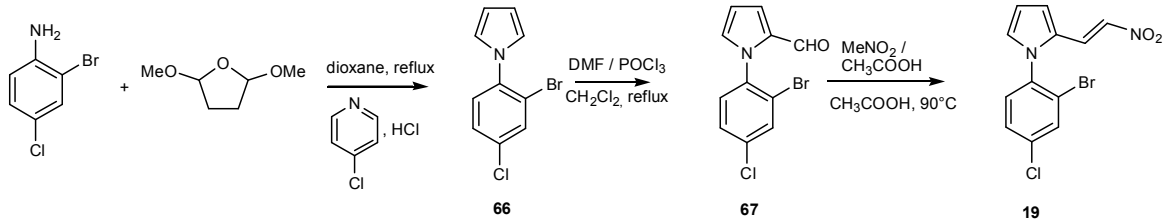

66 67 19

Synthetic procedure for compound (**19**) is is similar as that described for compound (**1**) and spectra data are shown below.

1-(2-Bromo-4-chlorophenyl)-1*H*-pyrrole (**66**).[8] Orange oil (89%). ^{1}H NMR (400 MHz, $CDCl_3$) δ 7.60 (d, *J* = 2.3 Hz, 1H), 7.25 (dd, *J* = 8.4 and 2.3 Hz, 1H), 7.15 (d, *J* = 8.4 Hz, 1H), 6.74 (t, *J* = 2.2 Hz, 2H), 6.24 (t, *J* = 2.3 Hz, 2H). ^{13}C NMR (100 MHz, $CDCl_3$) δ 139.2, 134.6, 133.6, 128.9, 128.5, 122.2, 120.4, 109.6.

1-(2-Bromo-4-chlorophenyl)-1*H*-pyrrole-2-carbaldehyde (**67**). White solid (30%). Mp: 102 °C. ^{1}H NMR (400 MHz, $CDCl_3$) δ 9.43 (s, 1H), 7.61 (d, *J* = 2.4 Hz, 1H), 7.31 (dd, *J* = 8.4 and 2.3 Hz, 1H), 7.20 (d, *J* = 8.3 Hz, 1H), 7.04 (dd, *J* = 4.1 and 1.7 Hz, 1H), 6.85 (m, 1H), 6.38 (dd, *J* = 3.9 and 2.6 Hz, 1H). ^{13}C NMR (100 MHz, $CDCl_3$) δ 178.5, 137.6, 135.4, 133.0, 132.8, 131.0, 129.6, 128.3, 123.0, 122.6, 111.1. LC-MS (ESI): t_R = 4.80 min; $[M+H]^+$ 284.30. HRMS for $C_{11}H_8BrClNO$ $[M+H]^+$ calculated mass: 283.9472, measured: 283.9470.

[8] Sugita, K *et al* . Preparation of tricyclic compounds such as pyrrolobenzoxazepine derivatives and analogs thereof for treatment of hypercholesteremia, hyperlipemia, and arteriosclerosis. Jpn. Kokai Tokkyo Koho, 2008291018, 04 Dec 2008

(*E*) 1-(2-Bromo-4-chlorophenyl)-2-(2-nitrovinyl)-1 *H*-pyrrole (**19**). Yellow solid (53%). Mp: 98 °C. ^{1}H NMR (400 MHz, $CDCl_3$) δ 7.79 (d, *J* = 2.2 Hz, 1H), 7.53 (d, *J* = 13.3 Hz, 1H), 7.48 (dd, *J* = 8.3 and 2.3 Hz, 1H), 7.32 (d, *J* = 8.3 Hz, 1H), 7.12 (d, *J* = 13.3 Hz, 1H), 6.99 (dd, *J* = 2.5 and 1.5 Hz, 1H), 6.95 (dd, *J* = 4.0 and 1.3 Hz, 1H), 6.49 (dd, *J* = 3.8 and 2.7 Hz 1H). ^{13}C NMR (100 MHz, $CDCl_3$) δ 136.6, 136.0, 133.7, 132.6, 130.4, 130.0, 129.0, 127.4, 125.7, 123.3, 116.9, 112.3. LC-MS (ESI): t_R = 5.23 min; $[M+H]^+$ 327.35. HRMS for $C_{12}H_9BrClN_2O_2$ calculated mass: 326.9530, measured: 326.9529

(*E*) 1-(4-Bromo-2-chlorophenyl)-2-(2-nitrovinyl)-1*H*-pyrrole (20).

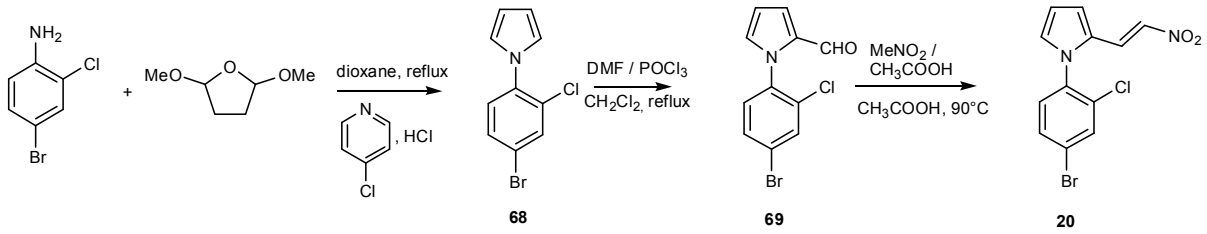

Synthetic procedure for compound (**20**) is similar as that described for compound (**1**) and spectra data are shown below.

1-(4-Bromo-2-chlorophenyl)-1*H*-pyrrole (**68**). Orange oil (90%). ^{1}H NMR (400 MHz, $CDCl_3$) δ 7.68 (d, *J* = 2.3 Hz, 1H), 7.47 (dd, *J* = 8.4 and 2.3 Hz, 1H), 7.22 (d, *J* = 8.4 Hz, 1H), 6.89 (t, *J* = 2.1 Hz, 2H), 6.35 (t, *J* = 2.2 Hz, 2H). ^{13}C NMR (100 MHz, $CDCl_3$) δ 137.9, 133.3, 130.8, 130.6, 128.8, 122.0, 120.8, 109.7. HRMS for $C_{10}H_8BrClN$ $[M+H]^+$ calculated mass: 255.9523, measured: 255.9523.

1-(4-Bromo-2-chlorophenyl)-1*H*-pyrrole-2-carbaldehyde (**69**). Beige solid (31%). Mp: 92 °C. ^{1}H NMR (400 MHz, $CDCl_3$) δ 9.52 (s, 1H), 7.68 (d, *J* = 2.1 Hz, 1H), 7.50 (dd, *J* = 8.4 and 2.2 Hz, 1H), 7.22 (d, *J* = 8.3 Hz, 1H), 7.13 (dd, *J* = 4.0 and 1.7 Hz, 1H), 6.94 (m, 1H), 6.46 (dd, *J* = 3.9 and 2.6 Hz, 1H). ^{13}C NMR (100 MHz, $CDCl_3$) δ 178.5, 136.5, 133.1, 132.9, 132.8 131.1, 130.7, 129.9, 123.2, 122.9, 111.2. LC-MS (ESI): t_R = 4.83 min; $[M+H]^+$ 284.25. HRMS for $C_{11}H_8BrClNO$ $[M+H]^+$ calculated mass: 283.9472, measured: 283.9468.

(*E*) 1-(4-Bromo-2-chlorophenyl)-2-(2-nitrovinyl)-1 *H*-pyrrole (**20**). Orange solid (57%). Mp: 124 °C. ^{1}H NMR (400 MHz, $CDCl_3$) δ 7.77 (d, *J* = 2.1 Hz, 1H), 7.59 (dd, *J* = 8.3 and 2.1 Hz, 1H), 7.54 (d, *J* = 13.3 Hz, 1H), 7.25 (d, *J* = 8.3 Hz, 1H), 7.16 (d, *J* = 13.3 Hz, 1H), 7.00 (dd, *J* = 2.7 and 1.4 Hz, 1H), 6.95 (dd, *J* = 4.0 and 1.4 Hz, 1H), 6.49 (m, 1H). ^{13}C NMR (100 MHz, $CDCl_3$) δ 134.8, 133.6, 133.7, 132.6, 131.4, 130.6, 130.0, 127.4, 125.7, 124.1, 116.7, 112.4. LC-MS (ESI): t_R = 5.26 min; $[M+H]^+$ 327.35. HRMS for $C_{12}H_9BrClN_2O_2$ calculated mass: 326.9530, measured: 326.9529.

(*E*) 1-(4-Chloro-2-iodophenyl)-2-(2-nitrovinyl)-1*H*-pyrrole (21).

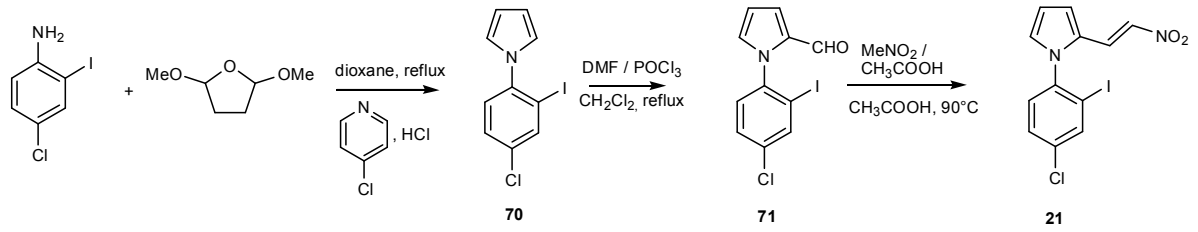

Synthetic procedure for compound (**21**) is similar as that described for compound (**1**) and spectra data are shown below.

1-(4-Chloro-2-iodophenyl)-1*H*-pyrrole (**70**).[9] Yellow solid (88%). Mp: 72 °C. ^{1}H NMR (400 MHz, $CDCl_3$) δ 7.84 (d, J = 2.3 Hz, 1H), 7.31 (dd, J = 8.4 and 2.2 Hz, 1H), 7.13 (d, J = 8.5 Hz, 1H), 6.74 (t, J = 2.2 Hz, 2H), 6.26 (t, J = 2.2 Hz, 2H). ^{13}C NMR (100 MHz, $CDCl_3$) δ 142.7, 139.2, 134.2, 129.1, 128.4, 122.1, 109.5, 96.0.

1-(4-Chloro-2-iodophenyl)-1*H*-pyrrole-2-carbaldehyde (**71**). Pink solid (30%). Mp: 62 °C. ^{1}H NMR (400 MHz, $CDCl_3$) δ 9.51 (s, 1H), 7.91 (d, J = 2.3 Hz, 1H), 7.42 (dd, J = 8.3 and 2.2 Hz, 1H), 7.24 (d, J = 8.3 Hz, 1H), 7.12 (dd, J = 4.0 and 1.7 Hz, 1H), 6.90 (m, 1H), 6.46 (dd, J = 4.0 and 2.6 Hz, 1H). ^{13}C NMR (100 MHz, $CDCl_3$) δ 178.5, 141.2, 138.8, 135.3, 132.5, 130.8, 129.1, 128.8, 122.9, 111.2, 97.8. LC-MS (ESI): t_R = 4.86 min; $[M+H]^+$ 332.23. HRMS for $C_{11}H_8ClINO$ $[M+H]^+$ calculated mass: 331.9333, measured: 331.9329.

(*E*) 1-(4-Chloro-2-iodophenyl)-2-(2-nitrovinyl)-1 *H*-pyrrole (**21**). Orange solid (57%). Mp: 100 °C. ^{1}H NMR (400 MHz, $CDCl_3$) δ 7.99 (d, J = 2.0 Hz, 1H), 7.52 (m, 2H), 7.28 (d, J = 8.2 Hz, 1H), 7.07 (d, J = 13.3 Hz, 1H), 6.94 (m, 2H), 6.49 (m, 1H). ^{13}C NMR (100 MHz, $CDCl_3$) δ 139.6, 136.5, 132.6, 132.5, 129.9, 129.8, 129.5, 127.5, 125.4, 117.2, 112.4, 98.6. LC-MS (ESI): t_R = 5.35 min; $[M+H]^+$ 375.29. HRMS for $C_{12}H_9ClIN_2O_2$ calculated mass: 374.9391, measured: 374.9391

(*E*) 1-(2-Chloro-4-iodophenyl)-2-(2-nitrovinyl)-1*H*-pyrrole (22).

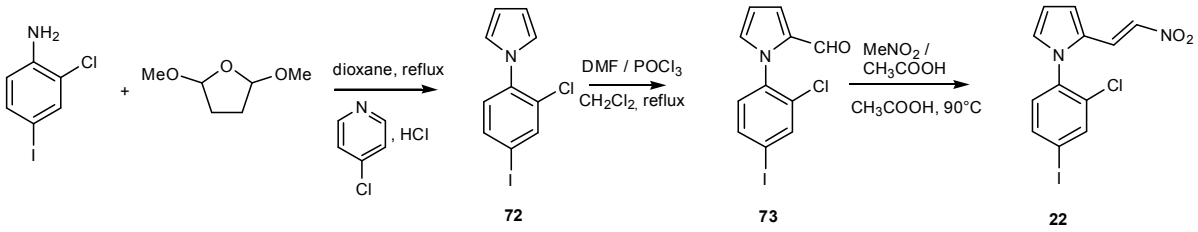

Synthetic procedure for compound (**22**) is similar as that described for compound (**1**) and spectra data are shown below.

1-(2-Chloro-4-iodophenyl)-1*H*-pyrrole (**72**). Orange oil (95%). ^{1}H NMR (400 MHz, $CDCl_3$) δ 7.78 (d, J = 2.0 Hz, 1H), 7.57 (dd, J = 8.3 and 1.9 Hz, 1H), 6.99 (d, J = 8.3 Hz, 1H), 6.80 (t, J = 2.3 Hz, 2H), 6.27 (t, J = 2.3 Hz, 2H). ^{13}C NMR (100 MHz, $CDCl_3$) δ 139.0, 138.6, 137.8,

[9] Chai, D. *et al* . Mechanistic Studies of Pd-Catalyzed Regioselective Aryl C-H Bond Functionalization with Strained Alkenes: Origin of Regioselectivity. *Chemistry - A European Journal*, **29**, 8175-8188, S8175/1-S8175/54 (2011).

130.5, 129.0, 122.0, 109.8, 91.6. HRMS for $C_{10}H_8ClIN$ $[M+H]^+$ calculated mass: 303.9384, measured: 303.9384.

1-(2-Chloro-4-iodophenyl)-1*H*-pyrrole-2-carbaldehyde (**73**). Yellow solid (32%). Mp: 92 °C. ^1H NMR (400 MHz, $CDCl_3$) δ 9.52 (s, 1H), 7.87 (d, *J* = 2.0 Hz, 1H), 7.69 (dd, *J* = 8.3 and 2.0 Hz, 1H), 7.13 (dd, *J* = 3.8 and 1.6 Hz, 1H), 7.07 (d, *J* = 8.3 Hz, 1H), 6.94 (m, 1H), 6.46 (dd, *J* = 3.9 and 2.7 Hz, 1H). ^{13}C NMR (100 MHz, $CDCl_3$) δ 178.5, 138.5, 137.2, 136.6, 133.0, 132.8, 131.0, 130.1, 123.2, 111.2, 94.1. LC-MS (ESI): t_R = 4.98 min; $[M+H]^+$ 332.28. HRMS for $C_{11}H_8ClINO$ $[M+H]^+$ calculated mass: 331.9333, measured: 331.9329.

(*E*) 1-(2-Chloro-4-iodophenyl)-2-(2-nitrovinyl)-1*H*-pyrrole (**22**). Orange solid (57%). Mp: 96 °C. ^1H NMR (400 MHz, $CDCl_3$) δ 7.96 (d, *J* = 2.0 Hz, 1H), 7.78 (dd, *J* = 8.2 and 1.9 Hz, 1H), 7.56 (d, *J* = 13.4 Hz, 1H), 7.17 (d, *J* = 13.3 Hz, 1H), 7.09 (d, *J* = 8.3 Hz, 1H), 7.00 (dd, *J* = 2.1 and 1.3 Hz, 1H), 6.95 (m, 1H), 6.49 (t, *J* = 3.3 Hz, 1H). ^{13}C NMR (100 MHz, $CDCl_3$) δ 139.3, 137.3, 135.5, 133.4, 132.6, 130.8, 130.0, 127.4, 125.7, 116.8, 112.4, 95.4. LC-MS (ESI): t_R = 5.35 min; $[M+H]^+$ 375.29. HRMS for $C_{12}H_9ClIN_2O_2$ calculated mass: 374.9391, measured: 374.9391.

(*E*) 1-(3-Chlorophenyl)-3-(2-nitrovinyl)-1*H*-pyrrole (23).

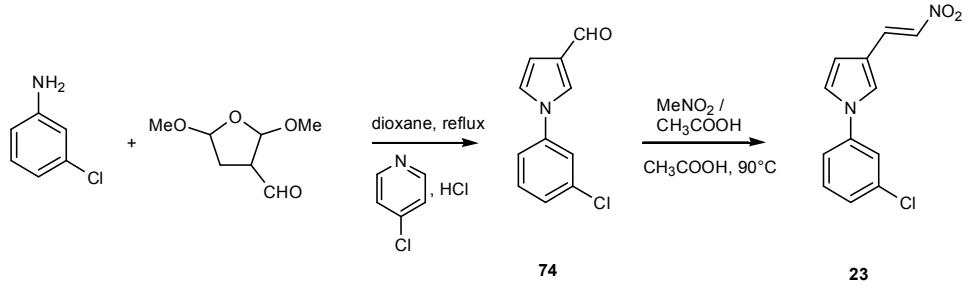

Synthetic procedure for compound (**23**) is similar as that described for compound (**2**) and spectra data are shown below.

1-(3-Chlorophenyl)-1*H*-pyrrole-3-carbaldehyde (**74**).[10] Brown solid (50%). Mp: 68°C. ^1H NMR (400 MHz, $CDCl_3$) δ 9.86 (s, 1H), 7.66 (t, *J* = 2.0 Hz, 1H), 7.44 (t, *J* = 2.0 Hz, 1H), 7.41 (d, *J* = 8.0 Hz, 1H), 7.37-7.31 (m, 2H), 7.07 (m, 1H), 6.81 (dd, *J* = 3.1 and 1.6 Hz, 1H). ^{13}C NMR (100 MHz, $CDCl_3$) δ 185.4, 140.5, 135.6, 131.0, 128.5, 127.4, 127.0, 122.2, 121.4, 119.2, 110,0. LC-MS (ESI): t_R = 4.42 min; $[M+H]^+$ 206.34.

(*E*) 1-(3-chlorophenyl)-3-(2-nitrovinyl)-1*H*-pyrrole (**23**). Brown solid (50%). Mp: 104 °C. ^1H NMR (400 MHz, $CDCl_3$) δ 8.01 (d, *J* = 13.3 Hz, 1H), 7.46 (d, *J* = 13.3 Hz, 1H), 7.43-7.40 (m, 3H), 7.33 (dt, *J* = 8.1 and 1.0 Hz, 1H), 7.39 (dt, *J* = 8.0 and 1.0 Hz, 1H), 7.11 (t, *J* = 2.7 Hz, 1H), 6.57 (dd, *J* = 3.0 and 1.6 Hz, 1H). ^{13}C NMR (100 MHz, $CDCl_3$) δ 140.4, 135.7, 134.3, 133.1, 131.0, 127.2, 124.9, 122.7, 121.1, 118.8, 118.2, 109.5. LC-MS (ESI): t_R = 5.15 min; $[M+H]^+$ 249.40. HRMS for $C_{12}H_{10}ClN_2O_2$ $[M+H]^+$ calculated mass: 249.0425, measured: 249.0424.

[10] McInnes, Campbell and Liu, Shu. Cyclin based inhibitors of CDK2 and CDK4. U.S. Pat. Appl. Publ., 20130289240, 31 Oct 2013.

(*E*) 1-(3,4-Dichlorophenyl)-3-(2-nitrovinyl)-1*H*-pyrrole (24) .

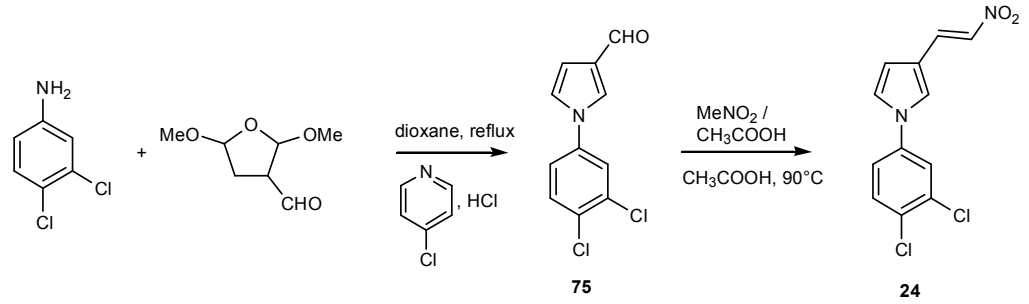

Synthetic procedure for compound (**24**) is similar as that described for compound (**2**) and spectra data are shown below.

1-(3,4-Dichlorophenyl)-1*H*-pyrrole-3-carbaldehyde (**75**).[11] Orange solid (30%). Mp: 112 °C. ^{1}H NMR (400 MHz, $CDCl_3$) δ 9.78 (s, 1H), 7.56 (t, *J* = 1.9 Hz, 1H), 7.48 (m, 2H), 7.21 (dd, *J* = 8.6 and 2.6 Hz, 1H), 6.98 (t, *J* = 2.6 Hz, 1H), 6.74 (dd, *J* = 3.0 and 1.7 Hz, 1H). ^{13}C NMR (100 MHz, $CDCl_3$) δ 185.4, 138.8, 134.0, 131.6, 131.4, 128.7, 126.8, 123.0, 122.1, 120.2, 110.0. LC-MS (ESI): t_R = 4.92 min; $[M+H]^+$ 240.26.

(*E*) 1-(3,4-Dichlorophenyl)-3-(2-nitrovinyl)-1*H*-pyrrole (**24**) . Brown solid (40%). Mp: 128 °C. ^{1}H NMR (400 MHz, $CDCl_3$) δ 8.01 (d, *J* = 13.2 Hz, 1H), 7.58 (d, *J* = 8.6 Hz, 1H), 7.54 (d, *J* = 2.9 Hz, 1H), 7.47 (d, *J* = 13.4 Hz, 1H), 7.41 (t, *J* = 2.0 Hz, 1H), 7.27 (dd, *J* = 8.6 and 2.6 Hz, 1H), 7.10 (t, *J* = 2.5 Hz, 1H), 6.59 (dd, *J* = 3.1 and 1.8 Hz, 1H). ^{13}C NMR (100 MHz, $CDCl_3$) δ 138.6 134.6, 134.0, 132.8, 131.6, 131.2, 124.7, 122.7, 122.6, 119.9, 118.4, 109.8. LC-MS (ESI): t_R = 5.37 min; $[M+H]^+$ 283.44. HRMS for $C_{12}H_9Cl_2N_2O_2$ $[M+H]^+$ calculated mass: 283.0035, measured: 283.0036.

(*E*) 1-(3,5-Dichlorophenyl)-3-(2-nitrovinyl)-1*H*-pyrrole (25).

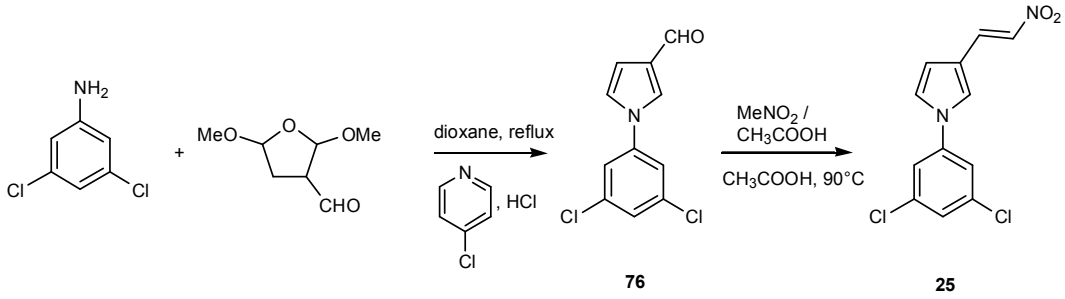

Synthetic procedure for compound (**25**) is similar as that described for compound (**2**) and spectra data are shown below.

1-(3,5-Dichlorophenyl)-1*H*-pyrrole-3-carbaldehyde (**76).** Brown solid (35%). Mp: 154 °C. ^{1}H NMR (400 MHz, $CDCl_3$) δ 9.86 (s, 1H), 7.65 (t, *J* = 2.1 Hz, 1H), 7.36-7.34 (m, 3H), 7.07 (t, *J* = 2.8 Hz, 1H), 6.83 (dd, *J* = 3.0 and 1.6 Hz, 1H). ^{13}C NMR (100 MHz, $CDCl_3$) δ 185.3, 141.1, 136.3, 128.8, 127.3, 126.7, 122.0, 119.7, 110.4. LC-MS (ESI): t_R = 4.85 min; $[M+H]^+$ 240.35. HRMS for $C_{11}H_8Cl_2NO$ $[M+H]^+$ calculated mass: 239.9975, measured: 239.9977.

[11] Haldar, P. *et al*. Sodium borohydride-iodine mediated reduction of γ-lactam carboxylic acids followed by DDQ mediated oxidative aromatization: a simple approach towards N-aryl-formylpyrroles and 1,3-diaryl-formylpyrroles. *Tetrahedron*, **14**, 3049-3056 (2007)

(*E*) 1-(3,5-Dichlorophenyl)-3-(2-nitrovinyl)-1*H*-pyrrole (**25**) .Brown solid (40%). Mp: 190°C. ^{1}H NMR (400 MHz, $CDCl_3$) δ 7.99 (d, *J* = 13.3 Hz, 1H), 7.45 (d, *J* = 13.4 Hz, 1H), 7.41 (t, *J* = 1.9 Hz, 1H), 7.34 (t, *J* = 1.7 Hz, 1H), 7.31 (d, *J* = 1.8 Hz, 2H), 7.10 (t, *J* = 2.7 Hz, 1H), 6.58 (dd, *J* = 3.0 and 1.6 Hz, 1H). ^{13}C NMR (100 MHz, $CDCl_3$) δ 140.9, 136.3, 134.7, 132.6, 127.1, 124.5, 122.6, 119.3, 118.6, 109.9. LC-MS (ESI): t_R = 5.49 min; $[M+H]^+$ 283.40. HRMS for $C_{12}H_9Cl_2N_2O_2$ $[M+H]^+$ calculated mass: 283.0035, measured: 283.0035.

(*E*) 1-(2,6-Dichlorophenyl)-3-(2-nitrovinyl)-1*H*-pyrrole (26).

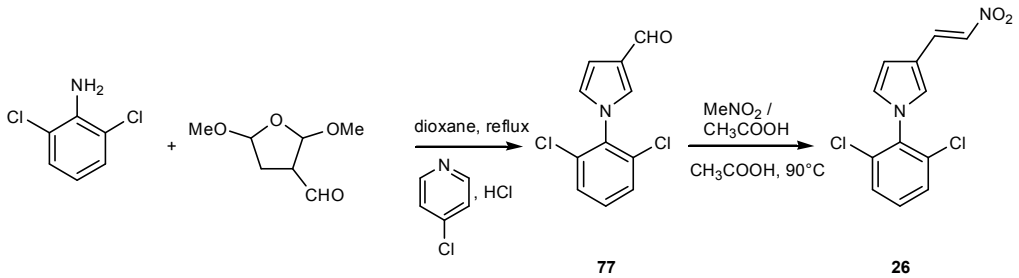

Synthetic procedure for compound (**26**) is similar as that described for compound (**2**) and spectra data are shown below.

1-(2,6-Dichlorophenyl)-1*H*-pyrrole-3-carbaldehyde (**77**).[6] White solid (30%). Mp: 92°C. ^{1}H NMR (400 MHz, $CDCl_3$) δ 9.79 (s, 1H), 7.42-7.39 (m, 2H), 7.30 (m, 1H), 7.27 (dd, *J* = 3.7 and 1.1 Hz, 1H), 6.75 (dd, *J* = 3.1 and 1.5 Hz, 1H), 6.66 (m, 1H). ^{13}C NMR (100 MHz, $CDCl_3$) δ 185.4, 135.5, 133.9, 130.6, 130.4, 128.9, 127.7, 124.7, 108.5. LC-MS (ESI): t_R = 4.85 min; $[M+H]^+$ 240.39.

(*E*) 1-(2,6-Dichlorophenyl)-3-(2-nitrovinyl)-1*H*-pyrrole (**26**) .Yellow solid (50%). Mp: 108 °C. ^{1}H NMR (400 MHz, $CDCl_3$) δ 8.04 (d, *J* = 13.2 Hz, 1H), 7.49-7.46 (m, 3H), 7.37 (dd, *J* = 8.8 and 7.3 Hz, 1H), 7.12 (m, 1H), 6.77 (m, 1H), 6.61-6.58 (m, 1H). ^{13}C NMR (100 MHz, $CDCl_3$) δ 134.1, 133.9, 133.4, 130.5, 129.9, 128.9, 128.1, 125.3, 117.1, 108.0. LC-MS (ESI): t_R = 5.08 min; $[M+H]^+$ 283.40. HRMS for $C_{12}H_9Cl_2N_2O_2$ $[M+H]^+$ calculated mass: 283.0035, measured: 283.0035.

(*E*) 3-(2-Nitrovinyl)-1-(2,4,6-trichlorophenyl)-1*H*-pyrrole (27).

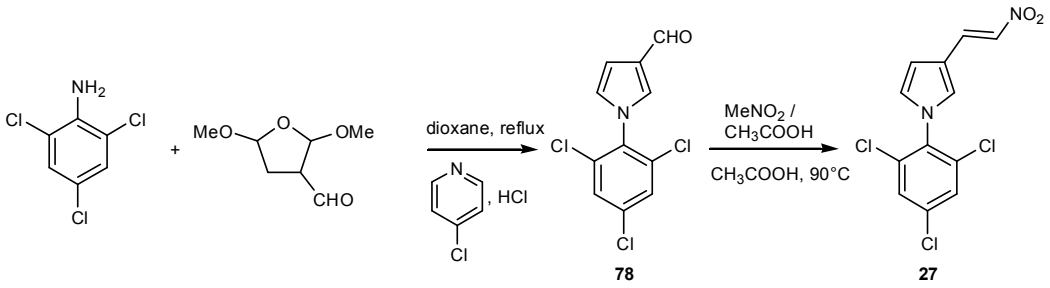

Synthetic procedure for compound (**27**) is similar as that described for compound (**2**) and spectra data are shown below.

1-(2,4,6-Trichlorophenyl)-1*H*-pyrrole-3-carbaldehyde (**78**)**.** Beige solid (30%). Mp: 74°C. ^{1}H NMR (400 MHz, $CDCl_3$) δ 9.87 (s, 1H), 7.50 (s, 2H), 7.31 (t, *J* = 2.0 Hz, 1H), 6.83 (dd, *J* = 3.1 and 1.5 Hz, 1H), 6.71-6.69 (m, 1H). ^{13}C NMR (100 MHz, $CDCl_3$) δ 185.3, 135.8, 134.6, 134.3, 130.1, 128.9, 127.9, 124.6, 108.8. LC-MS (ESI): t_R = 4.86 min; $[M+H]^+$ 274.31. HRMS for $C_{11}H_7Cl_3NO$ $[M+H]^+$ calculated mass: 273.9587, measured: 273.9582.

(*E*) 3-(2-Nitrovinyl)-1-(2,4,6-trichlorophenyl)-1*H*-pyrrole (**27**). Yellow solid (50%). Mp: 90 °C. ^{1}H NMR (400 MHz, $CDCl_3$) δ 8.02 (d, *J* = 13.2 Hz, 1H), 7.50 (s, 2H), 7.47 (d, *J* = 13.3 Hz, 1H), 7.08 (t, *J* = 1.7 Hz, 1H), 6.73 (t, *J* = 6.7 Hz, 1H), 6.58 (m, 1H). ^{13}C NMR (100 MHz, $CDCl_3$) δ 135.8, 134.5, 134.3, 134.2, 133.1, 128.9, 127.9, 125.2, 117.3, 108.3. LC-MS (ESI): t_R = 5.39 min; $[M-H]^-$ 315.31. HRMS for $C_{12}H_8Cl_3N_2O_2$ $[M+H]^+$ calculated mass: 316.9645, measured: 316.9645.

(*E*) 1-(2-Bromo-4-chlorophenyl)-3-(2-nitrovinyl)-1*H*-pyrrole (28).

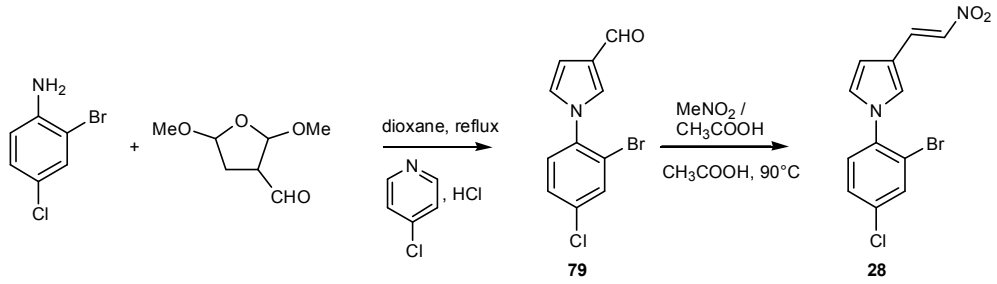

Synthetic procedure for compound (**28**) is similar as that described for compound (**2**) and spectra data are shown below.

1-(2-Bromo-4-chlorophenyl)-1*H*-pyrrole-3-carbaldehyde (**79**). Rose solid (32%). Mp: 86 °C. ^{1}H NMR (400 MHz, $CDCl_3$) δ 9.85 (s, 1H), 7.74 (d, *J* = 2.3 Hz, 1H), 7.44 (t, *J* = 1.8 Hz, 1H), 7.42 (dd, *J* = 8.4 and 2.2 Hz, 1H), 7.30 (d, *J* = 8.3 Hz, 1H), 6.83 (m, 1H), 6.78 (dd, *J* = 3.0 and 1.7 Hz, 1H). ^{13}C NMR (100 MHz, $CDCl_3$) δ 185.4, 137.8, 135.3, 133.7, 130.1, 128.7, 128.7, 127.7, 124.9, 120.4, 108.7. LC-MS (ESI): t_R = 4.72 min; $[M+H]^+$ 284.25. HRMS for $C_{11}H_8BrClNO$ $[M+H]^+$ calculated mass: 283.9472, measured: 283.9470.

(*E*) 1-(2-Bromo-4-chlorophenyl)-3-(2-nitrovinyl)-1 *H*-pyrrole (**28**). Yellow solid (53%). ^{1}H NMR (400 MHz, $CDCl_3$) δ 8.08 (d, *J* = 13.2 Hz, 1H), 8.00 (d, *J* = 2.4 Hz, 1H), 7.93 (d, *J* = 13.1 Hz, 1H), 7.72 (t, *J* = 1.8 Hz, 1H), 7.61 (dd, *J* = 8.5 and 2.4 Hz, 1H), 7.53 (d, *J* = 8.6 Hz 1H), 7.13 (t, *J* = 1.8 Hz, 1H), 6.82 (dd, *J* = 2.8 and 1.6 Hz, 1H). ^{13}C NMR (100 MHz, $CDCl_3$)

δ 138.2, 134.9, 134.5, 134.3, 133.3, 130.3, 130.0, 129.4, 126.4, 120.4, 117.4, 109.2. LC-MS (ESI): t_R = 5.36 min; $[M+H]^+$ 327.35. HRMS for $C_{12}H_9BrClN_2O_2$ $[M+H]^+$ calculated mass: 326.9530, measured: 326.9529.

(*E*) 1-(4-Bromo-2-chlorophenyl)-3-(2-nitrovinyl)-1*H*-pyrrole (29).

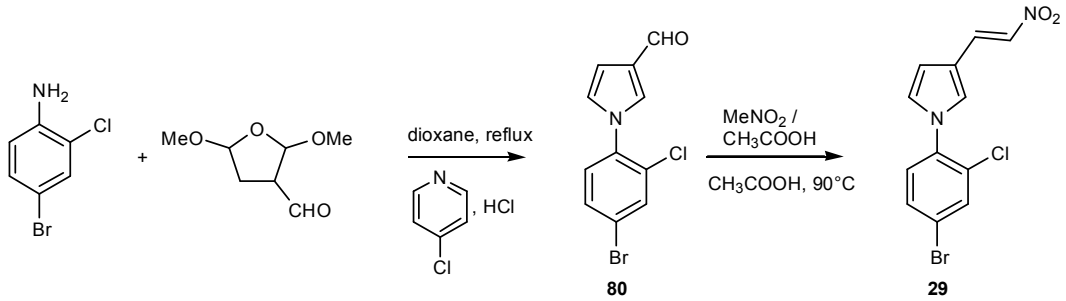

Synthetic procedure for compound (**29**) is similar as that described for compound (**2**) and spectra data are shown below.

1-(4-Bromo-2-chlorophenyl)-1*H*-pyrrole-3-carbaldehyde (**80**). Orange solid (34%). Mp: 100 °C. ^{1}H NMR (400 MHz, $CDCl_3$) δ 9.88 (s, 1H), 7.75 (d, *J* = 2.1 Hz, 1H), 7.55 (dd, *J* = 8.4 and 2.1 Hz, 1H), 7.50 (t, *J* = 1.7 Hz, 1H), 7.28 (d, *J* = 8.3 Hz, 1H), 6.89 (t, *J* = 2.7 Hz, 1H), 6.82 (dd, *J* = 2.9 and 1.5 Hz, 1H). ^{13}C NMR (100 MHz, $CDCl_3$) δ 185.4, 136.6, 133.6, 131.2, 130.8, 130.0, 128.7, 127.8, 124.8, 122.5, 108.9. LC-MS (ESI): t_R = 4.76 min; $[M+H]^+$ 284.21. HRMS for $C_{11}H_8BrClNO$ $[M+H]^+$ calculated mass: 283.9472, measured: 283.9470.

(*E*) 1-(4-Bromo-2-chlorophenyl)-3-(2-nitrovinyl)-1 *H*-pyrrole (**29**).Yellow solid (55%). Mp: 182°C. ^{1}H NMR (400 MHz, DMSO-d_6) δ 8.09 (d, *J* = 13.3 Hz, 1H), 8.00 (dd, *J* = 2.1 and 0.9 Hz, 1H), 7.93 (d, *J* =13.3 Hz, 1H), 7.76 (bs, 1H), 7.71 (ddd, *J* = 8.5, 2.1, and 0.9 Hz, 1H), 7.49 (dd, *J* = 8.4 and 0.8 Hz, 1H), 7.17 (m, 1H), 6.83 (m, 2.8 and 1.6 Hz, 1H). ^{13}C NMR (100 MHz, DMSO-d_6) δ 136.9, 134.8, 134.6, 133.3, 132.0, 130.2, 130.1, 130.0, 126.3, 122.1, 117.6, 109.3. LC-MS (ESI): t_R = 5.38 min; $[M+H]^+$ 327.35. HRMS for $C_{12}H_9BrClN_2O_2$ $[M+H]^+$ calculated mass: 326.9530, measured: 326.9528.

(*E*) 1-(2,4-Dibromophenyl)-2-(2-nitrovinyl)-1*H*-pyrrole (30).

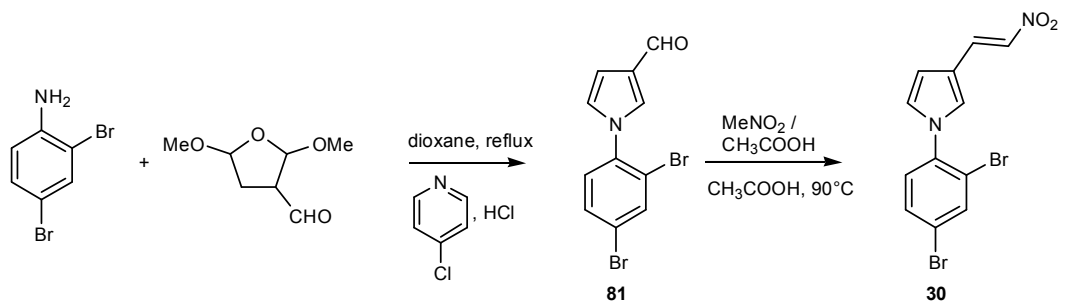

Synthetic procedure for compound (**30**) is similar as that described for compound (**2**) and spectra data are shown below.

1-(2,4-Dibromophenyl)-1*H*-pyrrole-3-carbaldehyde (**81**). Pink solid (32%). Mp: 86 °C. ^{1}H NMR (400 MHz, $CDCl_3$) δ 9.85 (s, 1H), 7.89 (d, *J* = 2.1 Hz, 1H), 7.57 (dd, *J* = 8.5 and 2.1 Hz, 1H), 7.45 (t, *J* = 1.8 Hz, 1H), 7.24 (d, *J* = 8.4 Hz, 1H), 6.84 (m, 1H), 6.78 (m, 1H), . ^{13}C NMR (100 MHz, $CDCl_3$) δ 185.4, 138.2, 136.4, 131.7, 130.0, 129.1, 127.7, 124.8, 123.0, 120.6, 108.7. LC-MS (ESI): t_R = 4.81 min; $[M+H]^+$ 328.25.

(*E*) 1-(2,4-Dibromophenyl)-2-(2-nitrovinyl)-1 *H*-pyrrole (**30**). Yellow solid (52%). Mp: 190 °C. ^{1}H NMR (400 MHz, DMSO-d_6) δ 8.10 (s, 1H), 8.08 (d, *J* = 13.2 Hz, 1H), 7.92 (d, *J* = 13.1 Hz, 1H), 7.73 (dd, *J* = 8.4 and 2.1 Hz, 1H), 7.45 (d, *J* = 8.5 Hz, 1H), 7.12 (m, 1H), 7.17 (m, 1H), 6.80 (dd, 3.0 and 1.6 Hz, 1H). ^{13}C NMR (100 MHz, DMSO-d_6) δ 138.6, 136.0, 134.9, 134.5, 132.4, 130.3, 130.2, 126.4, 122.6, 120.6, 117.4, 109.2. LC-MS (ESI): t_R = 5.44 min; $[M+H]^+$ 369.37. HRMS for $C_{12}H_9Br_2N_2O_2$ $[M+H]^+$ calculated mass: 370.9025, measured: 370.9023.

(*E*) 1-(4-Chloro-2-iodophenyl)-3-(2-nitrovinyl)-1*H*-pyrrole (31).

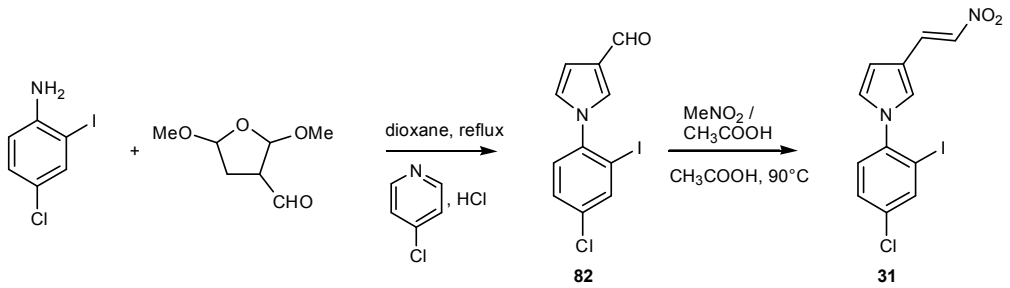

Synthetic procedure for compound (**31**) is similar as that described for compound (**2**) and spectra data are shown below.

1-(4-Chloro-2-iodophenyl)-1*H*-pyrrole-3-carbaldehyde (**82**). Yellow solid (31%). Mp: 102 °C. ^{1}H NMR (400 MHz, $CDCl_3$) δ 9.79 (s, 1H), 7.89 (d, *J* = 2.4 Hz, 1H), 7.38 (dd, *J* = 8.4 and 2.3 Hz, 1H), 7.31 (t, *J* = 1.8 Hz, 1H), 7.18 (d, *J* = 8.4 Hz, 1H), 6.71 (m, 2H). ^{13}C NMR (100 MHz, $CDCl_3$) δ 185.4, 141.3, 139.5, 135.5, 130.0, 129.5, 128.2, 127.7, 124.8, 108.8, 95.6. LC-MS (ESI): t_R = 4.81 min; $[M+H]^+$ 332.23. HRMS for $C_{11}H_8ClINO$ $[M+H]^+$ calculated mass: 331.9333, measured: 331.9328.

(*E*) 1-(4-Chloro-2-iodophenyl)-3-(2-nitrovinyl)-1*H*-pyrrole (**31**).Yellow solid (53%). ^{1}H NMR (400 MHz, $CDCl_3$) δ 8.03 (d, *J* = 13.3 Hz, 1H), 7.96 (d, *J* = 2.3 Hz, 1H), 7.47 (d, *J* = 13.3 Hz, 1H), 7.45 (dd, *J* = 2.3 and 8.3 Hz, 1H), 7.24 (d, *J* = 8.4 Hz, 1H), 7.16 (t, *J* = 1.8 Hz, 1H), 6.82 (t, *J* = 2.8 Hz, 1H), 6.55 (dd, *J* =2.9 and 1.6 Hz, 1H). ^{13}C NMR (100 MHz, $CDCl_3$) δ 139.3, 138.9, 137.2, 137.1, 134.2, 133.2, 130.5, 128.7, 127.8, 125.3, 117.3, 108.3. LC-MS (ESI): t_R = 5.40 min; $[M-H]^-$ 373.32. HRMS for $C_{12}H_9ClIN_2O_2$ $[M+H]^+$ calculated mass: 374.9391, measured: 374.9390.

(*E*) 1-(2-Chloro-4-iodophenyl)-3-(2-nitrovinyl)-1*H*-pyrrole (32).

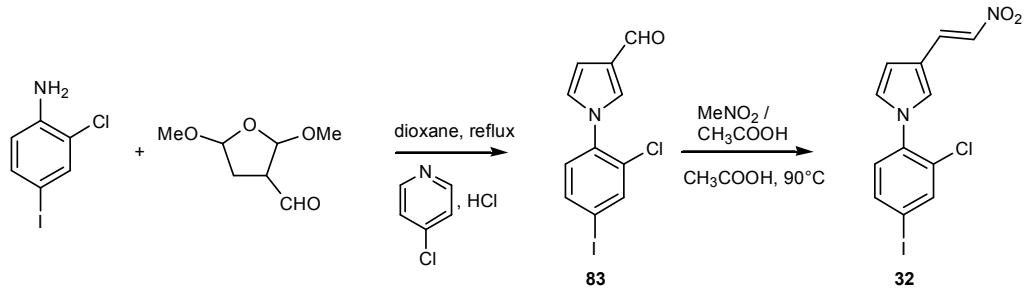

Synthetic procedure for compound (**32**) is similar as that described for compound (**2**) and spectra data are shown below.

1-(4-Chloro-2-iodophenyl)-1*H*-pyrrole-3-carbaldehyde (**83**). Beige solid (35%). Mp: 118 °C. ^{1}H NMR (400 MHz, $CDCl_3$) δ 9.85 (s, 1H), 7.91 (d, J = 1.8 Hz, 1H), 7.72 (dd, J = 8.3 and 1.8 Hz, 1H), 7.48 (t, J = 1.8 Hz, 1H), 7.10 (d, J = 8.3 Hz, 1H), 6.87 (m, 1H), 6.79 (dd, J = 3.2 and 1.7 Hz, 1H). ^{13}C NMR (100 MHz, $CDCl_3$) δ 185.4, 139.3, 137.2, 137.1 130.6, 130.0, 128.9, 127.8, 124.7, 108.8, 93.5. LC-MS (ESI): t_R = 4.87 min; $[M+H]^+$ 332.28. HRMS for $C_{11}H_8ClINO$ $[M+H]^+$ calculated mass: 331.9333, measured: 331.9328.

(*E*) 1-(2-Chloro-4-iodophenyl)-3-(2-nitrovinyl)-1*H*-pyrrole (**32**). Yellow solid (53%). ^{1}H NMR (400 MHz, $CDCl_3$) δ 8.02 (d, J = 13.4 Hz, 1H), 7.91 (d, J = 1.9 Hz, 1H), 7.72 (dd, J = 8.2 and 2.0 Hz, 1H), 7.46 (d, J = 13.5 Hz, 1H), 7.25 (t, 1.9 Hz, 1H), 7.08 (d, J = 8.4 Hz, 1H), 6.91(m, 1H), 6.55 (m, 1H). ^{13}C NMR (100 MHz, $CDCl_3$) δ 139.3, 138.9, 137.2, 137.1, 134.2, 133.2, 130.5, 128.7, 127.8, 125.3, 117.3, 108.3. LC-MS (ESI): t_R = 5.47 min; $[M-H]^-$ 373.27. HRMS for $C_{12}H_9ClIN_2O_2$ $[M+H]^+$ calculated mass: 374.9391, measured: 374.9390.